

PLASMA INDUCED SOLID STATE POLYMERIZATION OF
N-ISOPROPYLACRYLAMIDE (NIPAM)

A THESIS SUBMITTED TO
THE GRADUATE SCHOOL OF NATURAL AND APPLIED SCIENCES
OF
MIDDLE EAST TECHNICAL UNIVERSITY

BY

ALPER ÜNVER

IN PARTIAL FULFILLMENT OF THE REQUIREMENTS
FOR
THE DEGREE OF DOCTOR OF PHILOSOPHY
IN
CHEMISTRY

JANUARY 2008

Approval of the thesis:

**PLASMA INDUCED SOLID STATE POLYMERIZATION OF
N-ISOPROPYLACRYLAMIDE (NIPAM)**

submitted by **ALPER ÜNVER** in partial fulfillment of the requirements for the degree of **Doctor of Philosophy in Chemistry Department, Middle East Technical University** by,

Prof. Dr. Canan Özgen
Dean, Graduate School of **Natural and Applied Sciences** _____

Prof. Dr. Ahmet M. Önal
Head of Department, **Chemistry** _____

Prof. Dr. Güneri Akovalı
Supervisor, **Chemistry Dept., METU** _____

Examining Committee Members:

Prof. Dr. Nesrin Hasırcı
Chemistry Dept., METU _____

Prof. Dr. Güneri Akovalı
Chemistry Dept., METU _____

Prof. Dr. Ahmet M. Önal
Chemistry Dept., METU _____

Prof. Dr. Erdal Bayramlı
Chemistry Dept., METU _____

Prof. Dr. Nursel Dilsiz
Chemical Engineering Dept., Gazi University _____

Date: January 31, 2008

I hereby declare that all information in this document has been obtained and presented in accordance with academic rules and ethical conduct. I also declare that, as required by these rules and conduct, I have fully cited and referenced all material and results that are not original to this work.

Name, Last Name : Alper, Ünver:

Signature :

ABSTRACT

PLASMA INDUCED SOLID STATE POLYMERIZATION OF N-ISOPROPYLACRYLAMIDE (NIPAM)

Ünver, Alper

Ph.D., Department of Chemistry

Supervisor: Prof. Dr. Güneri Akovalı

January 2008, 148 pages

Poly(N-isopropylacrylamide) (PNIPAM) is a smart polymer exhibiting an inverse temperature-solubility relationship with a sharp transition at 32°C in its aqueous solution. Due to its reversible thermo-responsive phase transition behavior at around body temperature, PNIPAM promise a potential for a variety of novel applications especially in biotechnology and medicine.

PNIPAM can be produced by conventional polymerization methods, as well as by use of ionizing radiation, primarily by gamma which leads mainly to a residual-free crosslinked polymer. In this study, RF plasma (glow discharge) technique is used as a novel synthesis method in solid state leading to higher proportions of linear polymer. Since plasma method is an additive-/initiator-free process, a residual-free polymer is expected.

To obtain a better understanding of the plasma induced solid state polymerization mechanism of NIPAM, X-ray data are used. It is found that crystalline structures of Acrylamide (AAM) and NIPAM are isomorphous. Plasma and post plasma aging effects on crystalline structure of NIPAM are followed.

From the Electron Paramagnetic Resonance (EPR) investigations it is observed that post plasma polymerization of NIPAM in solid state proceed by radicalic mechanism. After determination of temperature range in which the radical formed by plasma treatment of NIPAM is highly stable, decay kinetics of the propagating radical in solid state after plasma treatment has been studied in detail.

Keywords: N-isopropylacrylamide (NIPAM), smart behavior, EPR, plasma, solid state polymerization.

ÖZ

N-İZOPROPİLAKRİLAMİDİN (NIPAM) KATI FAZDA PLAZMA ETKİSİ İLE POLİMERİZASYONU

Ünver, Alper

Doktora, Kimya Bölümü

Tez Yöneticisi: Prof. Dr. Güneri Akovalı

Ocak 2008, 148 sayfa

Poli(N-izopropilakrilamid) (PNIPAM) sulu çözeltisinde 32°C civarında keskin bir geçişle ters sıcaklık-çözünürlük ilişkisi gösteren akıllı bir polimerdir. Vücut sıcaklığı civarındaki ısıya duyarlı, tersinir faz geçiş davranışı ile PNIPAM özellikle biyoteknoloji ve ilaç alanlarında çeşitli yenilikçi uygulamalar için potansiyel vadetmektedir.

PNIPAM geleneksel polimerleştirme metotları ile üretilebileceği gibi, iyonlaştırıcı radyasyon kullanımı ile ve özellikle kalıntısız çapraz-bağlı polimer veren gama ile yapılabilmektedir. Bu çalışmada, daha yüksek oranlarda doğrusal polimer veren yeni bir sentez metodu olarak RF plazma (ışıl deşarj) tekniği kullanılmıştır. Plazma metodu katkı-/başlatıcı eklenmemiş bir işlem metodu olduğundan dolayı kalıntısız bir polimer ürün eldesi beklenir.

NIPAM in plazma etkisi ile katı fazda polimerizasyon mekanizmasını daha iyi anlayabilmek için X-ray verileri kullanılmıştır. Akrilamit (AAm) ve NIPAM in kristal yapılarının izomorfolojik oldukları bulunmuştur. Plazma ve plazma sonrası yaşlandırmanın NIPAM in kristal yapısı üzerindeki etkileri izlenmiştir.

Elektron Paramanyetik Rezonans (EPR) alıřmaları ile NIPAM in katı fazda plazma sonrası polimerizasyonunun radikalik mekanizma ile gerekleřtiėi gözlemlenmiřtir. NIPAM in, plazma ile muamelesi sonrası oluřan radikal kararlılıėının yüksek oranda olduėu sıcaklık aralıėının belirlenmesinin ardından, plazma sonrası polimerizasyona devam eden radikalın sönümlenme kinetiėi ayrıntılı bir řekilde alıřılmıřtır.

Anahtar Kelimeler: N-izopropilakrilamid (NIPAM), akıllı davranıř, EPR, plazma, katı faz polimerizasyonu.

To My Parents

ACKNOWLEDGMENTS

The author wishes to express his deepest gratitude to his supervisor Prof. Dr. Güneri Akovalı and co-supervisor Prof. Dr. Nursel Dilsiz for their guidance, advice, criticism, encouragements and insight throughout the research.

The author would also like to thank Prof. Dr. Nesrin Hasırcı for valuable NIPAM discussions, Prof. Dr. Ali Usanmaz for X-ray discussions and Prof. Dr. Ahmet Önal for EPR discussions.

The technical assistances of Elif Kemeröz, Seha Tirkeş, Fatoş Polat, Ayşe Aksoy, Semih Seyyidoğlu and Tolga Depçi in various instrumental studies are gratefully acknowledged.

This study was supported by the State Planning Organization (DPT) Grant No: BAP-01-03-DPT 2003K120920-14.

TABLE OF CONTENTS

ABSTRACT.....	iv
ÖZ.....	vi
DEDICATION.....	viii
ACKNOWLEDGMENTS	ix
TABLE OF CONTENTS.....	x
CHAPTER	
1. INTRODUCTION.....	1
1.1 PLASMA.....	1
1.1.1 A Brief History on Plasma and Some Related Fundamental Literature	1
1.1.2 Advantages of Plasma as a Novel Process	3
1.1.3 Thermal Characteristics of Plasmas.....	3
1.1.4 Some Applications of Plasma in Modern Technology	4
1.1.5 Plasma Process Parameters.....	7
1.1.6 Plasma Chemistry	8
1.1.6.1 Homogeneous Reactions.....	9
1.1.6.2 Heterogeneous Reactions	10
1.1.7 Plasma Discharge Phenomenon.....	11
1.1.8 Glow Discharge Polymerization	12
1.1.9 Polymer Formation Mechanism in Glow Discharge	13
1.1.9.1 Plasma-induced Polymerization (P-iP) Mechanism	14

1.1.9.2	Plasma Polymerization (PP) Mechanism	14
1.1.10	Interaction of Plasmas with Surfaces	15
1.1.10.1	Ablation Effect (Cleaning, Sputtering or Etching).....	16
1.1.10.2	Effect of Radiation Produced by Plasma.....	16
1.1.10.3	Surface Modification (Activation)	17
1.1.10.4	Deposition (Thin Film Coating – Chemical Vapor Deposition).....	17
1.2	Radiation Initiated Polymerization	18
1.2.1	Radiation Initiated Polymerization in Solid-State.....	19
1.2.1.1	Some Characteristics of Polymerization Mechanisms in the Solid State.....	19
1.2.1.2	Nucleation Mechanisms in the Solid State Crystals.....	22
1.2.1.3	Some Characteristics of Polymerization Kinetics in Solid State.....	23
1.3	Fundamental Principles of EPR Spectroscopy	26
1.3.1	Magnetism and Interaction with a Magnetic Field	27
1.3.2	The Zeeman Effect.....	29
1.3.3	The Resonance Conditions in EPR.....	30
1.3.4	Nuclear Hyperfine Structure	33
1.3.5	The Examination of EPR Spectra of Alkyl Radicals	36
1.3.6	EPR Absorption Line Shapes and Symmetry Considerations of Factor	39
1.3.7	Radical Concentration Measurements	42
1.4	Smart Polymers and Applications	44
1.4.1	Poly(N-isopropylacrylamide), (PNIPAM)	47

1.4.2	Solution Properties of PNIPAM	48
1.4.3	Molecular Designs for Tuning of LCST and Characterization	50
1.5	Aim of the Study	52
2.	EXPERIMENTAL	53
2.1	Studies of Monomer Conversion by Percent Weight	53
2.1.1	Low Temperature Plasma System and Monomer	53
2.1.2	Reactor Design	54
2.1.3	Plasma Parameters for Monomer Conversion Experiments	55
2.1.4	Procedure Followed for the Determination of Percent Conversions	55
2.1.5	Bromide—Bromate Titration Method	56
2.1.6	Fourier Transform Infrared (FTIR) Analysis	57
2.1.7	Nuclear Magnetic Resonance (NMR) Analysis	58
2.1.8	Differential Scanning Calorimetric (DSC) Analysis of PNIPAM Hydrogels	58
2.1.9	Scanning Electron Microscopy (SEM) Studies	58
2.2	Studies of Crystallinity and its Effects on Polymerization in Solid State	59
2.2.1	Vacuum Plasma System for Surface Modification of Polymer Materials	59
2.2.2	X-ray Diffraction (XRD) Studies	62
2.2.2.1	X-ray Experiments	62
2.3	Studies of Radicalic Phenomenon by Electron Paramagnetic Resonance (EPR)	62
2.3.1	Plasma Setup for EPR Studies	62

2.3.2	EPR Measurements	63
2.3.3	Reactor Design for EPR Studies	64
3.	RESULTS AND DISCUSSION.....	67
3.1	Plasma Processing of NIPAM — Chemical and Microscopic Characterization of Final Products	67
3.1.1	Geometric Optimizations of Plasma Reactor and Electrodes	67
3.1.2	Effects of Plasma Parameters on Monomer Conversion	69
3.1.3	Some Complications Involved in Isolation Steps.....	72
3.1.4	Product Recognition after Plasma Processing and Isolation.....	74
3.1.4.1	FTIR Results.....	74
3.1.4.2	Structure Elucidation by ^{13}C - and ^1H -NMR Analysis	79
3.1.4.3	DSC Studies	83
3.1.4.4	Scanning Electron Microscopy (SEM)	84
3.1.5	Plasma – surface Interactions	86
3.2	Polymerization in Solid State.....	88
3.2.1	Crystallinity Studies.....	89
3.2.2	X-Ray Investigations of Products	90
3.2.3	Aging Studies	91
3.2.4	Mosaic Block Model and Kinematical Diffraction Approximation	96
3.2.5	Crystalline Structure and Polymerization in Solid State.....	99
3.2.6	Discussions of Polymerization in Crystalline State.....	100

3.3 EPR Studies and Post Plasma Radical Decay Kinetics of NIPAM	103
3.3.1 Characterization of the Radical	104
3.3.2 Thermal Decay of the Radical Signal	107
3.3.3 Data Collection for Post-plasma Decay Kinetics of Propagating PNIPAM	109
3.3.4 Decay Kinetics of PNIPAM Radicals	112
3.3.5 Formation and Decay of the Peroxide Radical after Vacuum Break.....	124
4. CONCLUSIONS.....	130
REFERENCES	131
CURRICULUM VITAE	149

LIST OF TABLES

TABLES

Table 1 Summary of the quantum numbers and their restricted values to define an electrons quantum state	27
Table 2 Several line intensity ratios for the nuclei with $I = \frac{1}{2}$	36
Table 3 Several environmental stimuli	45
Table 4 EPR Parameters for PNIPAM radical monitoring	64
Table 5 Plasma discharge parameters for several discharge periods.....	70
Table 6 Percent compositions of obtained raw product mixtures for the samples treated at 20W and 40W RF plasma	74
Table 7 Chemical shifts in ^{13}C and ^1H -NMR spectra of NPAM and PNIPAM.....	83
Table 8 X-Ray pattern revealed from comparison AAm with NIPAM	101
Table 9 Post-plasma decay data of sample stored at 7°C	109
Table 10 Post-plasma decay data of sample stored at 22°C	110
Table 11 Post-plasma decay data of sample stored at 30°C	110
Table 12 Data used in calculation of activation energy of post-plasma radical decay	116
Table 13 Second-order decay data of peroxide stored at 22°C	125

LIST OF FIGURES

FIGURES

Figure 1 Changes in T_e and T_g with respect to pressure of the system	5
Figure 2 Complexity of interaction between plasma parameters	9
Figure 3 Schematic representation of reactions in a plasma reactor	11
Figure 4 Overall possible interactions in the glow discharge plasma medium	13
Figure 5 Possible initiation pathways in plasma-initiated solid-state NIPAM	21
Figure 6 The precession of a magnetic dipole about the axis of an external magnetic field H_0 . The angular velocity of precession is ω_0	28
Figure 7 The normal Zeeman effect.....	29
Figure 8 The Zeeman energy levels of an electron ($S = 0$) in an applied magnetic field for a fixed microwave frequency	31
Figure 9 Block diagram of general interactions in an ordinary EPR Measurement.....	34
Figure 10 Energy level diagram in a high magnetic field, resulting from the interaction of an unpaired electron $S = \frac{1}{2}$ with a nucleus of $I = \frac{1}{2}$	35
Figure 11 The spin polarization of a $C-H$ bond.....	37
Figure 12 (a) Overlap of π orbitals (b) The effect of dihedral angle θ on overlap of electronic orbitals in a CCH_3 fragment	39
Figure 13 Magnetic field, H_0 , situation according to the g tensor ellipsoid in the x, y and z axes	41

Figure 14 Theoretical line shapes for a species with g tensors of isotropic, axially symmetric and orthorhombic	42
Figure 15 Uses of smart polymers in biotechnology and medicine	47
Figure 16 Effect of copolymerization on the LCST	51
Figure 17 Low temperature (RF) plasma discharge system used in the monomer conversion experiments.....	54
Figure 18 Block diagram of isolation procedure for the solid state plasma initiated PNIPAM	56
Figure 19 TPVD-300/PG System is in the course of diagnostic tests	60
Figure 20 General diagram of vacuum plasma system for surface modification of polymer materials (TPVD300/PG)	61
Figure 21 Schematic representations of plasma irradiation and ESR spectral measurement	63
Figure 22 Plasma effect on quartz under vacuum and under open air conditions	65
Figure 23 Designed plasma polymerization glassware for EPR studies	66
Figure 24 Designed external electrode reactors for the plasma initiated polymerization of NIPAM	69
Figure 25 Pressure change (average of the values for all discharges is shown) in the glass reactor with plasma discharge times	71
Figure 26 Gravimetric and volumetric ($C = C$) determination of monomer deprivations in % by plasma discharges at 20 and 40 W	73
Figure 27 s-cis conformation is favorable for dimers with less steric hindrance (a), while s-trans conformation is common in case of polymers having more steric restrictions (b)	75
Figure 28 FTIR spectrum of PNIPAM polymerized in solid state by plasma initiation.....	77
Figure 29 FTIR spectra of to NIPAM monomer (sampled from inner parts), PNIPAM polymer (sampled from the surface) and their mixture.....	78

Figure 30 NMR spectra of solid state plasma polymerized PNIPAM. (a) ^{13}C and (b) ^1H	80
Figure 31 NMR spectra for isolated NIPAM monomer. (a) ^{13}C and (b) ^1H	81
Figure 32 ^1H -NMR spectrum (in D_2O) for raw product mixture	82
Figure 33 DSC thermogram of the solid state PNIPAM hydrogel at a heating rate of $2^\circ\text{C}/\text{min}$ from 25 to 40°C	83
Figure 34 SEM micrographs of crystalline monomer	85
Figure 35 SEM micrographs of amorphous linear polymer isolated by Extraction	85
Figure 36 SEM micrographs of sample taken after plasma process having both crystalline inner cores beneath amorphous plasma polymerized, amorphous surface layer.....	86
Figure 37 Schematic diagram of surface and underneath layers including linear polymer and crystalline monomer bulk after plasma processing.....	89
Figure 38 X-ray diffraction pattern of NIPAM monomer	90
Figure 39 X-ray diffraction patterns of linear and hydrogel PNIPAM.....	91
Figure 40 Diffractogram set showing plasma and post-plasma effects on X-ray spectrum of NIPAM pellet stored in open-air.....	93
Figure 41 Diffractogram set showing plasma and post-plasma effects on X-ray spectrum of NIPAM pellet stored in a closed vial	94
Figure 42 Weight losses of NIPAM pellets stored in closed vial (covered) and open-air after plasma treatment at 30°C	95
Figure 43 Mosaic model of a NIPAM crystal and effect of aging conditions on orientations of mosaic blocks in the crystal structure.....	98
Figure 44 Molecular structures of (1) AAm and (2) NIPAM.....	103
Figure 45 Splittings in stable radical formed under plasma conditions	105
Figure 46 Conformation of protons in the position in growing chain end.....	106

Figure 47 Formation of stable radical under plasma conditions and its signal endurance at ambient temperature in 5 weeks period	107
Figure 48 Rapid signal deteriorate at 45°C in 2 hours	108
Figure 49 First derivative (a) and absorption (b) curves of 4-amino-TEMPO used as a standard for quantitation of spin concentration	111
Figure 50 First-order decay lines of PNIPAM radicals at 7, 22 and 30°C.....	114
Figure 51 Decay radical profiles of PNIPAM radical at 7, 22 and 30°C.....	115
Figure 52 Arrhenius plots of first order PNIPAM radical decay	117
Figure 53 EPR spectrum set for decaying PNIPAM radical at 7°C	118
Figure 54 Integrated absorption curve set for decaying PNIPAM radical at 7°C	119
Figure 55 EPR spectrum set for decaying PNIPAM radical at 22°C	120
Figure 56 Integrated absorption curve set for decaying PNIPAM radical at 22°C	121
Figure 57 EPR spectrum set for decaying PNIPAM radical at 30°C	122
Figure 58 Integrated absorption curve set for decaying PNIPAM radical at 30°C	123
Figure 59 Peroxide formation by vacuum break and its decay at 22°C	124
Figure 60 Formation of peroxide radical on growing chain end of PNIPAM.....	125
Figure 61 Decay radical profiles of peroxide radical at 22°C	126
Figure 62 Second-order decay line of PNIPAM radicals at 22°C	126
Figure 63 EPR spectrum set for decaying peroxide radical at 22°C	128
Figure 64 Integrated absorption curve set for decaying peroxide radical at 22°C	129

CHAPTER 1

INTRODUCTION

1.1 Plasma

The word plasma is a Greek word meaning to be formed or to be molded, and shares the same root with another well-known word, plastic [1]. Several definitions can be made in relation to plasma.

Plasma can also be defined shortly by industrial terms, as “a gas with electricity going through it” [2].

With more scientific words, plasma is the state of matter in which a collection of significant number of the atoms and/or molecules are electrically excited or partially ionized, with positive and negative charge carriers having equal (quasi-neutral state) densities [3].

1.1.2 A Brief History on Plasma and Some Related Fundamental Literature

The earliest roots of plasma science extend as far back as to 18th century, i.e., to the discoveries of G. C. Lichtenberg (1752–1799), who was a mathematics professor at Göttingen University in Germany who observed beautiful brush-like patterns for the first time on insulating surfaces followed by discharges from a pointed electrode [1]. A very first attempt to explain such phenomena, however, is due to Michael Faraday (1791–1867), the discoverer of electromagnetism. In fact, the first glow (gas) discharge “*vacuum tube*” was made by him in 1838 using brass electrodes and a vacuum approximately at 2 Torr. Sir William Crookes (1832-1919) firstly described it as the “4th state of matter” for a vacuumed gas under

electromagnetic field, because its unique physical properties are as far removed from those of a gas as this is from a liquid [4]. He correctly postulated the existence of electrically charged particles and ions, in a partially evacuated and voltage applied tube, in 1879 [5]. At 1857, Werner von Siemens, a German engineer, patented the first technological application of gas plasma; most probably he was not aware of the underlying science at that time. Siemens' ozonizer made of glass, the forerunner to what is, even today, one of the largest industrial applications of plasma-chemical technology: the synthesis of ozone from molecular oxygen unraveled [1].

In the last decade of 19th century, pioneering inventions marking a new epoch in working of radio transmitters were made. In 1891 Nikola Tesla made an antenna of the high-voltage (also known as "*Tesla coil*", with the patent number US 454,622 –System of Electric Lighting–) which became a powerful radio transmitter and utilized as transmission antennas in most of the practicable radios in the early decades of radio [6]. Two more complementary patent numbers are: US 645,576 – System of Transmission of Electrical Energy – [7] and US 649,621 – Apparatus for Transmission of Electrical Energy – [8].

In 1897, J.J. Thompson started his studies on cathode rays that led him to the identification of electron (which he called a "*corpuscle*") in 1898 [9]. In 1919 Johannes Stark awarded with Nobel Prize for the effect named after him, which is the splitting of spectral lines from a gas discharge under the effect of an intense electric field. Stark's textbook "*Electricity in Gases*", published in 1902, can be considered as the first full theoretical account of gas discharge physics. Another Nobel laureate, an industrial scientist Irving Langmuir, discovered "*plasma oscillations*" in ionized gases in 1923 [10], He and one of his co-worker L. Tonks are credited with using the term "*plasma*" for the first time, as we now use it [11]. He also made major contributions to the current understanding of plasma-related phenomena [12-14].

Although in this short account the widely known researchers are mentioned, there are a number of other scientists from all over the world that have contributed to our understanding of plasma and plasma science a lot.

1.1.3 Advantages of Plasma as a Novel Process

The success of plasma is derived, to a large extent, from several unique characteristics:

- It is an enabling technology, which are not capable of being obtained through other means;
- Plasma processes can be readily controlled and performed with perfect reproducibility and high quality; this makes them highly liable to automation, which is a desired case in large scale manufacturing operations;
- Environmentally favoring plasma operations can increasingly and economically replace wet-chemical, polluting “traditional” processes due to low emission of hazardous chemicals involved.

Furthermore, plasma processes can be conducted at lower temperatures than their conventional counterparts; hence they are less damaging to the materials being treated, and a number of temperature sensitive materials, including polymers can be used safely in plasma. In addition, from industrial point of view, this means a considerable reduction of the required energy budget [1].

1.1.4 Thermal Characteristics of Plasmas

If the plasma is to be investigated with respect to thermal properties, one will come across two subsystems. One of those subsystems is electrons, and the other one is heavy species (including ions, neutral atoms, and neutral molecules). At the low pressure region of plasma (e.g. 10^{-2} - 10^{-3} Torr) created

by either DC or AC, it is found that temperature of the electrons (T_e) is on the order of 10^4 K, and the energy transfer from electrons to the heavy species in the plasma media is not sufficiently high due to decreased number of elastic collisions in vacuum conditions. As a result, at the low pressure region, the temperature of gas (T_g) remain at ambient temperature (~ 300 K) level; while the energy of electrons can be utilized safely. This is called as the low-temperature (non-equilibrium) plasma state. Non-equilibrium plasma is a very active and preferred area for plasma polymerizations as well as plasma modifications of polymer surfaces [1]. The low-temperature (non-equilibrium) plasmas are also known as gas discharges.

On the contrary to low pressures, at atmospheric or higher pressures, mean free path is very short and energy of electrons can be transferred to heavy species by sufficient number of elastic collisions; hence gas temperature can reach to electron temperatures. If supplied energy is enough, beyond these conditions it is possible to obtain thermal (equilibrium) plasma, at high pressure levels (i.e., arcs). Thermal (equilibrium) plasmas are also known as high-temperature (or fusion) plasmas. Those phenomena are schematized in Figure 1.

1.1.5 Some Applications of Plasma in Modern Technology

The plasma state is often referred to as the fourth state of matter. Much of the visible matter in the universe is in the plasma state. Because stars and all visible interstellar matter that makes up over 99% of the total matter in universe are in the plasma state [15].

Plasmas, equilibrium or non-equilibrium types, and directly or indirectly, play key role in our contemporary life: in bringing us sunlight outdoors during the daytime, street light at night, fluorescent light in the offices, plus, a number of treated and coated surfaces of more important objects in our life (including hardened artificial joints we might have in the body and high temperature

turbine blade coatings for the jets), flat panel displays for TVs, gas lasers, the welded joints that keep buildings from falling apart, the production of electrical energy from nuclear fusion, environmental cleanup, and space ship propulsion for interplanetary flights, and so on. Beyond all mentioned above there are many other examples, even other industrially important applications, to list in this brief overview [1].

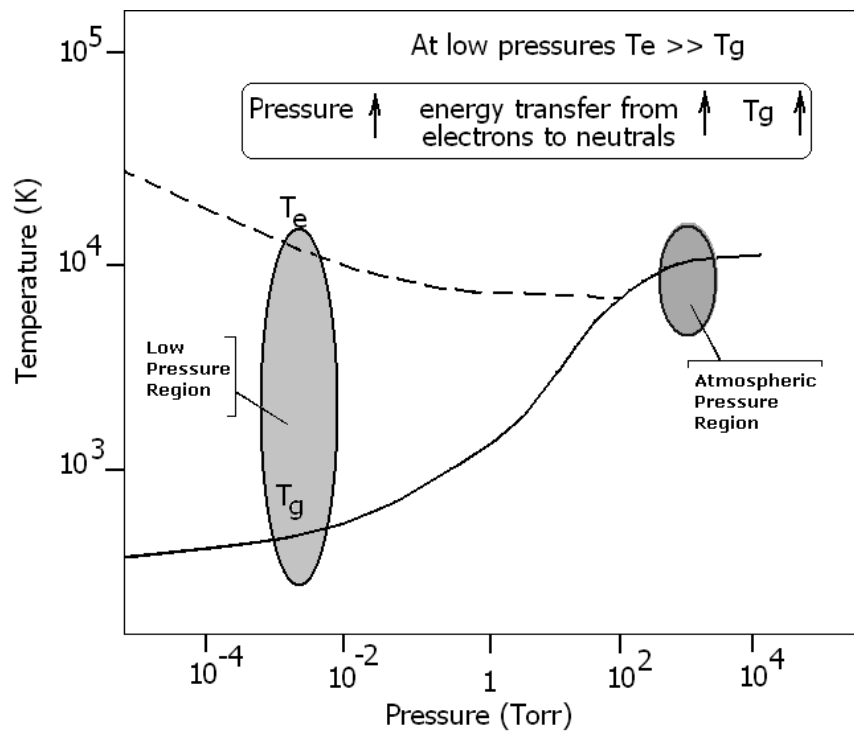


Figure 1 Changes in T_e and T_g with respect to pressure of the system [2].

In the following, some selected uses are referenced with featured articles and reviews.

- Polymer Surface Treatment:
 - Surface modifications (plastics, metals, etc.) [1, 15]
 - Etching [16, 17]
 - Grafting [16, 17, 18]
 - Crosslinking (CASING) [19]

- Bio Applications [20]:
 - Bio compatibility [21, 22]
 - Protein immobilization and cell patterning [23, 24, 25]
 - Bio-MEMS and bio-sensors [26, 27, 28]
 - Instrument sterilization [29, 30]
 - Cell therapy for Wounds [31]

- Textile [32]:
 - Surface treatment of synthetic cloth for dye adhesion [33]
 - Oil and water repellent textile surface [34]

- Automotive [1, 35]:
 - Cleaner exhaust compounds (reduce pollution) [36]
 - Plasma ignition (more reliable) [37]
 - Internal displays (Easy to read) [38]

- Special Chemical Synthesis:
 - Carbon nanotube growth [39, 40]
 - Plasma Assisted Chemical Vapor Deposition (PACVD) [41]
 - Diamond-like film deposition [42, 43]

- High Efficiency Light Sources:
 - High intensity discharge (arc) lamps [15]
 - Low pressure lamps (fluorescent lamps) [15]

- Metallurgical Processing / Thermal Plasma Technology [44, 45]:
 - Plasma arc cutting metals and ceramics [46, 47]
 - Plasma arc welding [48, 49]
 - Metal purification by plasma arc melting [50, 51]

- Environmental Technologies [52]:
 - Air pollution control [53, 54]

- Waste treatment [55, 56]
- Waste destruction [45]
- Spectroscopic Analysis:
 - Inductively Coupled Plasmas (ICP) [57, 58]
 - Astrophysics (Plasma Spectroscopy) [59]
- Propulsion:
 - Plasma ion thrusters for space flight [60, 61]
- Flat-Panel Displays:
 - Field-emitter arrays [62]
 - Plasma displays [63]
 - Organic Light Emitting Diode – OLED [64, 65]
- Semiconductor and Microelectronics [66]:
 - Etching [67, 68]
 - Ion implantation [69]
- Optoelectronics [70, 71]:
- Sensor Devices [72, 73]:

1.1.5 Plasma Process Parameters

The high energy density of the plasma medium makes it possible to obtain large radical fluxes which carry a high energy flow at low densities. Practically everything is possible in such a media: deposition of crystalline or amorphous thin layers, etching, surface modification, chemical conversion, synthesis and destruction, cluster formation (fragmentations) and production of powders [74]. Through wise and correct selection of some parameters such as precursor gas mixtures, regime of energy input, and process

chamber geometry, one can optimize the conditions for a wide range of technological process applications as will be shown below.

When the plasma conditions are sustained in a discharge medium the resultant radiation produces primary active particles i.e., radicals, ions, electrons and so forth. These particles are then undergo some succeeding transformations which result in the formation of new radicals, atoms, final radiolysis products and electrons known as secondary particles.

In an ordinary cold plasma system, which usually consists of RF powered electrode(s), final quantity and quality of product depends on several parameters. The most important ones are summarized below:

- Pressures of the feed gases (total/partial), or flow rates of the different gases
- Total pressure in plasma chamber (reactor)
- Substrate temperature
- Reactor geometry and material
- Electrode shape and distance
- Energy input and regime applied to the plasma

To achieve desired product properties, these parameters are needed to be optimized with utmost care. The complicated relationship between plasma processing parameters is charted in Figure 2.

1.1.6 Plasma Chemistry

The chemical reactions in a plasma reactor can be classified into two main categories: homogeneous and heterogeneous reactions. The former occurs between species in the gaseous phase; while the latter is between the plasma species and the solid surfaces (immersed or in contact with the plasma).

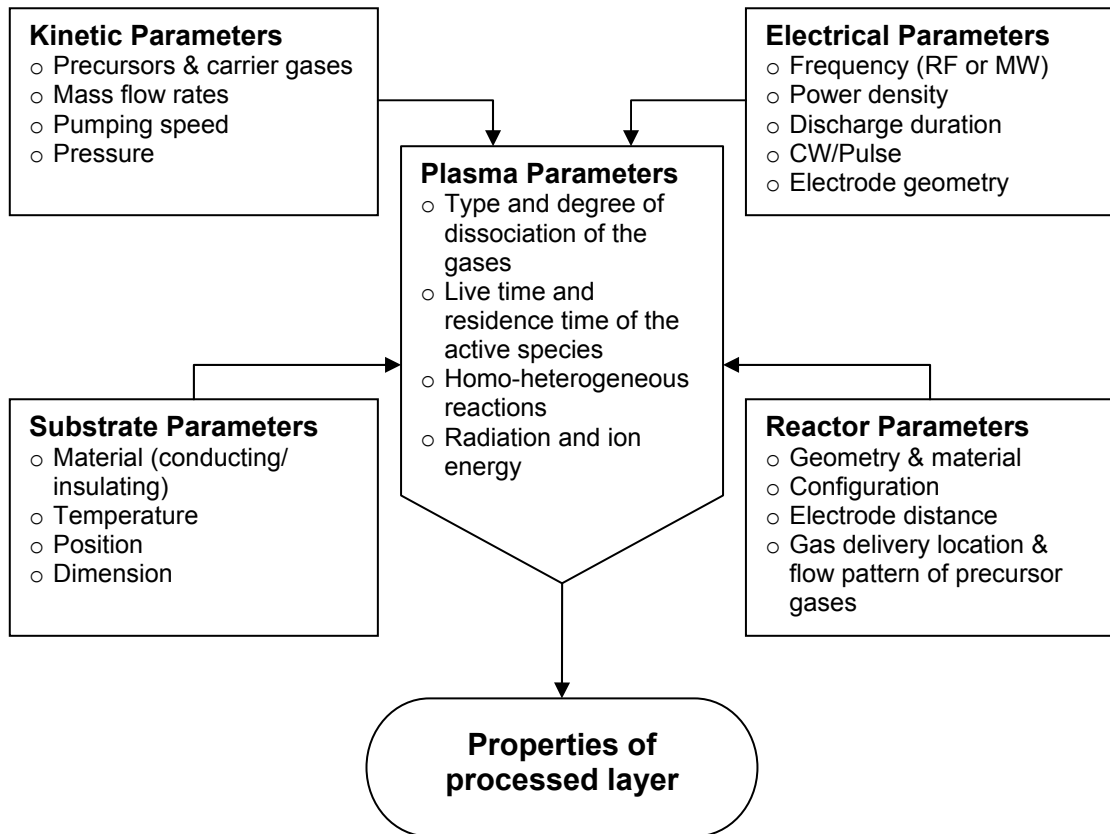


Figure 2 Complexity of interaction between plasma parameters [75, 76, 77].

1.1.6.1 Homogeneous Reactions

The energy gained by electrons in the plasma from the applied electromagnetic field is transferred to the gaseous medium, to excite and sustain the plasma. The major part of this energy transfer is handled by inelastic collisions which can lead to a variety of reactions. The list of some chemical reactions expected are presented below [76, 78]:

- Reactions of electrons with heavy species (i.e., excitation, dissociation, polar dissociation, dissociative attachment, ionization, dissociative ionization, dissociative recombination, two-body recombination, electron impact detachment);

- Some ion-molecule reactions (i.e., positive-negative ion recombination, charge transfer, associative detachment);
- Some radical-molecule reactions (i.e., Penning ionization / dissociation, electron transfer);
- Recombination of radicals;
- Chemiluminescence reactions.

1.1.6.2 Heterogeneous Reactions

These are the reactions which occur as a result of reactions between a solid surface exposed to the plasma and plasma species, as mentioned above. The plasma species can be electron, individual atom, a monomer molecule, a simple radical, or even a polymer formed in the plasma. Typical heterogeneous reactions are as follows [76]:

- Adsorption,
- Deposition of a solid film,
- Etching,
- Sputtering,
- Metastable de-excitation,
- Polymerization,
- Ion implantation,
- CASING (cross-linking by activated species in inert gas plasma).

A schematic summary of the different types of reactions that can take place in a cold plasma reactor is presented in Figure 3.

Due to the large number of the simultaneously competing phenomena affecting the plasma and the resulting complexity of the plasma chemistry, it is not always possible to control the pathways of the chemical reactions or to foresee beforehand the correct combination of process parameters needed for a product looked for. Therefore extensive studies have been carried out to

develop general mechanistic models by measuring, identifying and characterizing chemical reactions between plasma species, taking place in the plasma discharge media [76, 79, and 80].

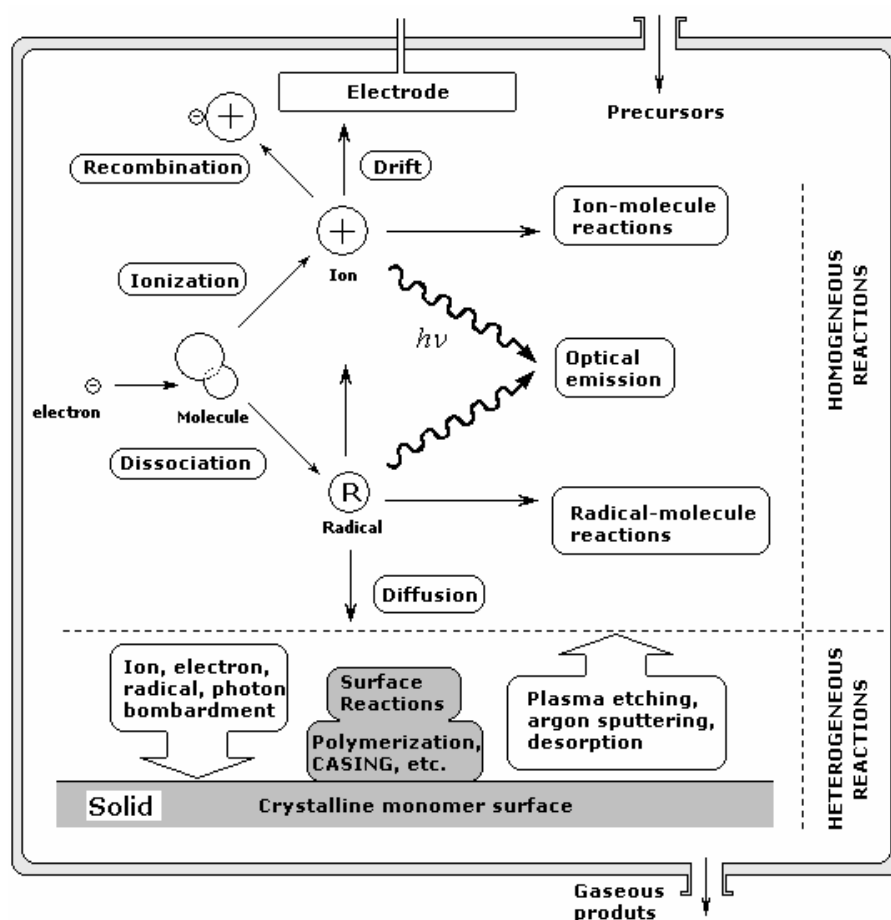


Figure 3 Schematic representation of reactions in a plasma reactor.

1.1.9 Plasma Discharge Phenomenon

The chemical reactions initiated by the ionized species and chemical reactions in which they are taking place in a plasma reactor are shown in Figure 3. In spite of the fact that the primary species created by ionization may not play the dominant role, this ionization process is found essential to sustain the glow discharge. Therefore, it is important to realize how to initiate ionization in a discharge system activated by the RF (radio frequency)

produced electric field near the surface of the cathode.

In this electric field region electrons are accelerated as the first step. When an electron reaches sufficient energy, it can collide with and ionize an (i.e., argon) atom. Due to these collisions metastables, positive ions, electrons and free radicals are generated. Electrons produced from those processes induce successive similar cascade reactions, until the system reaches the *quasi neutral* plasma state. In this highly ionized plasma medium the distribution of electron temperature (energy of electrons) and population varies from cathode to anode in reactor.

At frequencies above 100 kHz, i.e., RF (13.56 MHz.) and MW (2.45 GHz.) discharges, oscillation within a cycle becomes the major motion for electrons. In such cases ionization usually occurs by the collision of oscillating electrons with atoms or molecules in the middle section of the inter-electrode space.

In the argon plasma medium, excited species of argon dissipate their energy mainly by optical emission or transferring the excess energy to other gas atoms and molecules in the plasma volume. In the case of an organic gas molecule, excitation can occur by breaking of (covalent) bonds, such as $C-H$ and $C-C$, which needs much less energy than the ionization of it [81]. As a result, in an ordinary plasma medium, electrically charged and excited (i.e. radicals) particles, neutral atoms and molecules are the most common species.

1.1.10 Glow Discharge Polymerization

Plasmas can be deliberately created on the Earth's surface, for example, in the laboratory or in an industrial environment, by applying direct or alternating high voltage to a gas. If the gas is at low-temperature, non-equilibrium "glow discharge" type of plasma is produced. This type of plasma is of particular importance for the types of technological applications with thermally sensitive

materials. If an organic vapor is introduced into a glow discharge of an inert gas such as argon, the deposition of polymeric films on to an exposed surface is often observed by a process which is generally called as *glow discharge polymerization*.

1.1.10 Polymer Formation Mechanism in Glow Discharge

In a glow discharge medium, the individual steps of reactions involved in the process of polymer formation are extremely complex as discussed under previous titles. However by choosing suitable plasma process conditions, one can make generalizations to suggest a picture of glow discharge polymerization. As can be seen from Figure 4 glow discharge polymerization can be branched into two major types of polymerization mechanisms. One of them is *plasma-induced polymerization (P-iP)*, and the other is *plasma polymerization (PP)*.

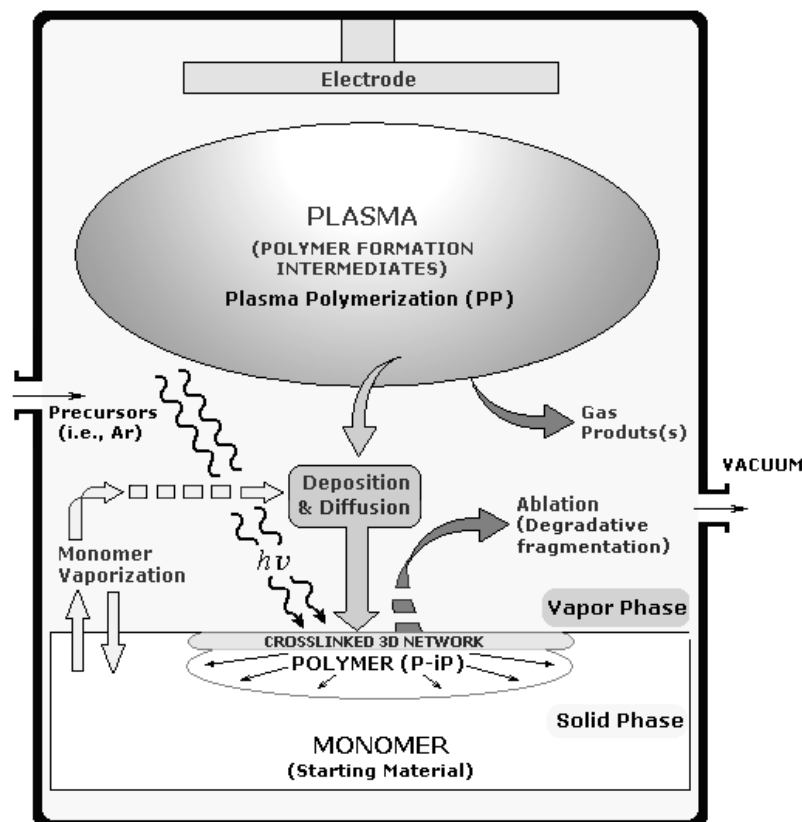
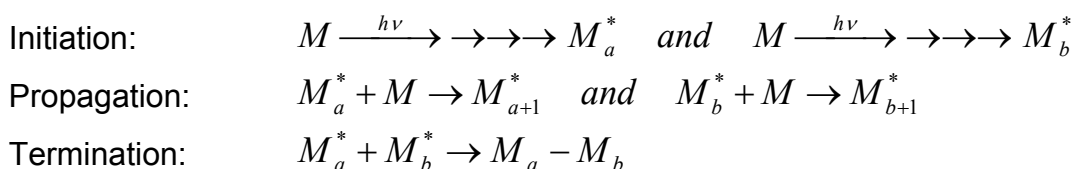


Figure 4 Overall possible interactions in the glow discharge plasma medium.

1.1.10.1 Plasma-induced Polymerization (P-iP) Mechanism

In P-iP mechanism, polymerization triggered by a reactive species that is created in plasma discharge medium, therefore it resembles the conventional (molecular) polymerization reactions where the molecular structure of monomer is retained in the polymer formed. In this mechanism, polymerization mostly occurs on the surface of solid monomer phase. In order to produce polymers by P-iP method, the starting material must contain polymerizable structures such as conventional olefinic double bonds, triple bonds, or cyclic structures; and so on. A representative chain propagation mechanism for plasma-induced polymerization can be given as follows:



where a and b are the numbers of repeating units and M^* represents reactive species. Monomers that can be polymerized by P-iP are limited and not all monomers can be polymerized by this method [82].

1.1.10.2 Plasma Polymerization (PP) Mechanism

In the PP mechanism, polymerization takes place only in the plasma state. The growth-mechanism of plasma polymerization cannot be expressed by the growth mechanism that is specific to the functional groups existing in the molecule, i.e., neither classical chain-growth nor step-growth mechanisms are applicable to plasma polymerization. Varying polymerizable species, which can be an ion of either charge, an excited molecule, a free radical, produced from M or even a fragment or an atom detached from the original starting material (M'), are created in glow discharge depending on the operational conditions of plasma polymerization. Therefore it is also called as elemental (or atomic) polymerization. A polymer formed by this mechanism

cannot be identified by the starting material, since the molecular structure of the starting material is not retained in the final polymer structure (i.e., PP styrene does not have the known polystyrene structure). This mechanism often results in three-dimensional networks made of highly crosslinked atomic level constitutional units. The complex nature of plasma polymerization was explained by the rapid step-growth polymerization (RSGP) in that the recombination of free radicals constitutes the main mechanism to increase the size of molecules [82, 83].

It should be emphasized that, in general, polymerizations in a glow discharge consists of both *plasma-induced polymerization* and *plasma polymerization*. In other words, polymer formation and the properties of polymers formed as expected by glow discharge polymerization are controlled by the balance among P-iP, PP, and even the ablation; as shown in Figure 4. Which of these two main polymerization mechanisms plays the predominant role in the polymer formation in a glow discharge depends not only on the chemical structure of the starting material (monomer), but also on the parameters of the plasma discharge employed. During the experiments of the present thesis study, both mechanisms of glow discharge polymerization -with different proportions- are observed. As will be presented in results and discussion chapter of the thesis, the amount of crosslinked network structure is observed more due to PP, in which the evaporated monomer from the solid monomer surfaces is involved, while, P-iP mechanism is responsible for the formation of linear polymer content owing to the trapped radicals below the monomer surface.

1.1.11 Interaction of Plasmas with Surfaces

When a surface is exposed to plasma, a mutual interaction will take place (Figure 3 and Figure 4). The substrate surface is bombarded with ions, electrons, radicals, neutrals and UV radiation from the plasma phase. This bombardment can induce a flow of volatile products from the substrate to the

plasma medium. With these volatile products the chemical composition of the plasma phase and thus the plasma chemistry will change [84]. In comparison with high energy radiation such as γ -ray and electron beam, plasma energy and penetration are quite low. On the other hand, the photons in plasmas, equivalent of photons in the vacuum UV (V-UV) region, have certain penetrating power, and their effect on a polymer could penetrate into the bulk material to an extent of approximately 100 Å. In Ar plasma treatment of polymeric films, V-UV irradiation is considered to be the major factor in the process. The extent of penetration of the plasma into the surface is determined by both the transport rate and the chemical reaction rate [82].

Because molecular gas glow discharges are very complicated systems, there were very limited generalized understandings about the phenomena for the plasma effects on substrate surfaces (such as mechanisms of concurrent reactions and interactions in between plasma constituents and surface). Some of those can be categorized as follows:

1.1.10.1 Ablation Effect (Cleaning, Sputtering or Etching)

Noble gases (e.g. Argon) are often used for high ablation efficiency and chemical inertness. Plasma ablation involves the mechanical removal of surface contaminants by energetic electron and ion bombardment. It breaks down weak covalent bonds in polymeric contaminants through mechanical bombardment. Ablation affects only the contaminant layers and the outermost molecular layers of the substrate material [76, 85-87].

1.1.10.2 Effect of Radiation Produced by Plasma

The energetic UV radiation from the excited plasma species has several effects on organic materials. Firstly vacuum UV radiation with wavelengths of less than 178 nm can cause photo-ionization. Furthermore UV radiation can cause dissociation of bonds yielding free radicals. This radiation can lead to

chain scissions, rearrangements, elimination or even post irradiation polymerization on the surface. Under certain circumstances, crosslinking through plasma treatment with inert gases, which is also known as CASING (cross-linking by activated species in inert gas plasma), can also introduce additional wear or chemical resistance to a material. The radicals created on the surface can cause crosslinking, can react with species from the plasma phase or can react with oxygen to form peroxides, when exposed to air after plasma treatment [84].

1.1.10.3 Surface Modification (Activation)

Plasma surface modification involves the creation of several chemical functional groups on the substrate surface by use of definite working gases (such as oxygen, hydrogen, nitrogen and ammonia) which dissociate and react with the surface. In the case of polymers, surface activation requires the replacement of surface polymer groups with chemical groups from the plasma gas (e.g. highly reactive carbonyl, carboxyl, and hydroxyl groups) in the same manner. Such modification alters the chemical activity and characteristics of the surface, such as wetting and adhesion, yielding greatly enhanced adhesive strength and permanency of that property [76, 84].

1.1.10.4 Deposition (Thin Film Coating – Chemical Vapor Deposition)

Plasma deposition involves the formation of thin polymer coatings at substrate surfaces through polymerization of the process gas. The deposited thin coatings can possess various properties or physical characteristics, depending on the type of the gas and process parameters selected. Such coatings' in general, exhibit a high degree of crosslinking and much stronger adherence to the substrate, as compared to films derived from conventional polymerization methods [76, 84].

1.2 Radiation Initiated Polymerization

Radiation-initiated (or induced) polymerization of vinyl monomers is direct application of radiation chemistry to the synthesis of high polymers. “*The ionizing radiation*” provides the external energy needed for the initiation step for such polymerizations.

In fact, the use of ionizing radiation as a “catalyst” for the initiation of chain polymerizations of vinyl monomers is not a new application. In the first experiments done before World War II (WWII) in this field (i.e., 1938), relatively strong ionizing radiation sources (such as gamma-rays, fast neutrons, X-rays) were used, for mostly polymerizing liquid monomers of methyl methacrylate and styrene [88]. Unfortunately, most of these works had little technical value because of unsatisfactory experimental conditions involved, such as, ignorance of the dosimetric (radiation dose) parameters, inhomogeneous nature of radiation fields and presence of oxygen in reaction media. The present large-scale development of radiation-induced polymerizations, which is believed to have a promising industrial future, has started after WWII; when the powerful radiation sources, such as nuclear energy plants, become available [89]. The first post war studies of radiation polymerization were those of Dainton’s [90, 91]. He and his coworkers made some detailed investigations of X- and gamma-ray-initiated polymerization of aqueous solutions of acrylonitrile, methacrylonitrile and acrylamide. In the past 6 decades, many advances have been made in radiation-induced polymerization, and a number of books and reviews have been published in this field [89, 92, 93]. At present, radiation-induced polymerizations are still being investigated extensively by a large number of research groups in different parts of the world.

Irradiation of monomers can be done in the vapor, liquid and/or solid states and various kinds of excitations can be satisfied in each. The common point for all of these polymerizations is the strong dependency shown on the irradiation conditions.

1.2.2 Radiation Initiated Polymerization in Solid-State

The earliest successful radiation-initiated polymerization of vinyl compounds in the solid state was reported by Schmitz and Lawton, in 1951 [94]. Starting from 50's, a number of studies have been reported in the field of radiation induced solid-state polymerizations, especially those that covering the next 2 decades. There is also a great deal of knowledge accumulated during this time period for the solid-state polymerization in general, and mainly for acrylamide. Today it is well known that there are a number of factors that affect radiation initiated solid-state polymerizations, such as the crystal size and its quality, structure of monomers, irradiation conditions of the sample, (e.g., polymerization temperature, pressure, external electric and magnetic fields) etc. There are also a number of influential conditions, such as, the type of irradiation source, rate of the radiation (or dose rate), and the radiation regime. In case of plasma irradiation, most of these factors are generally categorized and postulated in previous parts of this chapter. By use of some characteristic physicochemical properties of polymers obtained in the solid-state polymerization, one can obtain some valuable information about the mechanism of the reaction.

The most systematic investigations in solid state polymerization are seen to be carried out with acrylamide, (AA), and in fact these studies acted as the pivot point for the solid state studies done in this thesis work. Such previous studies allowed us to make some predictions with certain correlations for another derivative, N-isopropylacrylamide (NIPAm).

1.2.1.2 Some Characteristics of Polymerization Mechanisms in the Solid State

Study of polymerization reactions in the solid and crystalline states have certain problems when compared to those done in the liquid state. Since the mobility of molecules in the solid phase is highly restricted, one can not

assume that the rate of a given reaction step will be determined by the bulk average concentration of a reagent. Moreover, changes in the crystal lattice during the course of the reaction may influence deeply the velocity of the polymerization reactions. However, there is a number of experiments performed in literature that are mostly based on the solid state polymerization of crystalline vinyl monomers, initiated by exposing the monomer crystals to high energy ionizing radiation. For these experiments it has also been proved that polymerization in irradiated monomer crystals may continue through long-living radicals, sometimes even for months after the sample has been removed from the radiation source. The polymerization mechanisms of such experiments are usually investigated in two separate steps: through the “in source” polymerization (polymerization under irradiation) and the “post-irradiation” polymerization (polymerization after removal of the radiation source).

One can easily expect that, the radiation-initiated polymerization of vinyl monomers in the crystalline state should proceed by a conventional free radical mechanism (with the classical initiation, propagation and termination steps). This expectation can be based on following two principal evidences:

1. An inhibitor sensitivity characteristic of free radical processes,
2. Monomer crystals exposed to ionizing radiation have electron paramagnetic resonance (EPR) spectra indicating a high radical concentration.

In the past, in a number of cases, it was shown that polymerizations of melted monomers in liquid phase induced by ionizing radiation proceeded undoubtedly by an ionic mechanism [95-97]. It is, therefore, logical to investigate whether the EPR spectra observed in irradiated acrylamide crystals are, in fact, result from the species responsible for the growth of the polyacrylamide chain. The close correspondence of the concentration of radicals calculated from the intensity of the EPR spectrum and the concentration of polymer chains obtained from the ratio of polymer yield and

molecular weight indicates that the radicals represent ends of polymer chains. However a detailed consideration of the probable mechanism of chain initiation shows that this assumption does not define clearly the polymerization mechanism [98]. An additional approximation from the mechanistic point of view says that irradiation of solid monomers is expected to favor anionic processes. Because it is known that under irradiation, electrons are trapped in lattice defects of ionic crystals. It seems likely that long-lived negative ions could result from electron capture in lattice defects and this may be followed by their attachment to chemical groups having higher electron affinity which result in formation of negative ions responsible for the initiation of anionic polymerizations [89].

It is generally assumed that the primary process in the interaction of organic molecules with high energy radiation involves the detachment of an electron, i.e., after interaction of N-isopropylacrylamide monomer with the plasma, consecutive steps can possibly occur as shown in Figure 5.

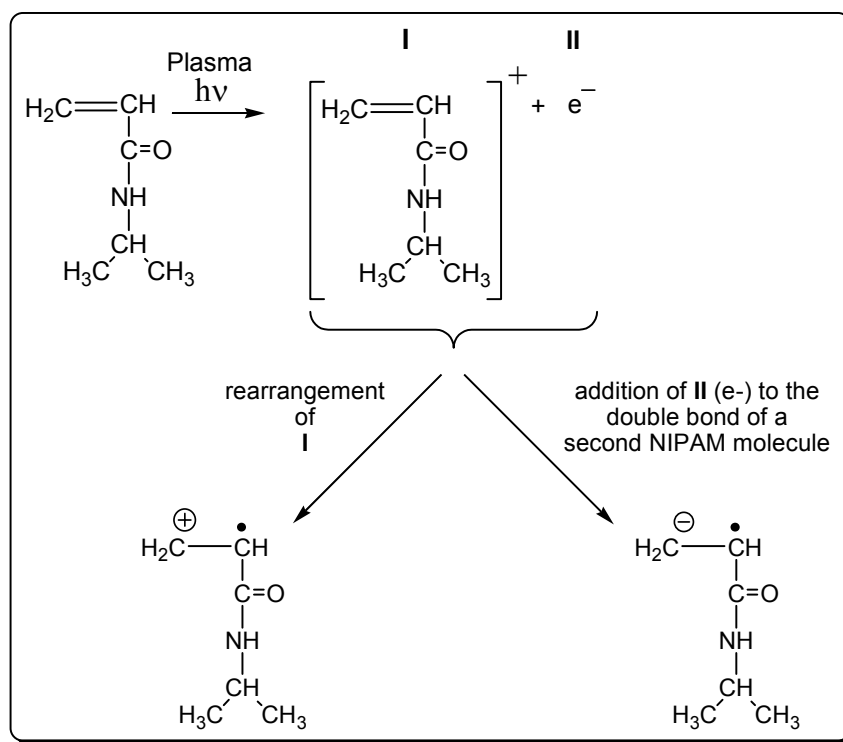


Figure 5 Possible initiation pathways in plasma-initiated solid-state NIPAM.

So, it can be said that the addition of monomer units to the radical cation or the radical anion by either a radical or an ionic mechanism will lead to chains with an unpaired electron at the chain end. Therefore it is difficult to decide the initiation of the polymerization reaction with high-precision from mechanistic point of view. However, at that point the sensitivity of the reaction to oxygen should also be considered as an argument favoring a radicalic mechanism. Hence, in principle, it is suggested by present evidences that, polymerizations with radicalic and ionic mechanisms are both possible in the solid state.

1.2.1.3 Nucleation Mechanisms in the Solid State Crystals

Generally, it is believed that both the in-source and post irradiation results can be explained on the basis of a solid state nucleation phenomenon, in which imperfections and defects especially located in borders and edges between crystal domains in the total structure, play a predominant role. An understanding of such phenomenon became possible only when theories of crystal dislocations and analysis of their role in transport processes provided a foundation for the interpretation of diffusion through crystals. As might be expected, diffusion in solids is very slow and is characterized by very high activation energy value. Also, it is characteristic that the mobility of various species through a crystal lattice may be drastically altered by an increase in the concentration of dislocations, caused either by mechanical damage or by the presence of impurities.

The kinetic pattern of solid-state reactions is generally rather complex. In the initial stages, a new solid phase has to be nucleated, so that the reaction typically exhibits an accelerating phase. It appears that the nucleation of a new phase in the interior of a perfect crystal is impossible and that nuclei are thus formed only at the crystal surfaces, or near crystal imperfections. The nucleation rate is very sensitive to the concentration of such imperfections. The real crystal has many defects such as vacancies, edge and screw

dislocations, impurity molecules etc. each introducing some imperfections to the crystalline system. There is a bit more free volume at those sites leading to somewhat freer thermal motion and diffusion than the oriented lattice. Because of this, it would seem that the reaction could nucleate a bit more easily at these zones than elsewhere in the crystal. If the reaction does indeed nucleate at defects and crystalline boundaries, it implies that the rate of reaction would be non-uniform; that is, the highest where the defect population is highest [99] and may also be highly dependant on the composition of the atmosphere, particularly its content of water vapor [100]. It has been suggested that the radiation-induced solid-state polymerizations of crystalline monomers are heterogeneous reactions proceeding by two-phase mechanisms [101]. Once nuclei of the reaction-product phase have been formed, the reaction proceeds at the interface of the reagent and product phases, so that a quantitative interpretation of experimental data involves assumptions about the geometry of the interface. Also, the advance of the reaction front line need not be isotropic, but may favor certain crystallographic directions. Since the nucleation rate of the reaction product usually varies widely from crystal to crystal, kinetic data obtained with a single crystal are usually meaningless, and polycrystalline samples have to be employed in which the special characteristics of individual crystals average out [102].

1.2.1.4 Some Characteristics of Polymerization Kinetics in Solid State

One of the most widely studied monomer group for the radiation-induced, solid-state polymerization is acrylamide and its derivatives, (i.e., methacrylamide and various N-substituted derivatives of it). Throughout these studies, a number of different parameters affecting polymerization kinetics are examined, such as temperature [103, 104], structure of the N-substituent of monomer [105], pressure [95], sample preparation (crystallization rate) [98], polymerization environment (i.e., oxygen, humidity) [98], monomer orientations in crystalline structure [106], solid solution of acrylamide with selected monomers [107], and nucleation and propagation of

polymerization reaction at definite imperfection sites within the crystal [108] etc. According to the results obtained from these studies, several important outcomes for *in source gamma-irradiation* of acrylamide and its derivatives are obtained, which can be summarized as follows:

- For all series of N-substituted acrylamide and methacrylamide monomers, a very regular increase of polymerization rate with temperature rise was observed.
- The introduction of an N-substituent in the acrylamide, as well as the methacrylamide series causes an increase in the activation energy of solid state polymerization.
- The presence of the methyl substituent of the α -carbon of the vinyl group increases the activation energy of solid state polymerization due to hamper of the chain propagation by the formation of large steric hindrances.
- An increase in size and in structural asymmetry of the N-substituent in the structure of the monomer separately causes an increase in activation energy of solid state polymerization which means that lower polymerization rate and vice versa.
- In comparison with the values of activation energy in-source irradiation polymerization studies, values obtained for post-irradiation solid-state polymerization of the same monomers are much higher.
- There are differences in the effect of pressure at fixed temperature between the initial and further stages (i.e., propagation and termination) of polymerization, and the magnitude of the effect depending on the polymerization temperature at a constant applied pressure.
- In the polymerization of acrylamide and its derivatives, it is generally observed that the rate of polymerization is slightly faster in shock-cooled monomer crystalline medium than in the large annealed crystalline one.

- For gamma-irradiated, solid-state polymerization of acrylamide, the reaction is not affected by the presence of oxygen, which means that kinetic curves for polymerizations run under oxygen atmosphere and under vacuum are nearly identical.
- For gamma-irradiated, solid-state polymerization of acrylamide, the presence of a small amount of water (e.g., 0.12%) produces a small but noticeable acceleration in the rate of polymerization. Introduction of larger amounts of water completely changes the nature of polymerization process i.e., the times required to reach 20% conversion in the presence of 1% and 6% water are 1/25 and 1/100, respectively, of the time required in case of no water addition.
- The polymerization proceeds in planes of the crystal and often started from lattice defects and crystal boundaries. The reaction rate in slowly prepared monocrystals is found to increase, when the crystal is slightly distorted mechanically.
- It was also postulated that in some cases, the chain propagation takes place in a preferred crystallographic direction of the crystal which implies that the orientation of monomer in crystal lattice favors the propagation step. In other words, the monomer is arranged in crystal lattice in a regular head-to-tail sequence so that the polymerization does not require a significant reorientation of the molecules.
- Studies with solid solutions shows that mixing of acrylamide with an isomorphous molecule (e.g., propionamide) does not change the polymerization rate, while the use of a nonisomorphous molecule as a diluent increase the reaction rate for the same reason that increase in reaction rate in distorted crystal surface by a mechanical treatment.
- It is believed that several activated states contribute to the in-source polymerization, while only a long-lived radical contributes to the post polymerization.

As a result, if direct observation of active species (which are formed during irradiation of monomer and are responsible for polymerization) is possible, one can determine the polymerization mechanism easily. Hence for the radical polymerization studies, the electron paramagnetic resonance (EPR) method would provide valuable information.

Beginning from the 60's EPR studies have mostly been performed to elucidate a number of radical polymerization mechanisms and kinetics of acrylamide and its N-substituted derivatives.

Although the scope of this study, plasma-initiated solid state polymerization of NIPAM, has some differences (e.g., monomer structure, radiation penetration and its energy); the investigation of gamma irradiated solid-state polymerization of acrylamide provides important contributions to understanding the polymerization process in this case. Relying on that point, some analogies will be made in the *Results and Discussion* part by using the data obtained from the experiments and the acrylamide literature to comprehend kinetics and mechanisms of plasma initiated solid state polymerization of NIPAM.

1.4 Fundamental Principles of EPR Spectroscopy

In quantum system, a set of four numbers, called *quantum numbers*, is used to describe the energy levels of each electron in an atom. As well as orientation, angular momentum, spin etc. According to *Pauli Exclusion Principle* for electrons in a single atom, no two electrons can have the same four quantum numbers, that is, if n (principal quantum number), l (azimuthal or angular quantum number), and m (magnetic quantum number) are the same, s (spin quantum number) must be different such that the electrons have opposite spins. Names, symbols and allowed values for each quantum numbers are tabulated in Table 1.

Table 1 Summary of the quantum numbers and their restricted values to define an electrons quantum state [109].

Name	Symbol	Range of values
Principal Quantum Number	n	$n \geq 1$
Azimuthal Quantum Number	l	$0 \leq l \leq (n - 1)$
Magnetic Quantum Number	m	$-l \leq m \leq l$
Spin Quantum Number	s	$-\frac{1}{2}, \frac{1}{2}$

1.3.8 Magnetism and Interaction with a Magnetic Field

In particles with an odd number of electrons (i.e., most atoms, free radicals and some ions) the total spin magnetic moment is not equal to zero, i.e., these particles display magnetic properties. In accordance with the theory of magnetism, all substances are either paramagnetic, i.e., their atoms or molecules display magnetic properties or diamagnetic, i.e., their atoms or molecules have no permanent magnetic moment. Particles which are paramagnetic will respond to EPR.

For a free electron the spin angular momentum can have two possible orientations and these give rise to two magnetic moments or spin states of opposite polarity. In the absence of an external magnetic field the two spin states are degenerate. However, if an external magnetic field is applied then the degeneracy is lifted and the individual magnetic dipoles of the particle will become oriented at a certain angle to the field. Similarly electron tends to align itself with its magnetic moment along the field direction. Classically the energy of a magnetic dipole of moment μ in a field H_0 is given by

$$E = -\mu H_0 \cos \theta \quad (1.1)$$

where θ is the angle between the field strength vector and the magnetic moment as shown in Figure 6.

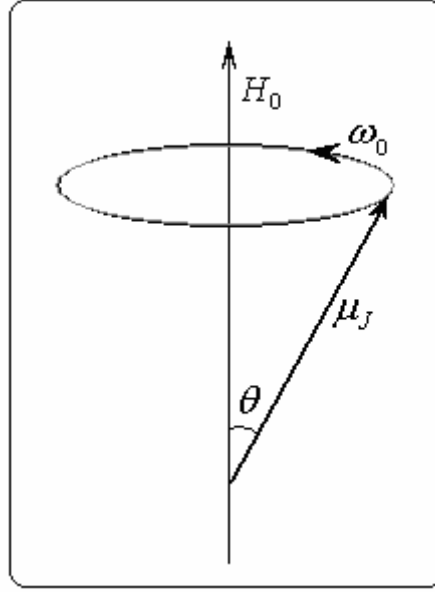


Figure 6 The precession of a magnetic dipole about the axis of an external magnetic field H_0 . The angular velocity of precession is ω_0 .

Actually for a particle with angular momentum, total magnetic moment vector μ_J is never aligned exactly along the direction of the applied field. Instead it executes a precessional motion about the axis of the field, such that the angle θ remains constant, just as a gyroscope precesses about the direction of the gravitational field [110, 111].

The angular frequency of precession ω_0 is called the Larmor frequency and is related to the applied field H_0 by the equation

$$\omega_0 = \gamma H_0 \quad (1.2)$$

where γ is the gyromagnetic ratio of the dipole, that is the ratio of the magnetic moment to the angular momentum.

1.3.9 The Zeeman Effect

By definition the *Zeeman Effect* is the splitting of a spectral line into several components in the presence of a stable magnetic field. The resulting spectral line in applied magnetic field has several excitation states with slightly different energies, which is also known as displacement from degeneracy of a quantum state. This splitting of energy levels can be studied by electron paramagnetic resonance (EPR), by optical spectroscopy in a magnetic field and by measuring magnetic susceptibility methods. In Figure 7, the *normal Zeeman Effect* is represented where the three lines in the spectrum is observed while, in the absence of the field, there is only one. In this case net spin of the system is zero ($S = 0$)

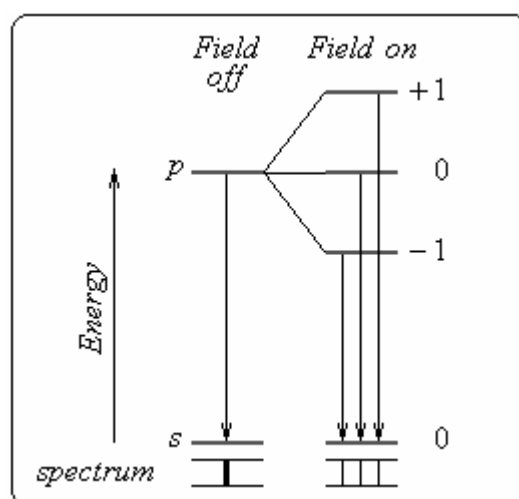


Figure 7 The normal Zeeman effect.

All atoms with one electron in valance shell (H, Na, etc.), those with $S = 1/2$, give an anomalous Zeeman Effect in a weak magnetic field in which the interaction between the magnetic moment of the atom and the applied field which is much weaker than the spin-orbit coupling. Because the spin magnetic moment of the electron affects the splittings in both the ground state and the excited state levels [112, 113].

1.3.10 The Resonance Conditions in EPR

If an external magnetic field is applied to a particle in the ground state with a lone unpaired electron ($l = 0, M_J = M_S = \pm 1/2$), a single transition between two magnetic levels with $s = +1/2$ and $s = -1/2$ will be observed. In such a system, for an electron to pass from a lower to a higher energy level, the amount of the required resonant energy absorption should be;

$$\Delta E = h\nu_0 = \hbar\omega = g_e\beta H_0 \quad (1.3)$$

With this equation the frequency of the quantum is also given. This phenomenon, i.e., the absorption of electromagnetic waves by paramagnetic substances in a magnetic field was discovered by E.K. Zavoiskii and is given the name electron paramagnetic resonance (EPR). EPR spectrometers may operate at different fields and frequencies. For example the most common two of these frequencies being 9.5 GHz and 35 GHz, known as X and Q band, respectively. In our study, the EPR Spectrometer is used at fixed frequency of X-Band and magnetic field is swept in the range of some several values as can be found in EPR measurement parameters in the experimental part. Figure 8 shows that the transition corresponding to EPR takes place as a result of resonant energy absorption equal to the energy difference between the two Zeeman levels.

It is necessary that EPR absorption can only takes place when the spin magnetic moment of the particle in the ground state is not zero. Such particles include ions of transition metals with vacancies in their inner electron shells, anion and cation radicals, systems in triplet state- biradicals, molecular ions, electrons, free radicals and even some point defects like trapped electrons and holes exist in solids.

If the magnetic vector of the applied oscillating electromagnetic field is perpendicular to the steady magnetic field H_0 , an absorption of the energy

occurs, and frequency of the oscillating field satisfies the resonance conditions with frequency ν . If the photon energy $h\nu$ matches the energy difference between Zeeman levels ΔE , then there will be a transition.

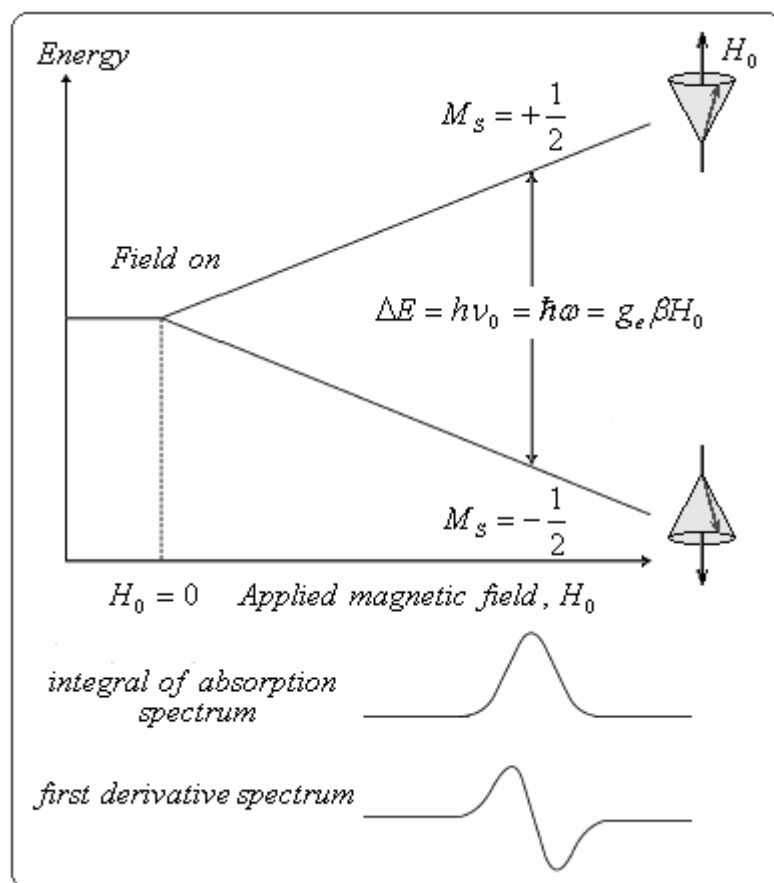


Figure 8 The Zeeman energy levels of an electron ($S = 0$) in an applied magnetic field for a fixed microwave frequency.

In Figure 8 the simplest form of EPR absorption line and its first derivative are also depicted. In fact the absorption lines for most free radical are not a single line, but a very complicated curve, consisting of several peaks, which are known as EPR spectra. The reason for this complexity is the extra interactions between analyzing free radical and various magnetic and electric fields located adjacent inside the substance besides the interaction with external field, H_0 . As shown in Figure 8 electron spins in a magnetic field

are characterized by two Zeeman energy levels, one with the magnetic moment parallel and the other state with the magnetic moment anti-parallel to the magnetic field. The moments will be randomly distributed between parallel and anti-parallel with slightly more in the lower energy state because the electronic system obeys Boltzmann statistics when it is in thermal equilibrium. Then, the ratio of populations of the two states is equal to:

$$\frac{N_{antiparallel}}{N_{parallel}} = e^{-\Delta E / kT} = e^{-g_e \beta H_0 / kT} \quad (1.4)$$

where N represents the populations of the two states, ΔE is the energy difference between the two states, k is Boltzmann's constant and T is the temperature. At room temperature (300 K) and in a magnetic field of 300 mT the populations of the two Zeeman levels are almost equal, but a slight excess exists in the lower level and that gives rise to a net absorption. In other words, to record an EPR signal, the number of electrons on the Zeeman levels must be different (different population levels). However, this would very quickly lead to the disappearance of the EPR signal as the absorption of energy would equalize these two states. For the further measurements to be made in a time dependant experiment (i.e., in a kinetic study) under reasonable conditions, the population excess between Zeeman levels should have to be maintained by some processes which are known as relaxation processes as given below [114];

- Spin-lattice relaxation
- Spin-spin relaxation

The EPR spectrum is characterized by the following parameters: the intensity, width and shape of the absorption line, the value of the g factor and the hyperfine structure. Among these the hyperfine structure of the EPR

spectrum is the most important characteristic for identifying the paramagnetic particle [113].

1.3.11 Nuclear Hyperfine Structure

The splitting of lines in an EPR spectrum arise not only from the interaction between unpaired electron and applied magnetic field, but also the interaction of the nuclear spin, I , produced by magnetic nucleus, with both applied field and unpaired electron. These interactions are depicted in Figure 9. From that point one can infer that when the paramagnetic centre contains one or more nuclei with non-zero nuclear spin ($I \neq 0$), the interaction between the unpaired electron and the nucleus with $I \neq 0$ produces further splittings of the Zeeman energies and consequently there are new transitions.

In EPR spectroscopy this splitting of lines is called *hyperfine splitting* and the resultant structure is *hyperfine structure*. Each nuclear spin I induces a splitting into $[2I + 1]$ levels. The magnitude of the splitting is defined by the hyperfine coupling constant, A , which is expressed in energy units (usually MHz). Where there are several nuclei, for example protons in a radical, each level is further split by each nuclear hyperfine interaction. The magnitude of the splitting is given the symbol a , expressed in magnetic field units.

For the simplest system as the hydrogen atom, which consists of a proton and an electron, the energy of its electron with spin quantum number M_S and the nucleus with spin quantum number M_I is given by

$$E(M_I, M_S) = g_e \beta H_0 M_S - g_N \mu_N H_0 M_I + h A M_I M_S \quad (1.5)$$

where A is the hyperfine coupling constant, g_N is the nuclear g factor and μ_N the nuclear magneton which is smaller than the Bohr magneton by a

factor of 1838, i.e. the ratio of the mass of a proton to that of an electron. The first term in the equation gives the contribution due to the interaction of an electron with an applied field, giving rise to two electron Zeeman levels. The second term is the contribution due to the interaction of the nucleus with the applied magnetic field, the nuclear Zeeman levels. The final term is the energy of interaction between the unpaired electron and the magnetic nucleus.

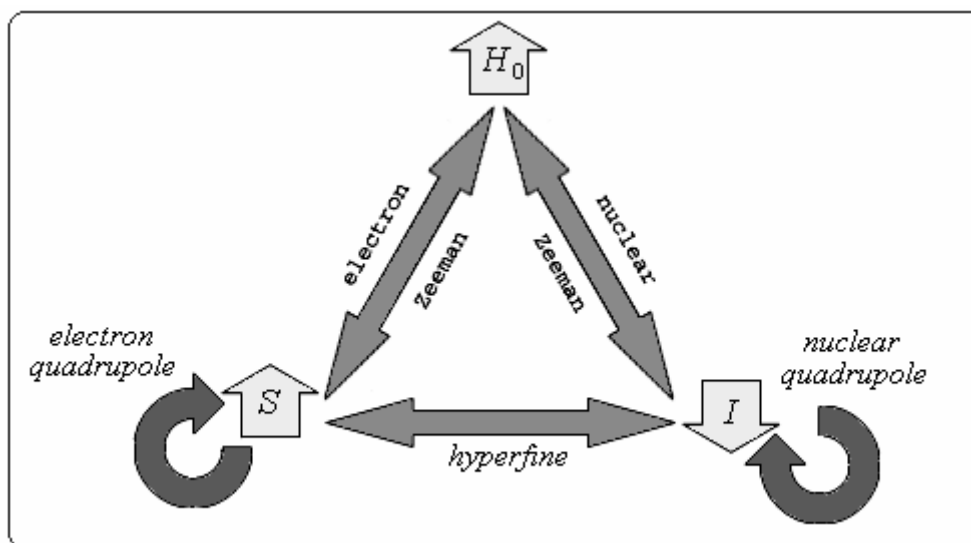


Figure 9 Block diagram of general interactions in an ordinary EPR measurement.

If we now substitute the values for M_S and M_I , then the interaction between an unpaired electron ($S=1/2$) and a single proton ($I=1/2$), gives rise to four energy levels, E_1 to E_4 [114]. The selection rules permit transitions only with $\Delta M_S = \pm 1$ and $\Delta M_I = 0$ as shown in Figure 10.

If we increase the number of equivalent nuclei in the measuring sample then the complexity of the spectrum expands. For the case of $I = \frac{1}{2}$ the line

intensities can be described by the expansion of $(X+1)^2$ and hence follow Pascal's triangle as given in Table 2.

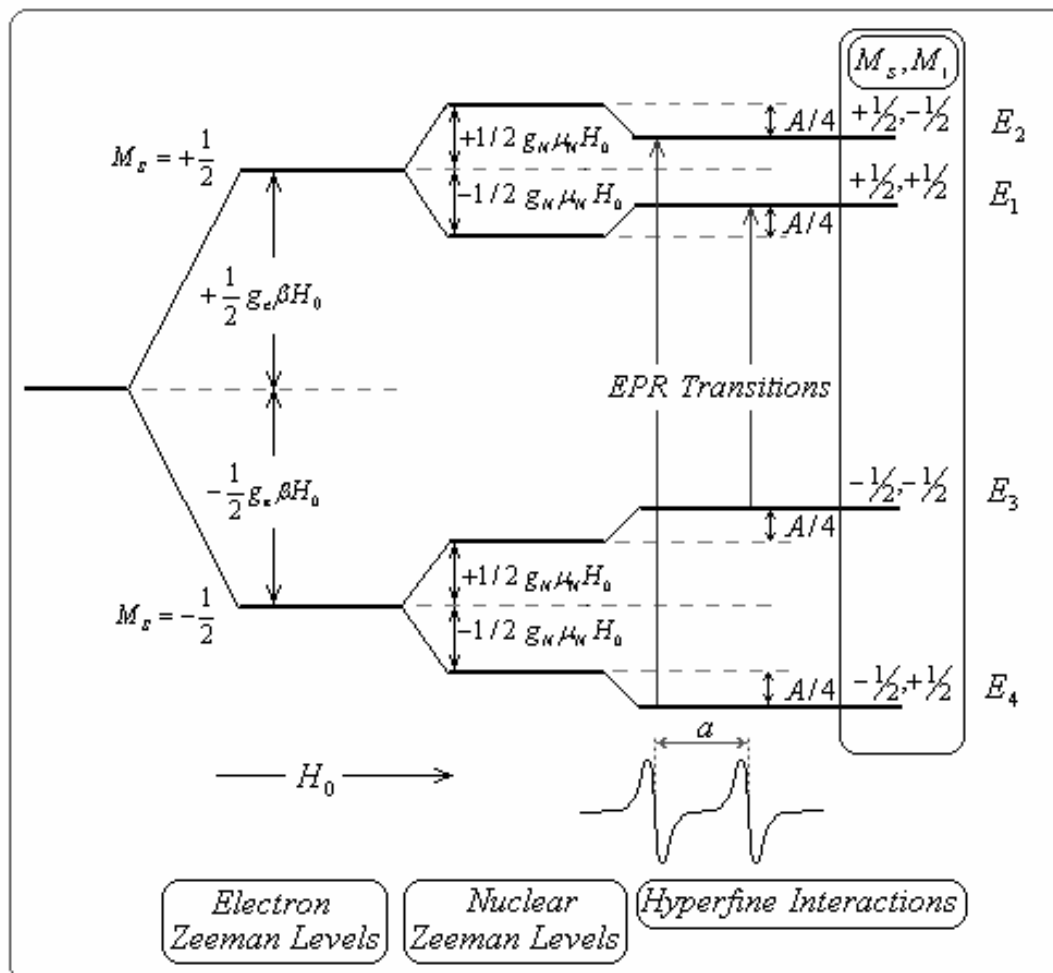


Figure 10 Energy level diagram in a high magnetic field, resulting from the interaction of an unpaired electron $S = 1/2$ with a nucleus of $I = 1/2$.

The resulting hyperfine patterns are highly characteristic and, mostly can be related in some detail to the spatial distribution of the unpaired electron in the whole extend of the radical or ion. Consequently, investigation of nuclear hyperfine structure can often lead to the recognition of the paramagnetic species, which is of great interest and value in the study of reaction

mechanisms of theoretical organic chemistry.

Table 2 Several line intensity ratios for the nuclei with $I = \frac{1}{2}$.

Nuclei ($I = \frac{1}{2}$, e.g. 1H)	Intensity of lines
Number of equivalent nuclei	
1	1
2	1 2 1
3	1 3 3 1
4	1 4 6 4 1

Most of the radicals encountered in chemical studies are π -radicals. These are either aromatic ion radicals with a system of conjugate bonds, such as $\cdot C_6H_6^-$, or alkyl radicals, such as $\cdot CH_3$ in which the unpaired electron is localized in a molecular π orbital or in an atomic p_z orbital. Actually the unpaired electron in these radicals is partially located in the s orbital of a hydrogen atom and the magnitude of the splitting depends on the distribution of the spin density [113].

1.3.12 The Examination of EPR Spectra of Alkyl Radicals

EPR spectra of alkyl radicals can be examined in two grounds as protons in α and β positions. By using some experimental findings about hyperfine splittings of these protons one can make some conformational considerations about active end of organic molecule as given in the following.

α -protons in organic radicals: The theoretical interpretation of isotropic hyperfine interaction of α -protons has been studied by some of authors, including McConnell [115], Bersohn [116], Weissman [117], and Jarrett [118]. After application of both valence bond and molecular orbital approximations,

all reach the same result. If we consider the fragment $\dot{C}-H$ the unpaired spin density which is mainly localized in the $2p_z$ orbital is introduced at the α -proton by a spin polarization effect and forms σ bond of $C-H$. Figure 11 illustrates this schematically that results in the evaluation of some spin density in the $1s$ orbital of the H atom and in turn causes an isotropic hyperfine interaction between the magnetic moment of the p_z electron and the magnetic field of the proton.

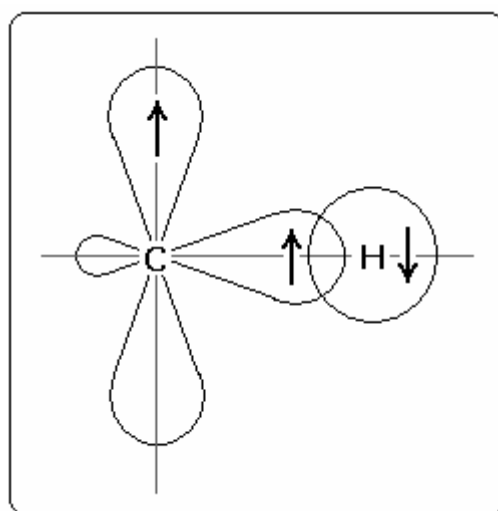


Figure 11 The spin polarization of a $C-H$ bond.

In an EPR spectrum analysis the relation between the magnitude of the splitting and the spin density (ρ_C) was obtained by McConnell with the equation named after him which is of great value for checking quantum mechanical calculations by experiment.

$$a_{\alpha}^H = Q_{CH}^H \cdot \rho_C \quad (1.6)$$

where Q_{CH}^H is a constant and the most accurate value of this constant for a

neutral π radical is 28 gauss. It has become customary to refer to the unpaired spin density on the carbon atom as ρ_C . This symbolize the fraction of the unpaired spin occupy in $2p_z$ orbital of the carbon. It is unity ($\rho_C = 1$) for the carbon atom in $\cdot CH_3$ and 1/6 for each carbon atom in $\cdot C_6H_6^-$.

The outcome which is achieved for the $\cdot \dot{C}-H$ fragment can also be extended with significant success to aromatic and aliphatic systems containing this fragment in a part of a larger molecule. The neighboring atoms and the total charge on the carbon atom will diverge the numerical value of Q_{CH}^C [110, 115].

β – protons in organic radicals : Although the hyperfine interaction mechanism is not fully understood, it is assumed that the splitting from interaction with protons in the β position is caused by *hyperconjugation* [119, 120]. Nevertheless in some cases the splitting is explained by *spin polarization mechanism* [121, 122]. In both of these mechanisms the value of the spin density is related with the degree of overlap of the atomic orbitals. In hyperconjugative mechanism the crucial necessity is that the overlap of π type orbitals having the same symmetry, which lead to delocalization of the unpaired electron into the hydrogen $1s$ orbitals in adjacent methyl group (Fig. 12-a). Here the interaction with all three methyl protons is the same, but if one proton is replaced by any other group, the hyperfine splittings of the two remaining protons will not be equal anymore (anisotropic). The overlap of the unpaired electron and the hydrogen is proportional to $\cos \theta$, where θ is the angle between the p_z orbital axis of the unpaired electron and the projection of the $C_\beta-H$ bond onto a plane perpendicular to the $C_\alpha-C_\beta$ bond (Fig. 14-b). Generally the semiempirical relation is adopted for a proton in the β position.

$$a_{\beta}^H \cong B_1 + B_2 \cos^2 \theta \quad (1.7)$$

where $B_1 \cong 4$ gauss is the spin polarization factor of the C_{β} —H bond, $B_2 \cong 50$ gauss [110, 123] and a_{β}^H is the magnitude of splitting due to proton in the β position.

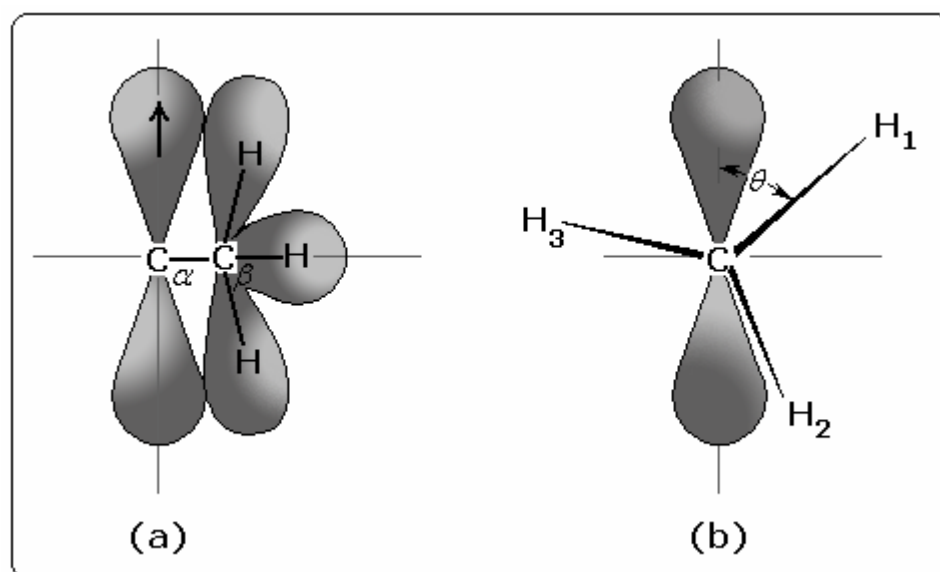


Figure 12 (a) Overlap of π orbitals (b) The effect of dihedral angle θ on overlap of electronic orbitals in a CCH_3 fragment.

1.3.13 EPR Absorption Line Shapes and Symmetry Considerations of g Factor

For a paramagnetic particle the total magnetic field acting on the magnetic moment of the electron equals the vector sum of the external and internal fields, i.e., spin-orbit coupling, crystal field. The latter is strongly concerned with particle's own coordinate system. Thus the magnitude of the effective magnetic field depends on the orientation of paramagnetic species

throughout the applied field. This alignment dependence causes a change in the *g factor* values along the three axes of the coordinate system which are denoted by g_{xx} , g_{yy} and g_{zz} . The intensity of the effective magnetic field may be represented as

$$H_{eff} = H_x \frac{g_{xx}}{g_e} i + H_y \frac{g_{yy}}{g_e} j + H_z \frac{g_{zz}}{g_e} k \quad (1.8)$$

where i , j and k are unit vectors directed along the x , y and z axes respectively. The *g factor* depends not only on the spin of the system and its electronic environment, but also on orientation of the molecule with respect to magnetic field [113]. Here g_e is a scalar value, while g is a second order tensor which represents the anisotropy of the interaction between the unpaired electron and the external magnetic field where it may be depicted as an ellipsoid whose principal elements (g_{xx} , g_{yy} , g_{zz}) depend upon the orientation of the symmetry axes of the paramagnetic entity with respect to the applied magnetic field. This ellipsoid geometry is given in Figure 13. The angles θ and ϕ are postulated to define the orientation of H_0 [114].

In many of the EPR analyses the samples are polycrystalline materials which are composed of numerous small crystallites that are randomly oriented in space. For such times the resultant powder EPR spectrum is the cumulative of spectra corresponding to all possible orientations of the paramagnetic species with respect to the magnetic field.

The general outline of the spectrum is found out by several parameters, such as the symmetry of the g tensor and the actual values of its components, and the line width of the resonance. The most common three possible cases can be distinguished with regard to the symmetry of the g tensor.

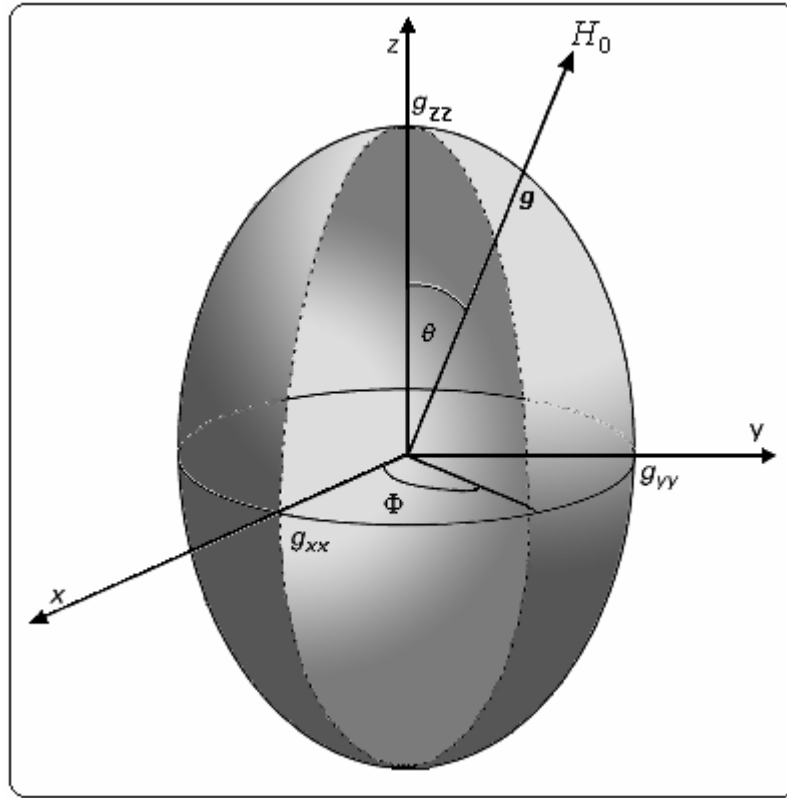


Figure 13 Magnetic field, H_0 , situation according to the g tensor ellipsoid in the x , y and z axes.

These are (i) symmetrical g tensor, which is characterized by $g_{xx} = g_{yy} = g_{zz} = g_{iso}$ and a single symmetrical absorption line, (ii) axially symmetric g tensor with $g_{zz} = g_{\perp}$ and $g_{xx} = g_{yy} = g_{\parallel}$ where the axis of the paramagnetic species is perpendicular and parallel to the applied magnetic field, respectively and (iii) unsymmetrical g tensor with $g_{xx} > g_{yy} > g_{zz}$ which is also known as orthorhombic symmetry. The concerned line shapes, tensor symmetries, absorption lines and their first derivatives for these cases are pictured schematically in Figure 14.

1.3.14 Radical Concentration Measurements

From general aspects the determination of free-radical concentration seems simple. However, the measurement of the absolute spin concentration is the one of the most difficult procedure which demand great care if reasonable accuracy is to be achieved.

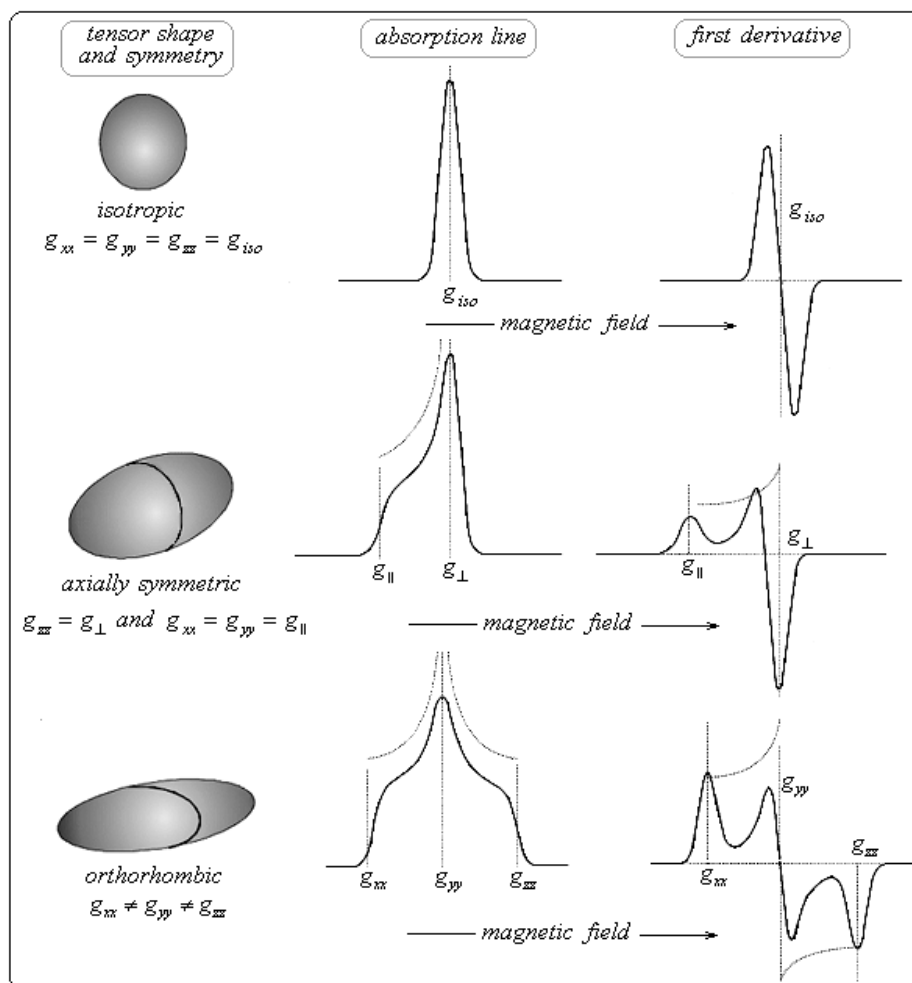


Figure 14 Theoretical line shapes for a species with g tensors of isotropic, axially symmetric and orthorhombic.

In this field there are two alternative methods proposed, an absolute and a comparison technique. In the former procedure the exact spectrometer

parameters are needed which will be used to find the relationship between the spin concentration and the magnetic susceptibility. Absolute measurement procedure is not feasible to perform because it demands knowledge of parameters such as crystal conversion loss, amplifier gain, microwave power, etc., none of which is specifically easy to obtain [110]. In the latter, as a more applicable method, the unknown is measured relative to a standard reference such as DPPH (1,1-diphenyl-2-picrilhydrazyl), TEMPO (2,2,6,6-tetramethylpiperidine-1-oxyl) or other calibrated standard substances having a long-term stable spin concentration over a wide ranges of temperatures. In the framework of our study we utilized the comparison procedures with standard 4-amino-TEMPO. In one of these techniques, the unknown spin concentration is calculated from the ratio of the area under the two EPR absorption lines recorded from the reference and from the unknown samples at identical thermal, electronic, and field conditions. Validity of the calculation is based on the scanning under identical spectroscopic parameters such as microwave power, scan width, averaged scan number, filling factor (sample size and geometry), field modulation amplitude, receiver gain, sampling time, and recording time constant [124, 125].

If the EPR measurements are done with great care under identical conditions, the concentration of the unknown radical can be found by the following equation.

$$\frac{N_1}{N_2} = \frac{A_1 M_1}{A_2 M_2} \quad (1.9)$$

where N_1 and A_1 stands for the number of radicals centers and the area under the absorption curve for the standard respectively; N_2 and A_2 stands for the same values for the sample. M_1 and M_2 are the mass of sample and the standard, respectively. Mass is not a variable in our case, because we study with one sample throughout the kinetic experiments at each

temperature. In another comparison approximation for species with the same spectral line width and shape function relative concentrations are readily determined by measuring the ratio of peak heights (h_1/h_2) on the first derivative curves. In this method identical size and identical conditions are needed.

$$\frac{N_1}{N_2} = \frac{h_1}{h_2} \quad (1.10)$$

where N_1 and N_2 are the numbers of unpaired electrons in standard and unknown, respectively. If the line shape function is the same (e.g. both Gaussian) but line widths differ, the equation can be modified as

$$\frac{N_1}{N_2} = \frac{h_1 \Delta H_1^2}{h_2 \Delta H_2^2} \quad (1.11)$$

in which ΔH_1 and ΔH_2 are the line widths corresponding the region between peak maxima of EPR signal [110].

1.5 Smart Polymers and Applications

Life is polymeric in its essence. Nature uses polymers both as constructive elements and as parts of complicated cell machinery. Recent decades have witnessed the appearance of synthetic functional polymers which respond in some desired way to a change in temperature, pH, electric or magnetic fields or other stimuli [126]. These polymers are nick-named as *stimuli-responsive*. They are also known as “intelligent”, “smart”, “signal-responsive” or “environmentally-sensitive” polymers. Many different stimuli have been investigated and they are listed in Table 3. These are the polymers that undergo relatively large and abrupt, physical or chemical changes in response to small external changes in the environmental conditions [127].

Table 3 Several environmental stimuli.

Type of Stimulus	Examples
Physical	Temperature, radiation ($h\nu$), ionic strength, electric field, magnetic field, mechanical stress, sonic radiation
Chemical	pH, specific ions, specific chemical substances
Biochemical	Metabolite, enzyme, affinity ligands

By more detailed definition, the “*smart polymer*” can be considered as macromolecules that undergo fast and reversible changes from hydrophilic to hydrophobic microstructures triggered by small changes in their environment. These microscopic changes are apparent at the macroscopic level as the formation of a precipitate of the smart polymer in solution, changes in wettability of the surface to which the smart polymer is grafted or dramatic shrinking/swelling of the hydrogel. The changes are relatively fast and reversible i.e. the system returns to its initial state when the trigger is removed [126].

These polymer systems recognize a stimulus as a signal, judge the magnitude of this signal, and then change their chain conformation in direct response [128]. The driving force behind these transitions could arise from differences between the nature of systems e.g. neutralization of charged groups, either by pH-shift or introduction of oppositely charged polymer, changes in the efficiency of hydrogen bonding with the increase in temperature or ionic strength, and so on. An appropriate balance of hydrophobicity and hydrophilicity in the molecular structure of the polymer is believed to be of key point in explaining the phase transition [126]. Chemical stimuli change the interactions between polymer chains or between polymer chains and solvents at the molecular level while physical stimuli will alter

molecular interactions at critical onset points [128].

Smart polymers may also be physically mixed with or chemically conjugated to biomolecules to yield a large family of polymer-biomolecule systems that can respond to biological as well as to physical and chemical stimuli, and they show such responsive behavior in aqueous solutions [129, 130]. These responses of polymer systems against physical, chemical and biochemical stimuli are very useful in bio-related applications such as drug delivery [131], biotechnology [132], and chromatography [133]. Therefore there are many successful applications in medicine and biotechnology for such smart polymer-biomolecule systems. Recent trends in uses are shown in Figure 15. Furthermore, in some cases by making some modifications (i.e., copolymerization) in structural architecture of the macromolecule, one can obtain dual-responsive polymer systems which response two simultaneously applied signals [128].

Recent advances in the design of stimuli-responsive polymers have created opportunities for novel biomedical applications. Stimuli-responsive changes in shape, surface characteristics, solubility, formation of a complex molecular self-assembly and a sol–gel transition enabled several novel applications of stimuli-responsive polymers in delivery of therapeutics, tissue engineering, bioseparations, sensors or actuator systems. These extensive studies, numerous published papers and patents are testifying the rapid advance in this field [132]. These polymers have been utilized in a number of forms. For instance, permanently cross-linked hydrogels [131], reversible (sol-gel transitive by stimulus) hydrogels [134], micelles [134], modified interfaces [135], conjugated solutions [136, 137], etc.

In the scope of present thesis the studies are concentrated on synthesis and characterization of the temperature responsive polymer, poly(N-isopropylacrylamide), (PNIPAM) by using plasma glow discharge technique in solid state.

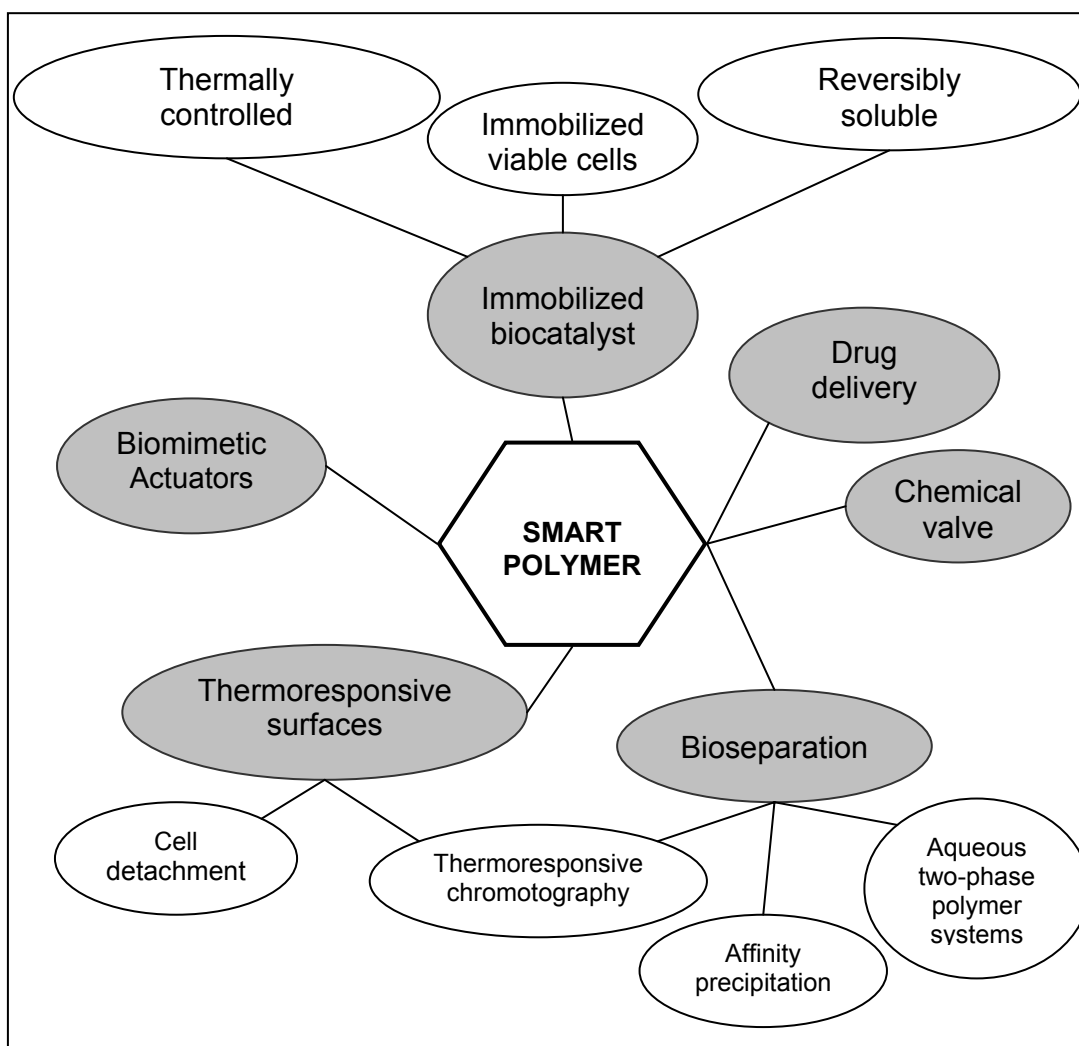


Figure 15 Uses of smart polymers in biotechnology and medicine [126].

1.4.4 Poly(N-isopropylacrylamide), (PNIPAM)

Poly (N-substituted acrylamide) is representative of the group of temperature-responsive polymers having lower critical solution temperature (LCST), defined as the critical temperature at which a polymer solution undergoes phase transition from a soluble to an insoluble state above that critical temperature. Among those polymer poly(N-isopropylacrylamide), PNIPAM is the most popular one since it exhibits a sharp phase transition in water (LCST) at around 32°C. [128] The often forgotten main reason for such biomedical popularity is not really the fact that the LCST of PNIPAM is close

to body temperature (other polymers exhibit LCST values even closer to 37°C) but rather the fact that its LCST is relatively insensitive to environmental conditions. Indeed, slight variations of pH, concentration, or chemical environment are generally affecting the LCST of PNIPAM by few degrees only, which is an appealing property for tuning LCST studies [138].

Historically, the first appearance of PNIPAM in literature is found in 1956 dealing with the synthesis and polymerization of the corresponding monomer N-isopropylacrylamide, NIPAM [139-141]. From that time, the different forms of PNIPAM have been studied such as single chains [142-145], microgels [146, 147], macroscopic gels [148, 149], latexes [150], gating membranes [151, 152], coatings [153] and fibers [154, 155] in a wide range of subjects including chemistry, physics, biology, biotechnology, pharmacy, photography and so on.

Today it becomes perhaps the most popular member of a class of polymers that possess inverse solubility upon heating, a property contrary to the behavior of most polymers in organic solvents under atmospheric pressure near room temperature. Its macromolecular transition from a hydrophilic to a hydrophobic structure occurs rather abruptly at lower critical solution temperature (LCST). Experimentally, this temperature lies between 30 and 35°C, the exact temperature being a function of the detailed microstructure of the macromolecule. Starting from the mid 80's PNIPAM has taken hits and citations in significant amounts, therefore it can be considered as relatively new polymer in literature [156].

1.4.5 Solution Properties of PNIPAM

One of the distinctive properties of temperature-responsive polymers is their critical solution temperature existence. This is the temperature at which the phase of polymer and solution is discontinuously changed according to their composition.

The behavior of a polymer in a given medium reflects the balance of like and unlike interactions among its own segments and the surrounding molecules. In case of aqueous solutions of temperature-responsive polymer besides the relationship between polymer and water molecules, there is another important interaction between polymer molecules. Therefore, both hydrogen bonding and hydrophobic interactions should be born in mind when volume phase transition is considered [157].

When hydrophobic solutes (i.e., polymers) are introduced into water, two phenomena are simultaneously observed. One is hydrophobic hydration, in which the water molecules form cage-like structures around the hydrophobic solutes. As a result of this hydration, nonpolar molecules become soluble in water. The other is hydrophobic interaction, or the association of hydrophobic solutes which is responsible for hydrogel shrinkage, micelle aggregation or the physical cross-link formation. In general, an increase in temperature results in a reduction of the total number of water molecules structured around the hydrophobic solutes, which promotes hydrophobic interaction. Consequently, a rise in temperature strengthens the hydrophobic interaction. This is quite contrary to other interactions such as dipole-dipole, van der Waals, and electrostatic forces [158-159].

From a thermodynamic point of view the phase transition phenomena can be explained as follows. Ordering of solutes such as PNIPAM in aqueous solution results from specific orientations required to hydrogen bond with the already somewhat arranged water molecules. This becomes especially important when water molecules must reorient around nonpolar regions of solutes, being unable to hydrogen bond with them. These have been claimed to be clathrate-like structures. This latter phenomenon, known as the hydrophobic effect, [160] results in a decreased entropy upon mixing (negative ΔS). At higher temperatures, the entropy term dominates the otherwise exothermic enthalpy of the hydrogen bonds formed between the polymer polar groups and water molecules that is the initial driving force for

dissolution. Once the free energy change (ΔG) becomes positive upon mixing, the consequence is phase separation above a lower critical solution temperature (LCST) such as exists in the case of PNIPAM. If the concentration of the polymer is high enough, this replacement of polymer-water interactions with polymer-polymer and water-water interactions is demonstrated by precipitation [156].

1.4.6 Molecular Designs for Tuning of LCST and Characterization

The chemical environment of the polymer strongly affects the thermo-sensitivity of the LCST polymers. The incorporation of hydrophilic and hydrophobic comonomers and the presence of ionic surfactants, salts, or organic cosolvents may alter or completely eliminate the temperature sensitivity [128, 161].

The LCST of a temperature responsive polymer is influenced by hydrophobic or hydrophilic moieties in its molecular chains. In general, to increase the LCST of temperature responsive PNIPAM, this polymer has been randomly copolymerized with a small ratio of hydrophilic monomers such as acrylamide [162]. By contrast, a small ratio of hydrophobic constituent was reported to decrease the LCST of NIPAAm as well as to increase its temperature sensitivity [163]. Further increase in hydrophilic monomers content would increase the LCST and even disappear, and more hydrophobic monomers such as N-butylacrylamide would decrease the LCST more as represented in Figure 16 [164].

Adjustment of LCST i.e., near body temperature by incorporation of hydrophobic or hydrophilic moieties to obtain a desired value is essential especially for some biotechnological applications such as controlled drug delivery.

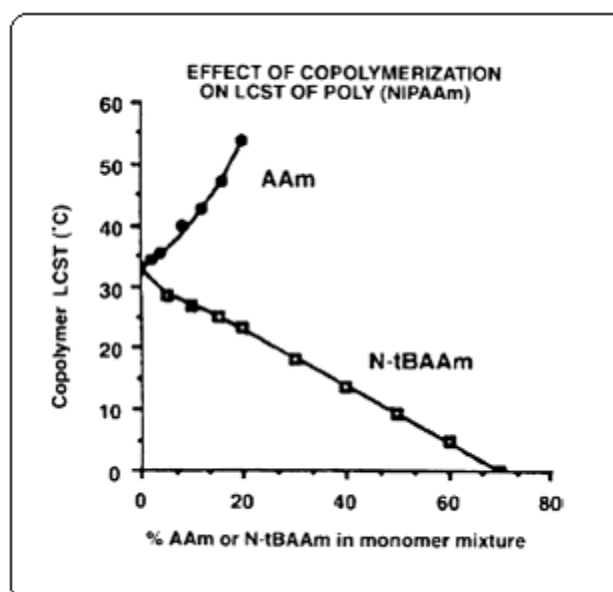


Figure 16 Effect of copolymerization on the LCST [164].

These modified PNIPAM polymers have been studied for several applications in various fields of material science such as in drug release; enzyme and cell immobilization; gene carrier systems; intelligent on-off systems for separation, permeation, actuation and detachment control; treatment of water; oil recovery; photo-response film technology; flocculation and artificial muscle [128, 156].

In the last three decades, both scientific and technological studies of the PNIPAM polymer have been extensively carried out. The transition phenomena or cloud point of the aqueous polymer solution have been investigated by a wide variety of techniques including U.V. turbidimetry [165-167], calorimetry [168-170], NMR [171], FTIR [172], time resolved optical spectroscopy (TROS) [173], fluorescence [174, 175], light scattering [176-178], neutron scattering [179], raman spectroscopy [180], and EPR [181, 182]. In many of these characterization methods analyses have been performed with bulk polymer in an aqueous solution.

1.5 Aim of the Study

With its sharp and reversible thermo-sensitive phase transition behavior at around body temperature, PNIPAM promise a prominent potential for a variety of novel applications especially in biotechnology and medicine. PNIPAM can be produced by conventional polymerization methods, in which several initiators and/or acceleration catalysts are employed in the media.

Although polymerization of NIPAM could be carried out by conventional polymerization methods, ionizing radiations has been generally preferred and distinguished as an eligible and practical tool for the synthesis of PNIPAM which is a simple and additive free process where no initiator or chemical accelerators are required. Use of powerful ionizing radiation, primarily the gamma, leads mainly to a residual-free crosslinked polymer with almost no linear polymer content. As a result, the crosslinked polymer obtained by this method brings limited utilization with no processability due to its insoluble nature.

In the present study, RF plasma (glow discharge) technique is proposed as a novel synthesis method in solid state leading to higher proportions of linear polymer, which is easily processable. Since RF plasma method offers an additive-/initiator-free process under clean atmospheres (vacuumed and argon fed), a side product-free polymer is expected. In addition, the product (linear PNIPAM) and unreacted monomer residue can easily be isolated by means of simple purification methods, which is considered another advantage.

CHAPTER 2

EXPERIMENTAL

2.1 Studies of Monomer Conversion by Percent Weight

2.1.1 Low Temperature Plasma System and Monomer

A schematic illustration of homemade low temperature radio frequency (RF) plasma discharge system, with frequency of the excitation voltage continuous at 13.56 MHz, was built for the monomer % weight conversion experiments. The system which is unique for present study is powered with Tegal™ made power supply which is able to operate between 1-40 W for the proposed reactor and electrode geometry as shown in Figure 17. To monitor the vacuum level of the plasma media, a capacitance manometer (Baratron®) and its readout unit is employed. The monomer NIPAM (97%) was purchased from Aldrich (Germany).

Polymerization reactions are carried out under identical conditions. Argon (Ar) is used as the working gas during plasma process, and its glow is maintained over the surface of crystalline monomer of NIPAM, (which is recrystallized from deionized water under vacuum just before plasma discharge).

The pressure in the reactor is altered precisely on wish by changing flow rate of Ar gas by means of MKS™ mass flow meter and its 4 channel MKS™ controller unit. It is known that the structural and chemical characteristics of plasma processed final product are strongly affected by many operational parameters of plasma. One of the most important parameters is the geometry which accounts the shape and nature of the material of both reactors inner

surfaces and electrodes, and amount (size) of the substrate (monomer) and its position with respect to electrode. To achieve desired consistent standard properties for the final product the same glass reactor is used and substrate is placed on the same location in the reactor.

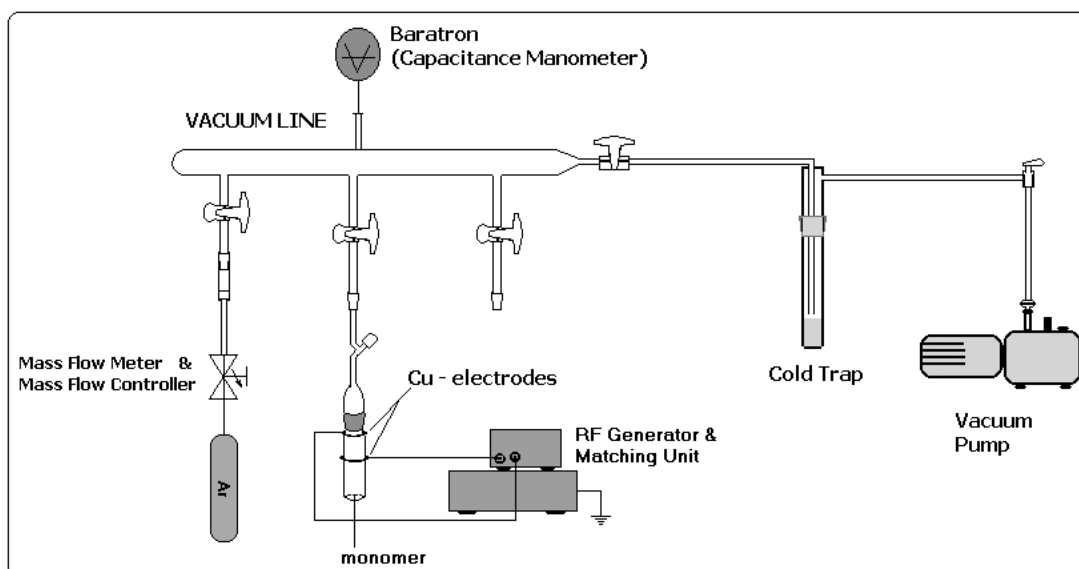


Figure 17 Low temperature (RF) plasma discharge system used in the monomer conversion experiments.

2.1.2 Reactor Design

In the present study most of the experiments for the plasma initiated polymerization processes are carried out in a homemade external electrode plasma system under low pressure, and at ambient conditions. Further details of the electrode and reactor geometry can be found in the following chapter.

After designing the reactor with optimized geometry, we intend to study dependence of conversion rate of monomer upon power delivered and duration of discharge.

2.1.3 Plasma Parameters for Monomer Conversion Experiments

By keeping reactor geometry, the amount (0.5 g for each charge) of the monomer, the regime of the flow rate and pressure in discharge media constant for all sets of experiments, we tried to determine the change in monomer conversions as well as its dependence on plasma power and plasma discharge time. To achieve this, one of these two parameters is changed while the other one is kept constant. For these, two different plasma discharge durations times (1hr and 5 hrs), and two different RF powers (20W and 40W) are selected.

Moving from some recorded plasma parameters (such as vacuum maintained throughout the plasma discharge) we aimed to have some idea about the physical changes on the sample surface during the plasma discharge.

2.1.4 Procedure Followed for the Determination of Percent Conversions

For a detailed investigation of plasma initiated polymerization of NIPAM in the solid (crystalline) state, we concentrated firstly on the examination of various experimental parameters that possibly are the most effective on evaluation of monomer conversion rate. These effects, which may arise either from the conditions throughout plasma processing step or they may be due to some complications of isolation method after plasma process. Throughout the study % weight conversions of monomer to polymer were measured after utilization of some dissolution and extraction methods successively. After each plasma treatment a mixture of unreacted monomer, linear and crosslinked polymer mixture is obtained. These fractions are then isolated by means of physical and wet chemical techniques such as filtration, water-ether heterogen extraction medium applied step by step as schematized in Figure 18. In this multi step isolation method firstly, insoluble

crosslinked polymer is separated by filtration from aqueous solution of raw product mixture. Secondly, unreacted monomer is successively extracted from diethyl ether-water heterogeneous system. Finally the amounts of unreacted monomer, linear polymer and crosslinked polymer contents are determined both gravimetrically and volumetrically.

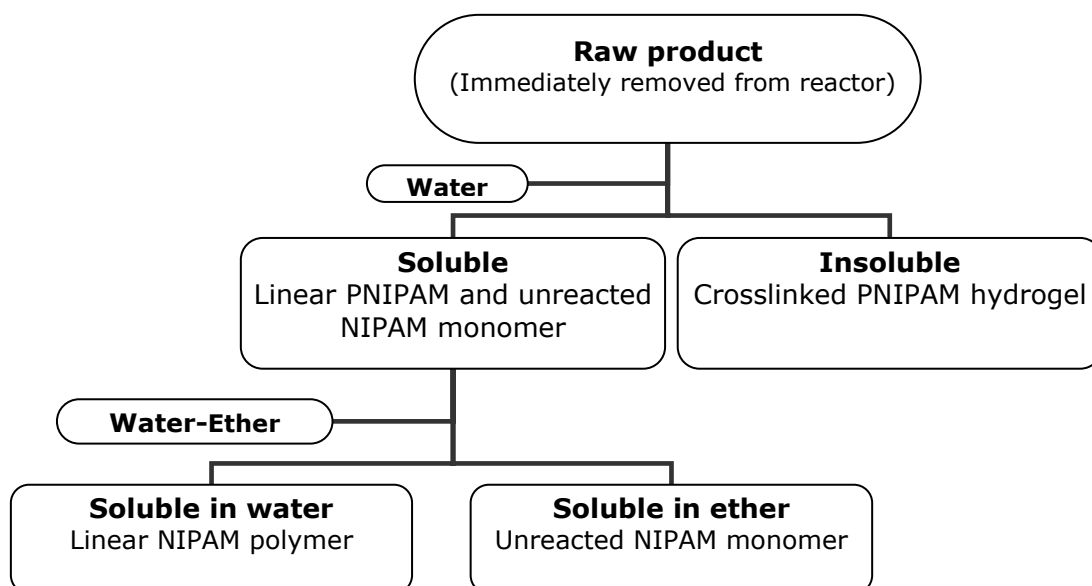


Figure 18 Block diagram of isolation procedure for the solid state plasma initiated PNIPAM.

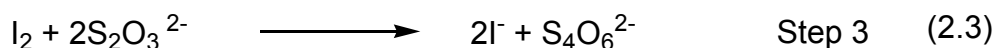
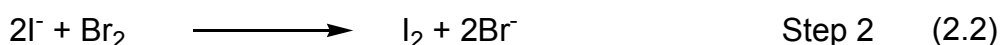
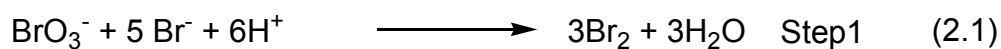
After isolation, evaporation and desiccation of each component, all constituents are dried under reduced pressure to constant weight then % weight values are calculated gravimetrically for all components of raw product such as, monomer, linear polymer and crosslinked polymer separately. In addition, monomer contents are determined by volumetric (bromide—bromate titration) method, quantitatively.

2.1.5 Bromide—Bromate Titration (Volumetric) Method

There are four common methods of determining carbon-carbon unsaturation: bromination; catalytic hydrogenation; addition of mercuric salts; and iodine

number. In this study quantitative analysis of vinylic monomer, NIPAM, depends on the basis of the bromination of the double bond. There are various bromination reagents commonly used for determining unsaturation (such as free bromine in a solvent, bromine generated from a bromide—bromate reagent using acid, pyridine sulfate dibromide reagent, and bromine generated electrically [183, 184]).

To avoid volatilization problems in the use of free bromine, stable bromate—bromide solution (0.1N) is used, and the bromine is generated by adding acid at the time of analysis after mixing of all other reagents with sample solution and waited for overnight. The reaction is catalyzed with mercuric sulfate (0.2N). Quantization was done by iodometric (back) titration of the excess Br_2 remaining after reaction with NIPAM. The addition reaction is found to proceed quantitatively without side reactions with good reproducibility. Reactions of Bromide—Bromate titration method are as follows.



2.1.6 Fourier Transform Infrared (FTIR) Analysis

FTIR analyses of components isolated from the final product mixture of solid state polymerized NIPAM are performed by BRUKER Vertex 70. A careful sampling is done from the highly polymerized surface and partially or non-polymerized inner layers of the plasma treated NIPAM. Spectra belonging to pure monomer, pure polymer and the mixture of them are obtained and plasma effect is fully elucidated.

2.1.7 Nuclear Magnetic Resonance (NMR) Analysis

In this study ^{13}C and ^1H -NMR spectra are recorded on a BRUKER Spectrospin Avance DPX400 Ultrashield, (^{13}C : 100 MHz and ^1H : 400 MHz) spectrometer. In all sample preparations for NMR study, D_2O is used as the solvent. Polymer formation at solid state under plasma conditions is confirmed by ^{13}C and ^1H -NMR spectra.

2.1.8 Differential Scanning Calorimetric (DSC) Analysis of PNIPAM Hydrogels

The volume phase transition temperature (VPTT) or lower critical solution temperature (LCST) measurements of PNIPAM hydrogels were determined by using TA-Modulated DSC V4.1C DuPont 2000. All hydrogels were immersed into deionized water at room temperature and allowed to swell for at least 30 mins to reach a certain swelling level. The thermal analyses were performed from 25 to 40°C at a heating/cooling rate of 2°C/min on the swollen hydrogels under a nitrogen atmosphere. Deionized water was used as the reference in the DSC measurement.

2.1.9 Scanning Electron Microscopy (SEM) Studies

The visual investigation of surface morphology of crystalline monomer before and after plasma treatment is done by using SEM micrograms which are taken on STEREOSCAN S4-10 Electron Microscope. Samples are prepared in three sets i.e., recrystallized monomer with no plasma treatment, a sample after 30W-1hr RF discharge treatment, and solid state plasma polymerized linear PNIPAM (pre-concentrated on holder drop by drop from its isolated solution). Specimens were fixed to the brass holders and coated with gold using a coating machine prior to the SEM examination.

2.2 Studies of Crystallinity and its Effects on Polymerization in Solid State

2.2.1 Vacuum Plasma System for Surface Modification of Polymer Materials

TPVD-300/PG is a fully automated plasma surface modification system developed and manufactured in cooperation with VAKSİS (Vakum Sistemleri) Bilkent University Campus, Cyber Park B Blok No:220 (former name was Teknoplasma A.Ş.).

This system was built in the scope of BAP-01-03-DPT 2003K120920-14 numbered project in 3 year continuum. After installation of the TPVD 300/PG some diagnostic studies had done for optimization of plasma operation parameters for several months. The components of this highly capable plasma processing system are as follows (Figure 19 and Figure 20).

- Vacuum Deposition Chamber, made of 304 grade stainless steel (SS), with set of lining SS view ports, gas connections and inlets.
- Gas flow control unit (AERA ROD-4) with two mass flow controllers (20 sccm), two more ports are available for different gas supplies.
- Rotary Mechanical Pump, VARIAN DS402 1Ph, 17.4 m³/hr pumping speed, with fore line roughing trap and oil exhaust filter.
- RF power supply (CESAR™ 136 Generator) and its impedance match (Dressler Variomatch) box, convertible to microwave (MW) power by top plate substitution.
- Multi-gauge controller unit (Varian®) and its RS232 Board is a terminal for operating whole plasma system.
- RF or MW Powered cathode (3 inch, SS and water cooled), earthed anode (3 inch and water cooled) and shutter.
- System equipped with 3-Position Pneumatic Gate Valve (VAT® Products), pneumatic right angle block valve (Varian®), pneumatic

- actuated bellow valves with micro switch, solenoid valves, and servo motor, and switch sensors.
- Capacitance Manometer (Baratron[®], MKS Absolute pressure transducers) for vacuum monitoring.
- PC-based and windows-based A&C hardware and software equipped with 15" LCD monitor (VESTEL)
- Thermocouple unit for measuring temperature of anode plate with RS232 Connection.

In the present study TPVD-300/PG is used for plasma surface treatments of prepared NIPAM monomer pellets in crystalline state. After treatment by plasma, crystallographic characterizations were performed by XRD Spectroscopy for these samples.



Figure 19 TPVD-300/PG System is in the course of diagnostic tests.

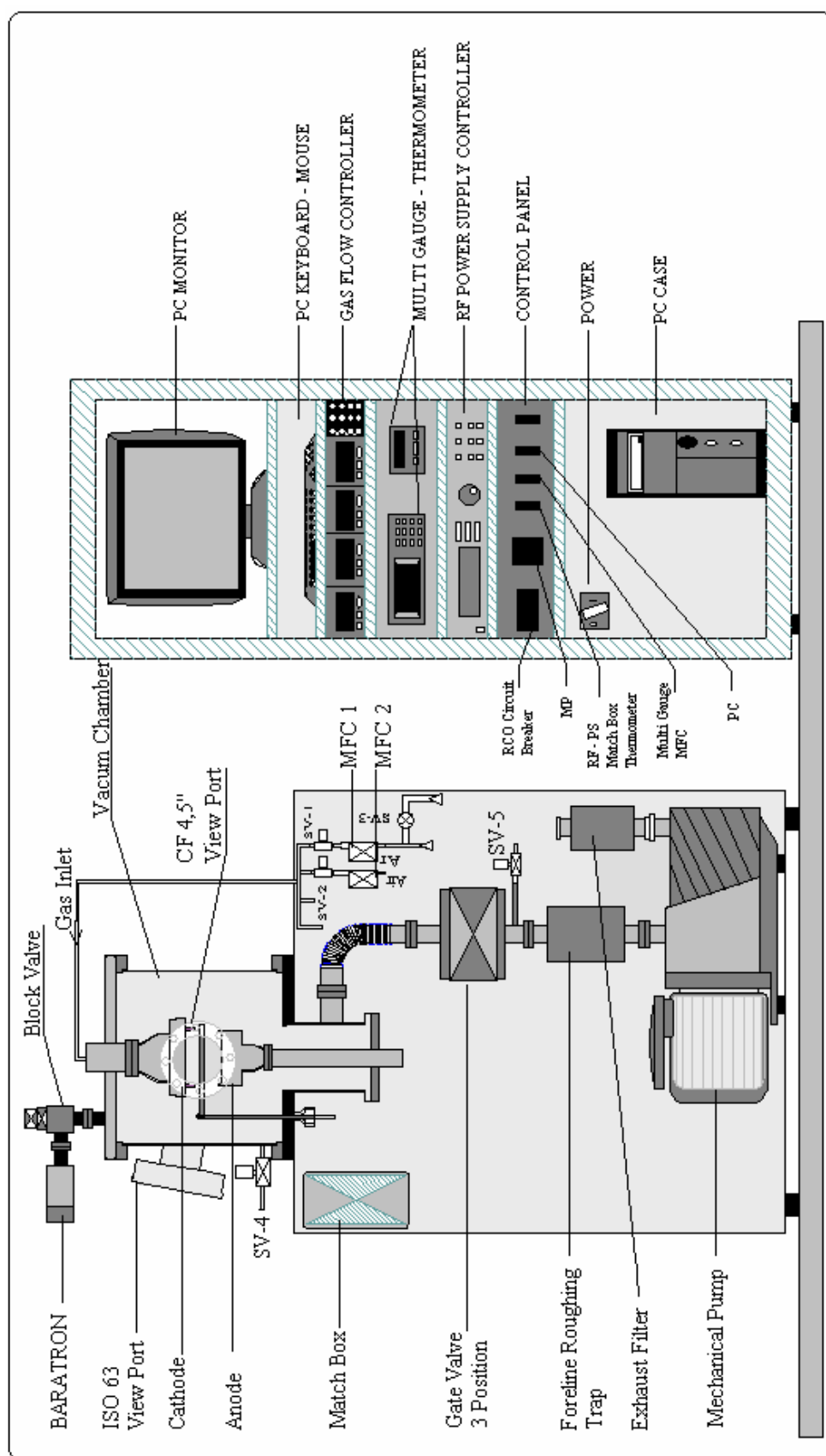


Figure 20 General diagram of vacuum plasma system for surface modification of polymer materials (TPVD300/PG).

2.2.2 X-ray Diffraction (XRD) Studies

X-ray patterns (XRD) were taken by Rigaku Miniflex Diffractometer with an CuK_{α} (30 kV, 10 mA, $\lambda=1.54051 \text{ \AA}$) radiation. Scanning was performed between $5^{\circ} < 2\theta < 60^{\circ}$ with $1^{\circ}\text{C}/\text{min}$ scan rate.

2.2.2.1 X-ray Experiments

For elucidation of plasma effects on surface of the crystalline solid-state monomer, X-ray technique is employed. For these experiments after recrystallization from water, pellets of NIPAM monomer is prepared with KBr Pellet Die Kit. Samples are prepared in two parallel sets for correspondence of data obtained. Plasma treatments of these identical pellets are performed under identical parameters by TPVD-300/PG plasma processing system. After loading both pellets, the system is evacuated to a desired base pressure of $1\text{E-}3$ Torr by its integrated mechanical pump. Then Ar is fed into system with the rate of 2 sccm until reaching a $2.7\text{E-}2$ Torr vacuum level. After 30W RF plasma ignition the system is sustained at $2.9\text{E-}2$ Torr for 30 minutes. Temperature is kept constant throughout plasma treatment at 19°C . Sets of pellet surfaces are then immediately investigated by XRD method, and post plasma effects on the surface are also studied for the same samples kept under predetermined conditions of opened to air and closed glass vial at 30°C .

2.3 Studies of Radicalic Phenomenon by Electron Paramagnetic Resonance (EPR)

2.3.1 Plasma Setup for EPR Studies

The experimental set-up for the plasma irradiation and EPR spectral measurement is schematically shown step by step in Figure 21. Because of its inert character, Ar is used as working gas (electron source) and to sustain pressure during plasma discharge process. All plasma processes were

performed for 10-15 minutes. Then the EPR signal was taken in the quartz part of the tube at various temperatures for each sample.

2.3.2 EPR Measurements

A Bruker ELEXSYS E 580 FT-EPR Spectrometer with 10" magnet interfaced to a PC computer was used to analyze data as well as coordinating all the parameters for acquisition of spectra.

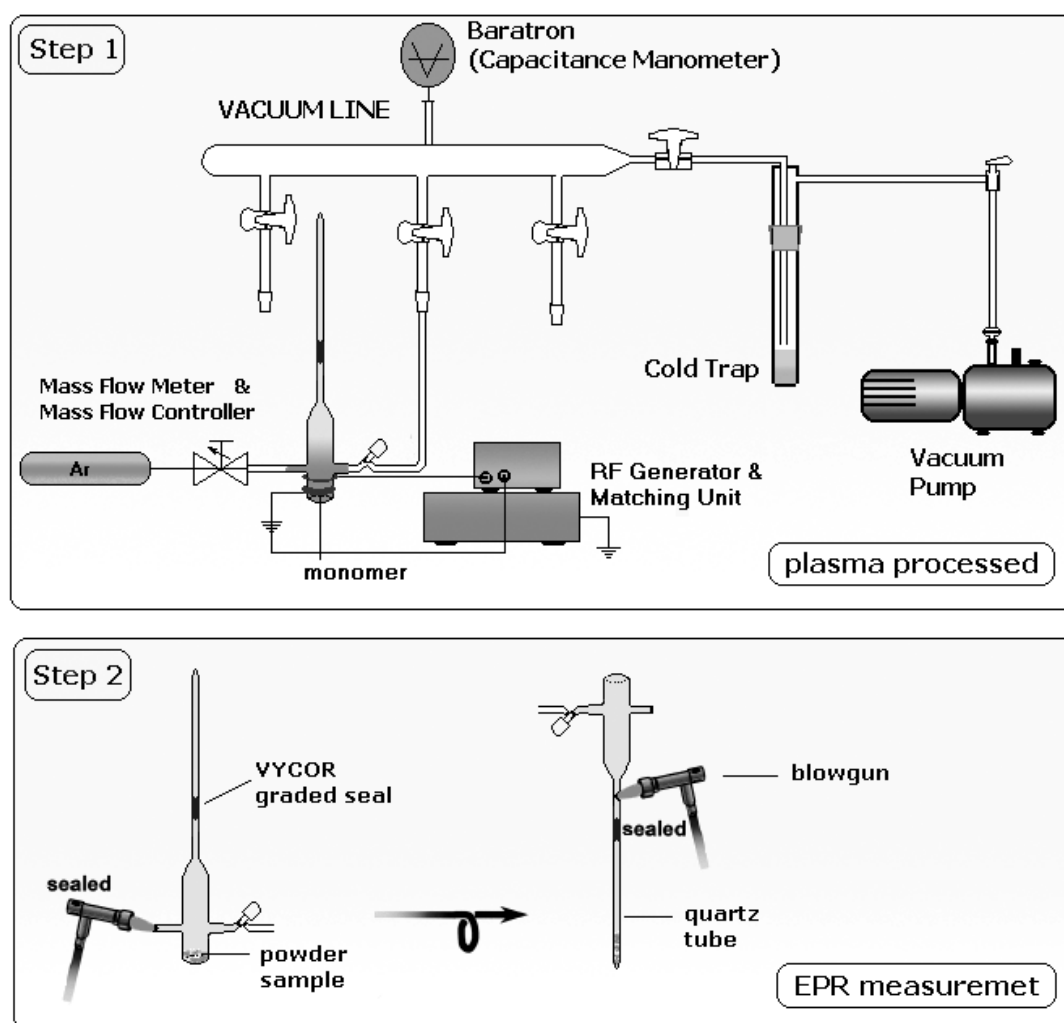


Figure 21 Schematic representations of plasma irradiation and ESR spectral measurement.

For further calculations the first order spectra are doubly integrated by help of integrated computer software to give peak areas and hence radical concentrations. A 4-Amino TEMPO with concentration of $2.97\text{E-}05$ mol/L standard reference sample with a radical concentration of $1.79\text{E+}19$ spins/cm was used to convert to peak areas to radical concentrations.

The EPR spectra of plasma processed NIPAM at various temperatures were recorded for kinetic and mechanistic studies. Spectrometer operated in the X-band region (9.8 GHz) in the course of scanning. The parameters which are used throughout the studies are given in Table 4.

Table 4 EPR Parameters for PNIPAM radical monitoring.

No. of Scans :	5
Scan Temperature (K)	300 approx.
Field Set (G):	3510.25
Sweep width (G):	300
Sampling time (s):	0.08192
Field Mod. Amplitude:	0.0001
Microwave Freq (Hz):	9.8 GHz
Microwave Power (W):	0.00002 (40dB)
Receiver Gain:	80
Rec. Time Const. (s):	0.08192

2.3.3 Reactor Design for EPR Studies

Specially designed glassworks were used for EPR Spectrometric analysis. In the first attempts to obtain EPR spectra of empty quartz tube after plasma processing under vacuum a strong first derivative singlet is observed which is resulted from Ar plasma in vacuum. After opening this sealed empty tube to air, existing singlet absorption peak is turned to a well-defined anisotropic

peroxide radical signal (Figure 22). Furthermore this intense singlet interferes with the expected signal of growing PNIPAM radical by overlapping with it.

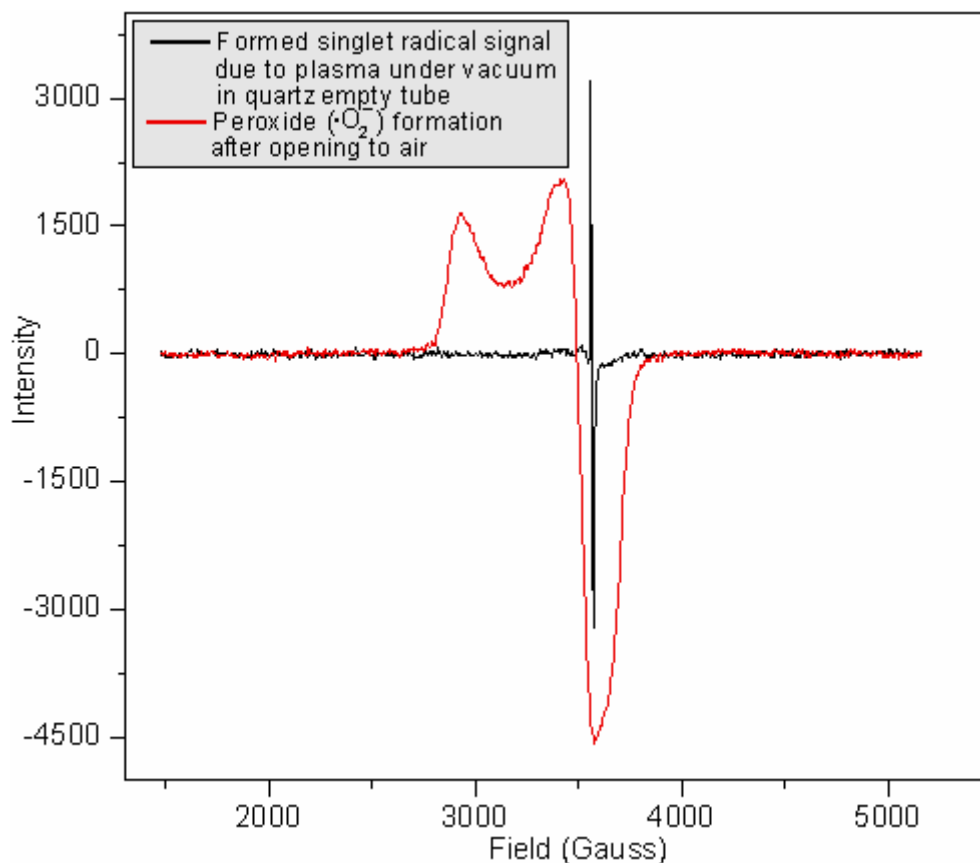


Figure 22 Plasma effect on quartz under vacuum and under open air conditions.

To get rid of this possible plasma adverse effect on quartz EPR glass, a special reactor is designed as shown in Figure 23. By the given geometry and dimensions of glass-made reactor the crystalline monomer is polymerized in the lower part of the Pyrex[®] reactor and then sample is drop into the quartz tube by keeping it upside down. Finally filled quartz tube is sealed under vacuum by use of a blowgun. Thus, the lower end part of the quartz tube fixed in the cavity of the EPR is prevented from plasma contact during sample preparation.

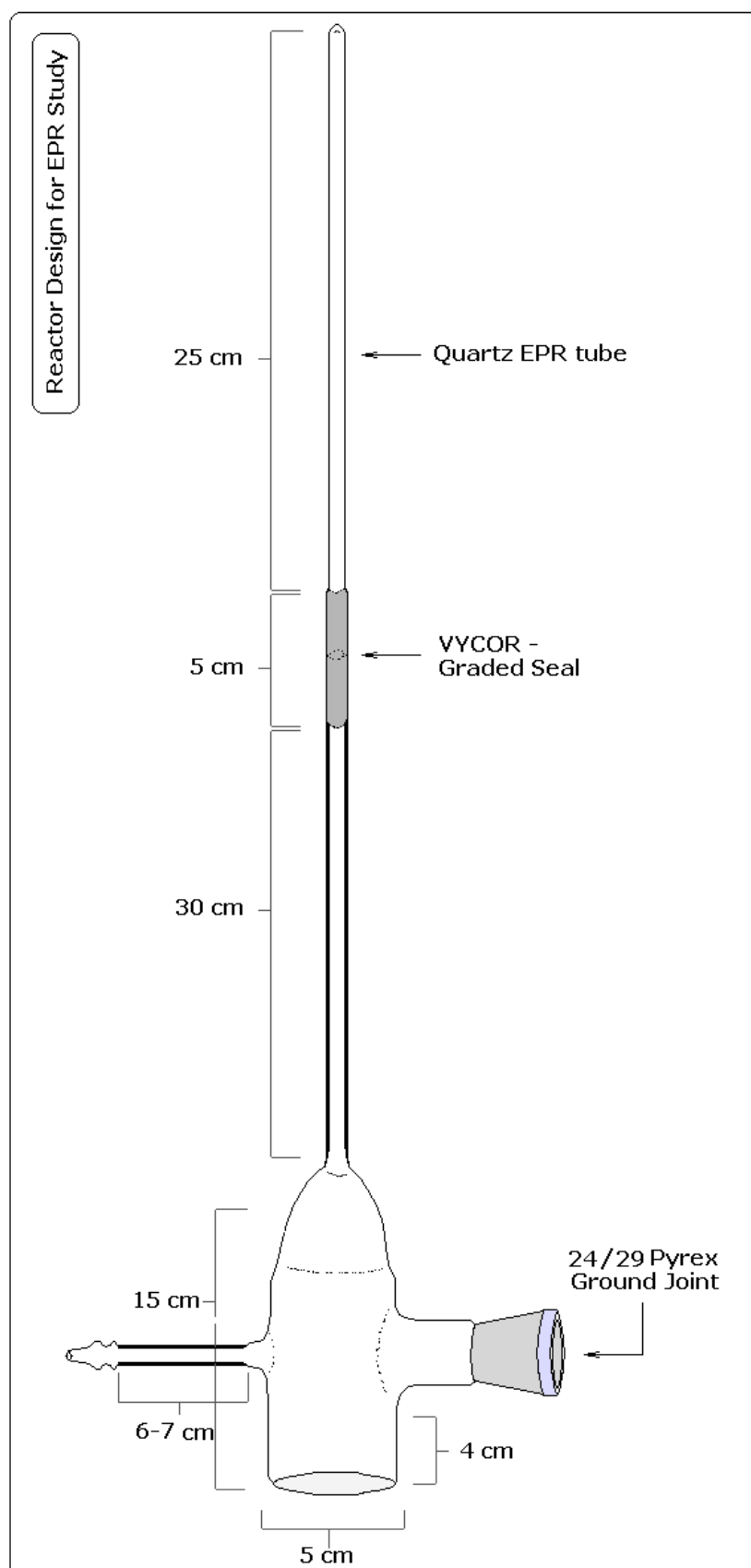


Figure 23 Designed plasma polymerization glassware for EPR studies.

CHAPTER 3

RESULTS AND DISCUSSION

Discussions of this thesis will be presented in three main subtitles. Plasma studies including optimization of process parameters, characterization of isolated species (i.e., monomer, linear polymer, and crosslinked polymer) obtained from raw product mixture left behind plasma initiated solid state polymerization of NIPAM, are going to be examined in the first part. In this part monomer percent conversion studies *in-source* polymerization will also be discussed.

In the second part, solid state plasma-initiated polymerization results will be presented and discussed from mechanistic point of view. The data obtained through XRD studies which are mainly used to explain plasma polymerization of NIPAM in solid (crystalline) state will also be presented in this part, therein.

The last part examines the results of EPR studies, which are used to clarify the mechanistic aspects of post irradiation polymerization reactions of NIPAM, and these data will be used for calculation of various kinetic parameters.

3.1 Plasma Processing of NIPAM — Chemical and Microscopic Characterization of Final Products

3.1.1 Geometric Optimizations of Plasma Reactor and Electrodes

In laboratory applications of plasma chemistry external electrode reactors using ring electrodes in most cases or an external coil around reactor tube from glass or silica, are usually preferred.

At onset of the experiments, it is aimed to have the most feasible type of reactor with proper geometrical configuration for the solid state polymerization of NIPAM. Firstly a tubular glass (borosilicate-Pyrex[®]) reactor (with the dimensions given in Figure 24-a) was used. After plasma processing at certain applied conditions (i.e., 30W, 15 min, 0.2 Torr, Ar), some undesirable issues are revealed, such as; after a certain time of plasma ignition, it was observed that the NIPAM crystals (mp: 63°C approx.) melted, and degraded subsequently during the discharge process. The final product was highly degraded throughout the reactor especially at the inner reactor sites of the wall encircled by electrode plates. It was almost impossible to dissolve that residual product within any solvent tested to facilitate its removal from the reactor. From this first phase of experiments, it was understood that a new reactor and electrode geometry was needed to provide milder conditions avoiding degradation during the plasma process.

The new reactor designed is depicted in Figure 24-b, which was proper to overcome all the mentioned problems. During the new reactor use, (a) crystalline NIPAM was laid on the bottom of the reactor (to keep monomer far from the local heated zone of the electrodes, situated about 6 cm distant from the monomer surface), and (b) a tiny ring electrode is used preferably for the larger volume discharge reactor (instead of previous larger plate electrode which makes the plasma medium more energetic and destructive for narrower discharge cavity). Another advantage obtained by the new design was the enlargement of the ground joint dimensions (from 14/35 to 40/40), which allows much more comfortable removal of samples from the reactor.

In plasma applications, the rule of thumb is that the plasma discharge parameters should be altered and optimized by looking for the most favorable and eligible patterns to achieve product in desired specifications, i.e., high conversion rates with low degradative fragmentation.

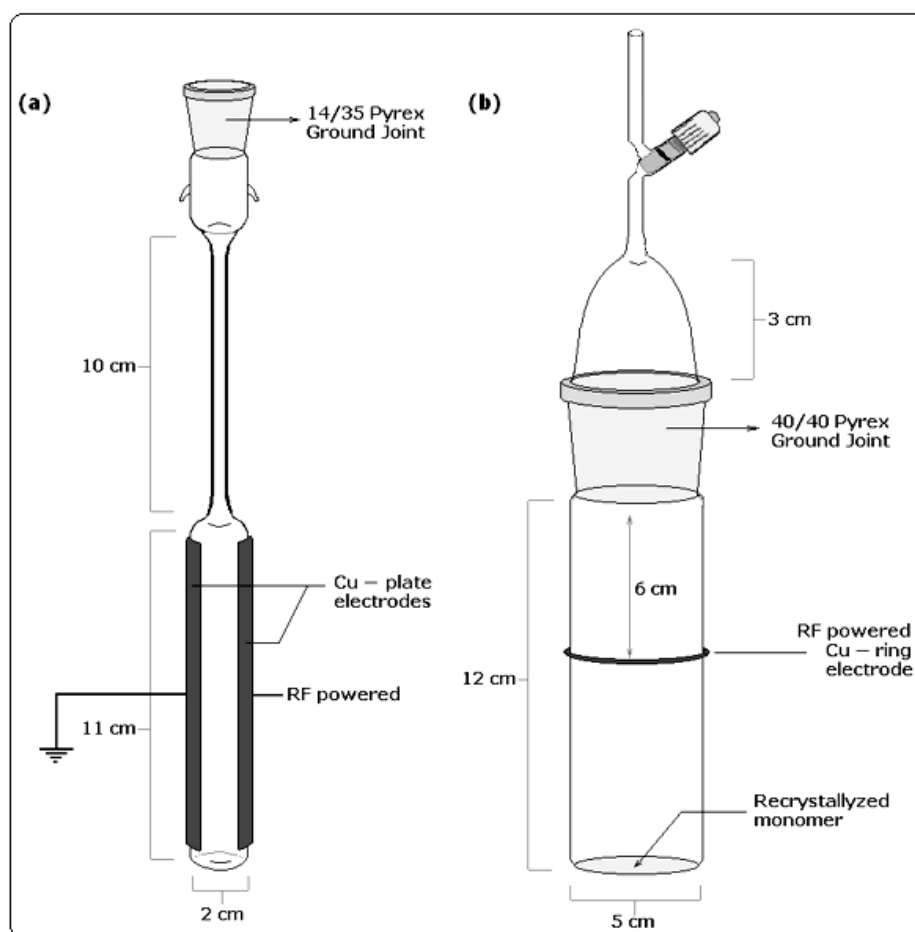


Figure 24 Designed external electrode reactors for the plasma initiated polymerization of NIPAM.

3.1.2 Effects of Plasma Parameters on Monomer Conversion

It is widely known that in a plasma reactor the physical and chemical characteristics of a final product (i.e., polymer) are strongly affected by many parameters. In the case of solid state polymerization, the most important parameters are the ones related to the inter-phases between plasma atmosphere and the polymerizing monomer surface for most of the time. During these experiments average values of plasma discharge parameters selected (e.g., flow rate of Ar and vacuum level) and their changes are followed and noted, with respect to the discharge time; which are all

tabulated in Table 5. In these groups of experiments, both the argon gas flow rate and the level of vacuum sustained in the reactor are consistently kept constant within experimental limits for both 1 hour and 5 hours discharges.

Table 5 Plasma discharge parameters for several discharge periods.

	Discharge Time (min)	Ar flow rate (sccm*)	Vacuum (Torr)
1hr discharge	0	3,0317	0,3550
	8	3,0143	0,3181
	15	3,0071	0,2936
	30	3,0157	0,2847
	45	3,1700	0,2794
	60	3,1783	0,2776
	Discharge Time (min)	Ar flow rate (sccm*)	Vacuum (Torr)
5 hrs discharge	0	3,0933	0,3480
	15	3,0433	0,3110
	30	3,1967	0,2860
	70	3,2100	0,2773
	120	3,2600	0,2787
	150	3,2650	0,2787
	180	3,2513	0,2803
	240	3,3167	0,2760
	300	3,3500	0,2777
*sccm: standard cubic centimeter per minute			

For every single plasma discharge experiment, an effort was paid to keep pressure change constant by making alterations in mass flow controller unit (Figure 25). In all discharge experiments, the pressure in the glass reactor decreased initially after ignition of plasma within the first hour period, and then it is stabilized at the level of 0.278 ± 0.002 Torr. This general trend can be attributed to the decrease in the rate of NIPAM sublimation by increasing the thickness of crosslinked layer produced on the surface of monomer, as the time goes on. At the end of this period, a crosslinked film of PNIPAM on the surface of crystals obviously has reached to a certain thickness, which prevents further monomer sublimation any more.

To keep the pressure at the selected level for each discharge, regulations were made in the flow rate of Ar feeding into the vacuum line, at all times. Some detailed interactions expected between the NIPAM surface and the plasma will be discussed in the forthcoming parts of this chapter.

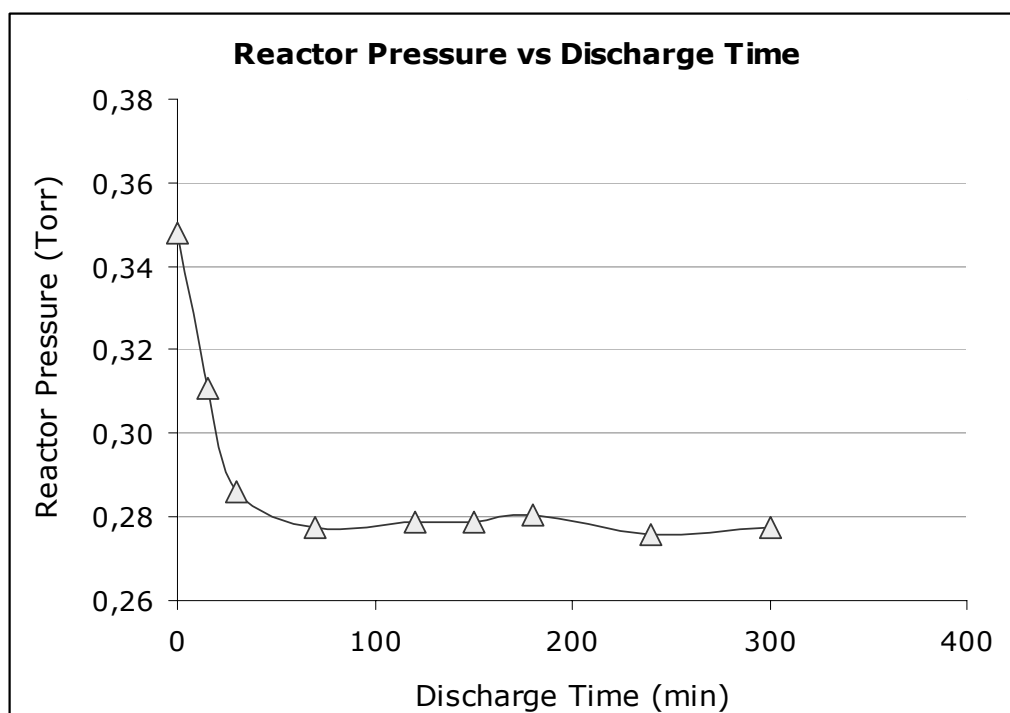


Figure 25 Pressure change (average of the values for all discharges is given) in the glass reactor with plasma discharge time.

3.1.3 Some Complications Involved in Isolation Steps

In all sets of the experiments, after plasma treatment of NIPAM, a reasonable difference in % conversion rates of monomer which are obtained from gravimetric and volumetric methods was observed. This is the case previously encountered and reported by O'Donnell et al [185]. These differences probably arise from continuation of the polymerization reaction during dissolution in extraction stage to some extent. As a consequence, the use of gravimetric method alone is not sufficient for precise determination of monomer conversion.

In this part of the study, referred to as *in-source polymerization*, monomer crystals are processed in plasma at several selected different plasma powers and plasma durations. Percent conversion rates of monomer to polymer given in terms of % loss of $C=C$ are plotted against time of plasma discharge (1hr-3h-5hr) for 20 and 40 W plasma conditions, are depicted in Figure 26. Additionally, the composition data of raw product mixtures in percent weight, obtained from both gravimetric and volumetric method are tabulated in Table 6.

The differences between gravimetric and volumetric data can be attributed to the formation of very low molecular weight oligomeric units (dimers, trimers, tetramers, etc.) at high rates under plasma glow discharge. Since the oligomeric content is very low-molecular weight (similar to monomer), it cannot be isolated from monomer by extraction method so that this portion is confined in monomer content. A big portion of this oligomeric content still remains in the monomer residue even after performing of repeatedly extracting process. Thus, a more precise determination method is needed for unreacted monomer. Since direct quantitative determination of vinyl group of monomer is possible by bromide—bromate titration (Volumetric) method, the amount of unreacted monomer can be found precisely.

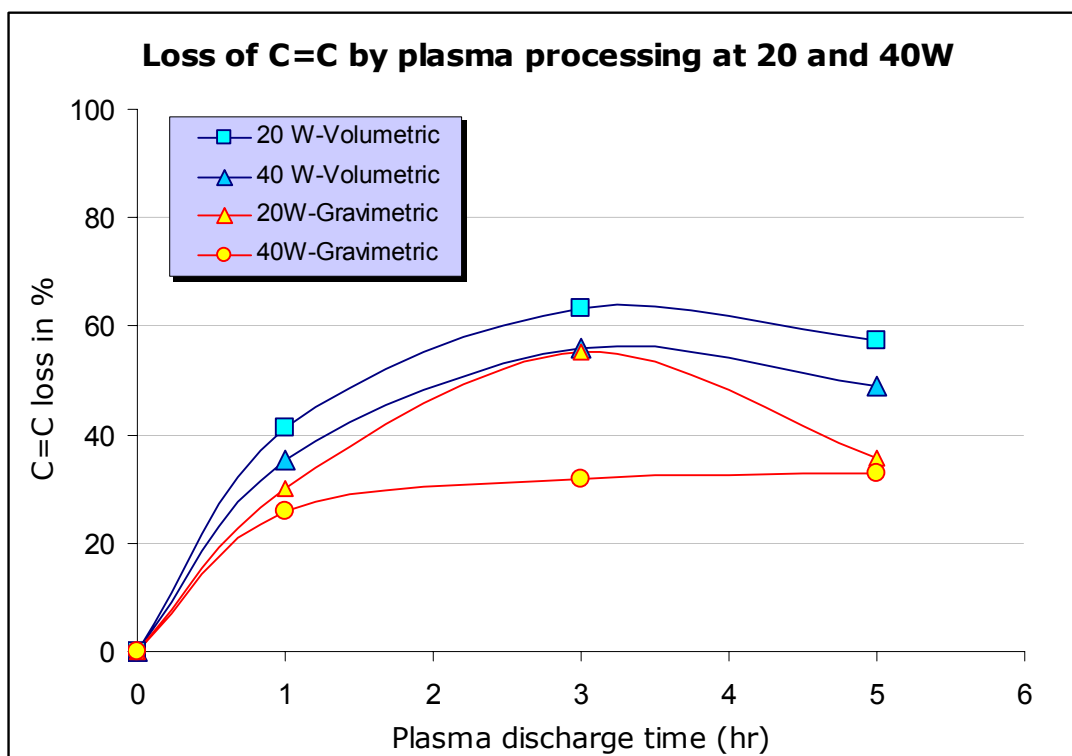


Figure 26 Gravimetric and volumetric ($C = C$) determination of monomer deprivations in % by plasma discharges at 20 and 40 W.

Additionally, the monomer conversions measured in both ways are found to increase to some extent and then slightly decrease along increasing plasma discharge period. The highest conversion rates are reached in 3 hour discharge time. Further plasma processing may cause decrease in conversion due to degradative fragmentation. There is a fluctuation for one of 40W processed sample for 3 hrs. Except this error all data are well-matched with each other.

At high plasma discharge watts, i.e. 40W, established powerful plasmon atmosphere can result in high degradation rates leading to large scale drop-offs in molecular weight of polymerized portions, especially at the surfaces in contact with the plasma. This may decrease in amount of linear polymer content in regions nearby surface in high-watt plasma experiments.

Table 6 Percent compositions of obtained raw product mixtures for the samples treated at 20W and 40W RF plasma.

Power (W)	Percent weight (%)				
	Discharge Time (hr)	Linear Polymer	Crosslinked Polymer	Unreacted Monomer (from volumetric method)	Oligomer
20	1	16	4	59	11
	3	19	4	37	17
	5	20	6	43	22
40	1	13	7	65	9
	3	22	6	44	14
	5	23	8	51	16

According to Table 6, linear and crosslinked polymer contents increase with increasing plasma discharge time. Oligomer contents are calculated from difference between unreacted monomer percentages obtained by volumetric and gravimetric methods. Oligomer formation rate is found to be higher for the low plasma power treatments. This can be attributed to high loss of degradative fragmentations of oligomeric species by Ar sweep in high-power plasma treatments.

3.1.4 Product Recognition after Plasma Processing and Isolation

3.1.4.1 FTIR Results

Figure 28 shows the FTIR spectra of the sample obtained by careful sampling from the polymerized surface layer after plasma treatment. Gradual conversion of NIPAM from monomer to its polymer form is presented in Figure 29 separately. From the interpretation of spectrum of isolated PNIPAM, the band of N—H stretching vibration is observed near 3313 cm^{-1} as typically in solid samples of secondary amides which exist mainly in the *s-trans* conformation (Figure 27). Broadening is attributed to intermolecular

hydrogen bonding. In this region a weak absorption band is also seen at 3078 cm^{-1} recognized as amide II band overtone.

All amides show a $\text{C}=\text{O}$ stretching band called as the *amide I band* which is observed at 1651 cm^{-1} in our monomer spectrum. The band seen at a frequency of 1547 cm^{-1} is assigned to $\text{N}-\text{H}$ stretching of secondary amides which is also another common absorption band known as *amide II band*. This band results from the interaction between $\text{N}-\text{H}$ bending (%60) and $\text{C}-\text{N}$ stretching (%40) of the $\text{C}-\text{N}-\text{H}$ group. Figure 29 shows *amide I* and *amide II* bands are protected in the spectrum of polymer. From this point one can insist that secondary amide structure is retained in the structure of isolated polymer.

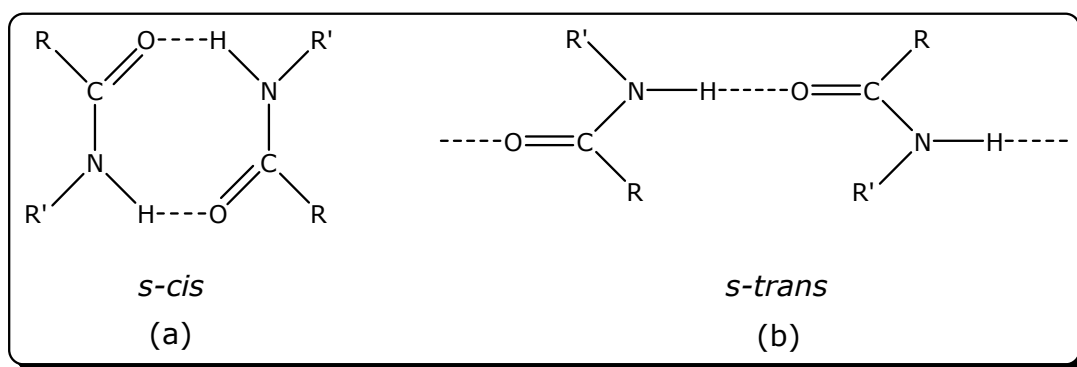


Figure 27 *s-cis* conformation is favorable for dimers with less steric hindrance (a), while *s-trans* conformation is common in case of polymers having more steric restrictions (b) [186].

In the range generally called as *aliphatic C—H stretching region* the absorption bands at 2878 cm^{-1} ($-\text{CH}_3$ symmetric stretching), 2935 cm^{-1} (asymmetric $-\text{CH}_2-$) and 2974 cm^{-1} ($-\text{CH}_3$ asymmetrical stretching) are observed successively as expected. Additionally the two moderate absorption bands at 1369 cm^{-1} and 1389 cm^{-1} are attributed to deformation of the two methyl groups on isopropyl ($-\text{CH}(\text{CH}_3)_2$) functionality. In light of

these findings isopropyl structure in monomer which is believed to contribute to the thermo responsive behavior of the polymer is retained apparently in the structure of plasma induced solid state polymerized PNIPAM [186]. From the comparison spectra in Figure 29, it can be observed the C=C bond absorption band near 1620 cm^{-1} in the spectrum of pure monomer diminished in the course of monomer conversion to polymer, and disappeared completely in pure polymer spectrum. Likewise, strong bands at 1411 cm^{-1} , at 991 cm^{-1} with its strong overtone at 964 cm^{-1} and another strong band which occurs at 918 cm^{-1} are weakened gradually from monomer to polymer. All of these absorption bands which are distinctive for vinyl groups are shaded in Figure 29. This regular transformation makes more clear the point of radicalic polymerization mechanism following the path of C=C vinyl bond cleavage somehow.

One of the last two striking vibration bands is the C—N stretching band of amide as a moderately intense peak near 1450 cm^{-1} which is overlapped and broadened by methylene ($\text{—CH}_2\text{—}$) deformations of the polymer chain. The other is a broad strong band in $650\text{--}800\text{ cm}^{-1}$ region results from out-of-plane N—H bending (or wagging) in secondary amide monomer structure. This band loses its intensity and broadens gradually in the polymer spectrum as expected.

As a consequence, in the course of solid state plasma initiated polymerization of NIPAM there is no sensible loss of chemical functionality due to energetic radiation in the most part of the final product. This may be a result of the protection of inner layers containing linear form of PNIPAM from the destructive fragmentation under energetic plasma discharge owing to highly crosslinked layer formed on samples surface. The low penetration nature of plasma plays another important role in the preservation of inner layers. From these spectral evidences one can conclude that, the thermo-responsive behavior is most probably maintained in PNIPAM polymer form which is polymerized by plasma initiation in the solid state.

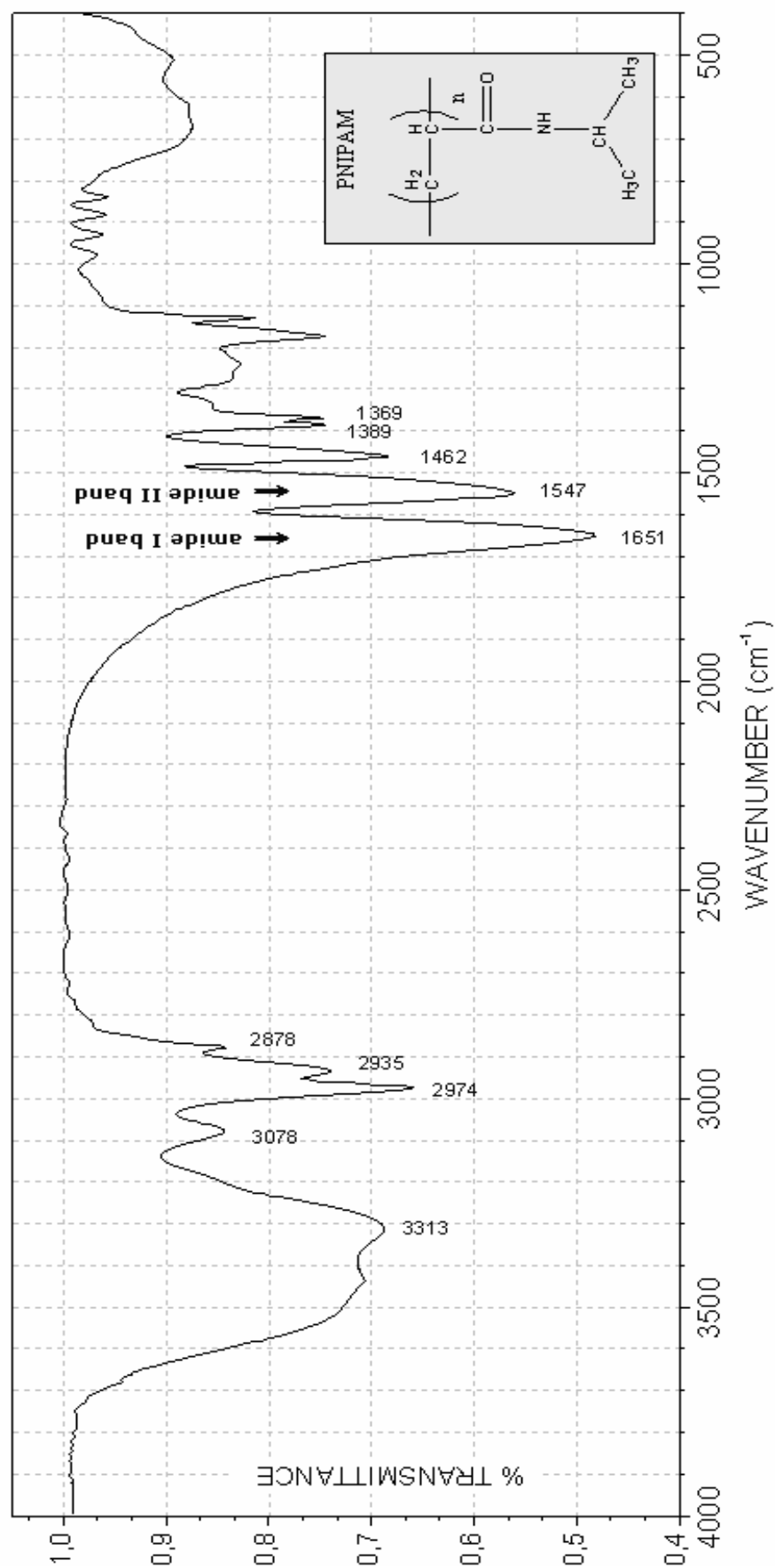


Figure 28 FTIR spectrum of PNIPAM polymerized in solid state by plasma initiation.

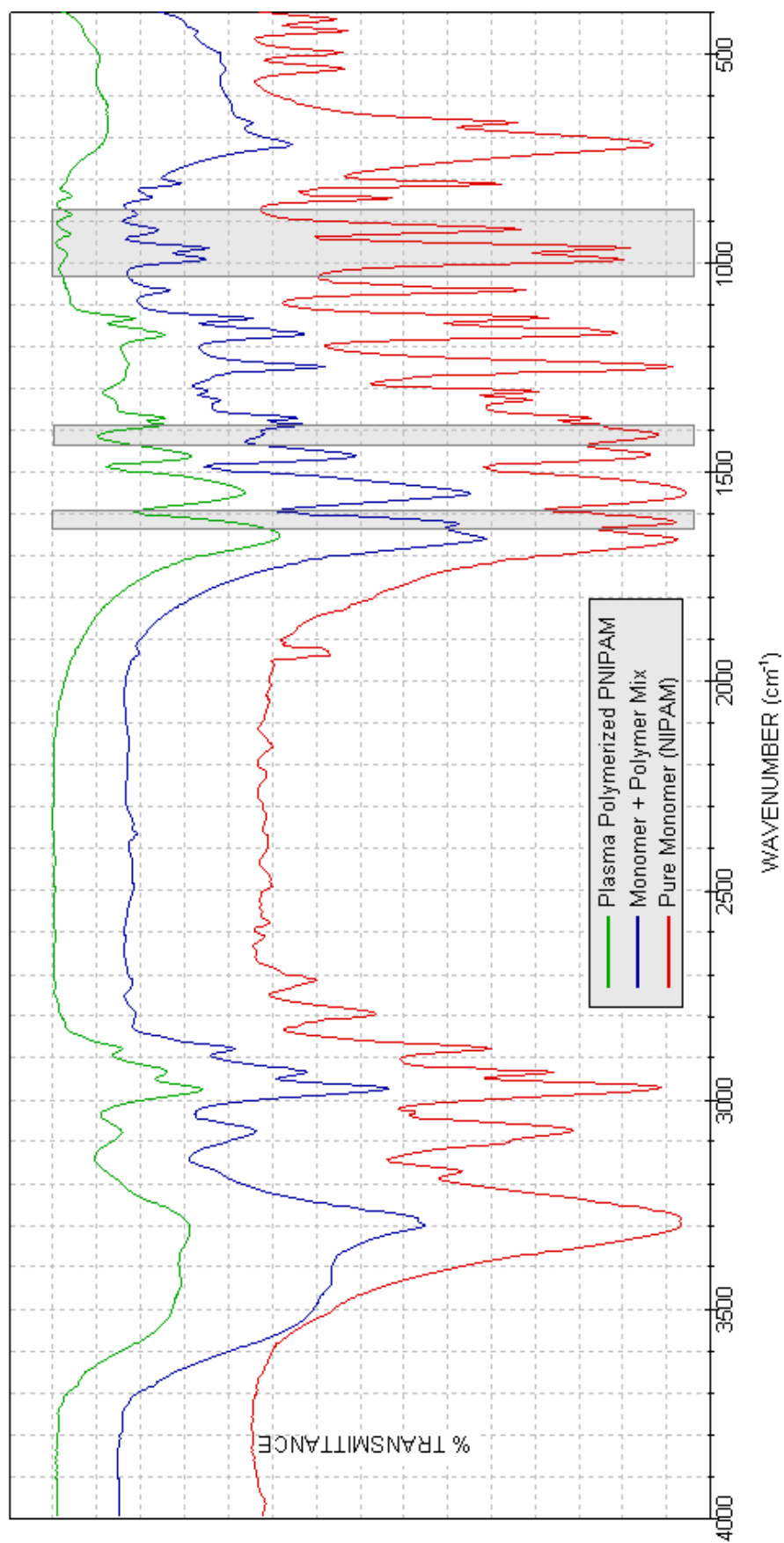


Figure 29 FTIR spectra of NIPAM monomer (sampled from inner parts), PNIPAM polymer (sampled from the surface) and their mixture.

3.1.4.2 Structure Elucidation by ^{13}C and ^1H NMR Analysis

^{13}C and ^1H spectra of plasma polymerized PNIPAM are given in Figure 30 (a, b), and the peak assignments are also present in each figure. For PNIPAM ^{13}C and ^1H spectra are obtained extremely clear, and peak assignments were performed according to the literature [187-190]. Observed chemical shifts are listed in Table 7. Analyzing the ^{13}C -NMR spectrum of PNIPAM, the most downfield peak can be assigned to the carbonyl carbon ($\text{C}=\text{O}$ at $\delta = 175.3$ ppm), followed by the main-chain methine overlapped pendant group methine (CH at $\delta = 41.8$ ppm), the peak corresponding to the methylene group on main-chain (CH_2 at $\delta = 34.6$ ppm) and finally the methyl groups of pendant isopropyl functionality (CH_3 at $\delta = 21.6$ ppm). The structure clarified by ^{13}C -NMR is also validated by proton NMR (Figure 30 (b)). There is a good correspondence between them. In ^1H NMR spectrum absorptions of unsaturated vinyl carbon protons ($\delta = 5.6$ ppm and $\delta = 6.0$ ppm in Figure 31(b)) found in monomer structure are disappeared. Instead, proton absorptions of saturated carbons constituting main-chain revealed with the chemical shifts of 2.0 ppm (1H) and 1.6 ppm (2H). Additionally absorptions of 6 methyl protons (CH_3 at $\delta = 1.1$ ppm) and proton of methine (CH at $\delta = 3.9$ ppm) of isopropyl functionality can be seen in the spectrum. Moreover NIPAM monomer structure is investigated by means of ^{13}C and ^1H NMR tests. The ^{13}C -NMR spectrum of NIPAM monomer is given in Figure 31 (b). From isopropyl moiety methyl carbons give an intense signal at $\delta = 20.9$ ppm and methine carbon absorption at $\delta = 41.3$ ppm. Vinyl carbons resonate at chemical shifts of 126.4 ppm and 129.9 ppm successively. Finally the least shielded carbonyl carbon absorbs at $\delta = 166.8$ ppm. In proton spectrum absorptions of 6 methyl protons (CH_3 at $\delta = 1.0$ ppm) and a proton of methine (CH at $\delta = 3.8$ ppm) from isopropyl functionality are observed. Carbons of vinyl moiety of monomer are detected as multiple peaks at $\delta = 5.6$ ppm and $\delta = 6.0$ ppm. Finally amide proton (NH at $\delta = 7.66$ ppm) is sometimes observed as an unsplitted broad peak due to its intermediate exchange rate that causes the prevention of coupling to protons on adjacent carbons and replacement by deuterons of D_2O so that the signal disappears.

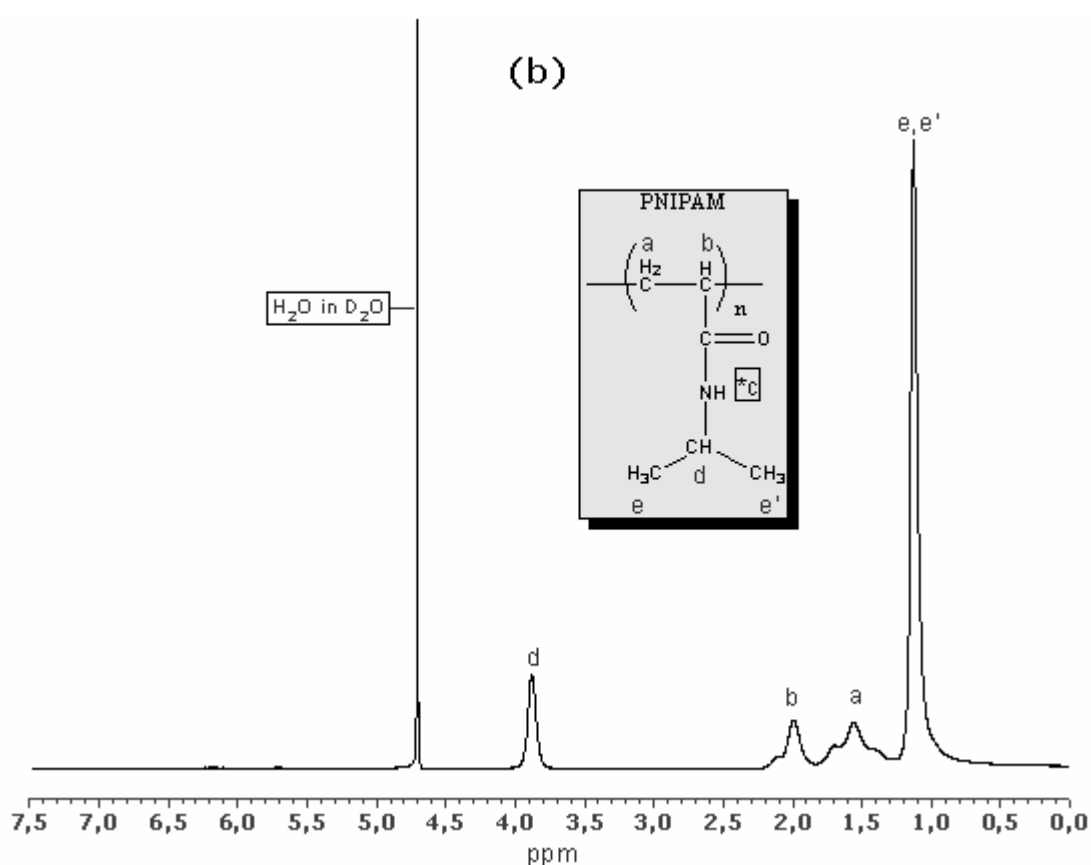
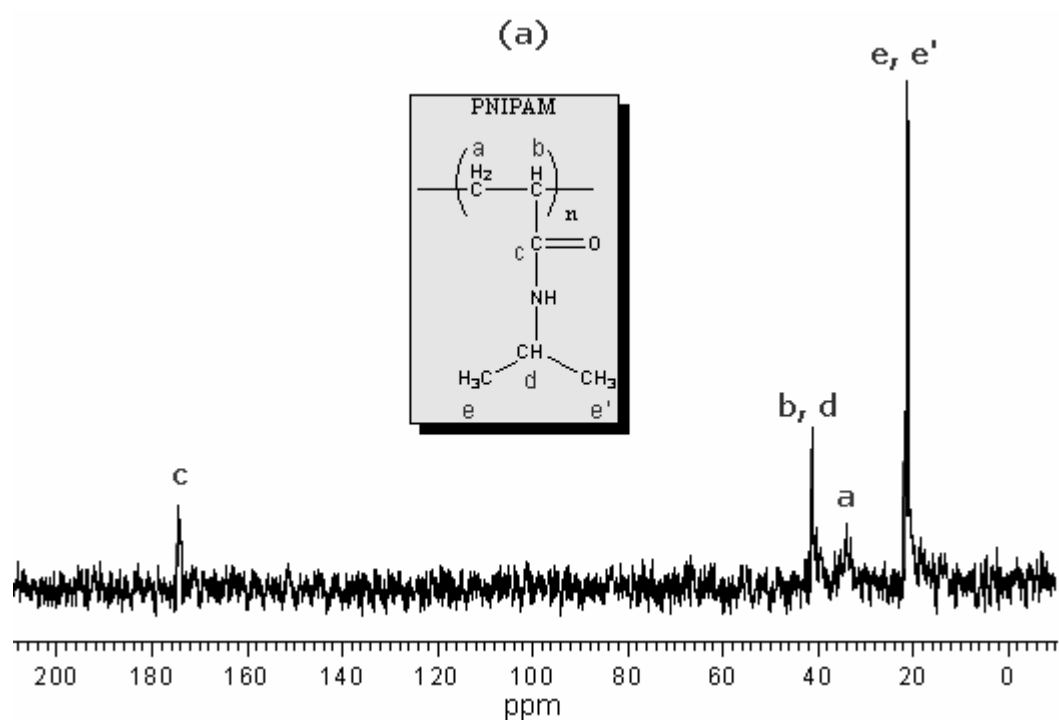


Figure 30 NMR spectra of solid state plasma polymerized PNIPAM. (a) ^{13}C and (b) ^1H

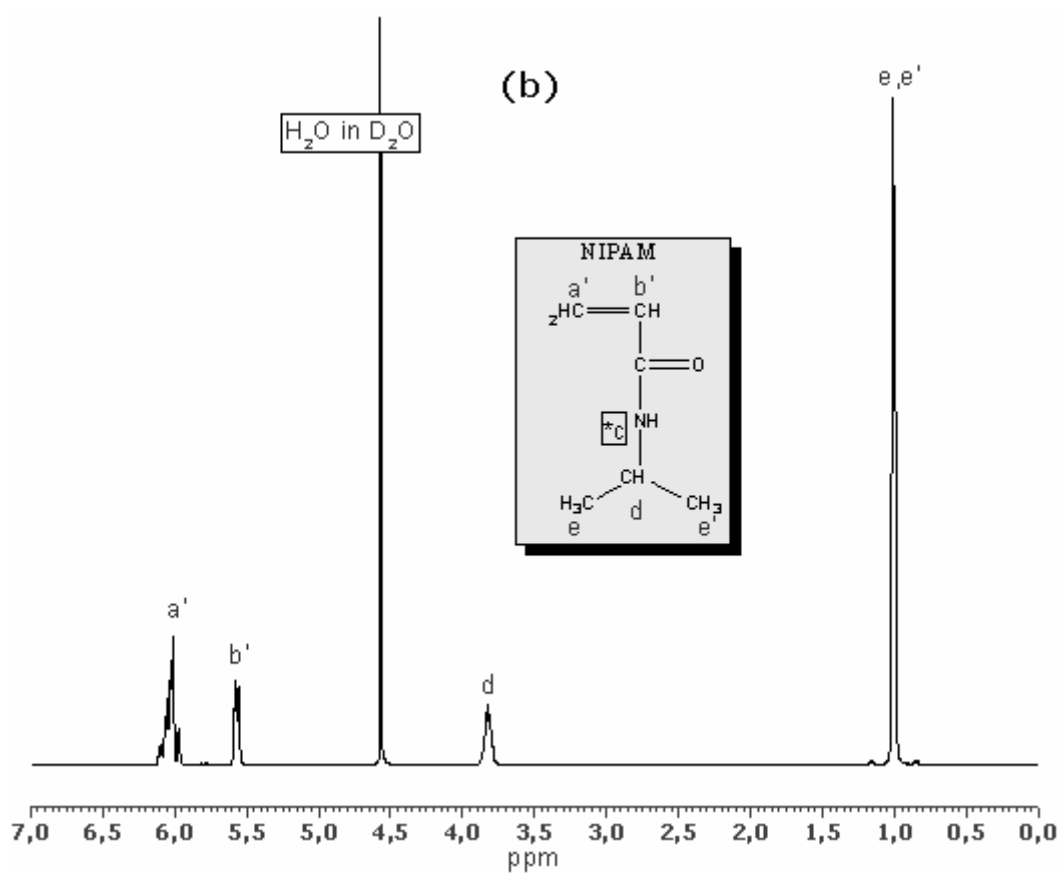
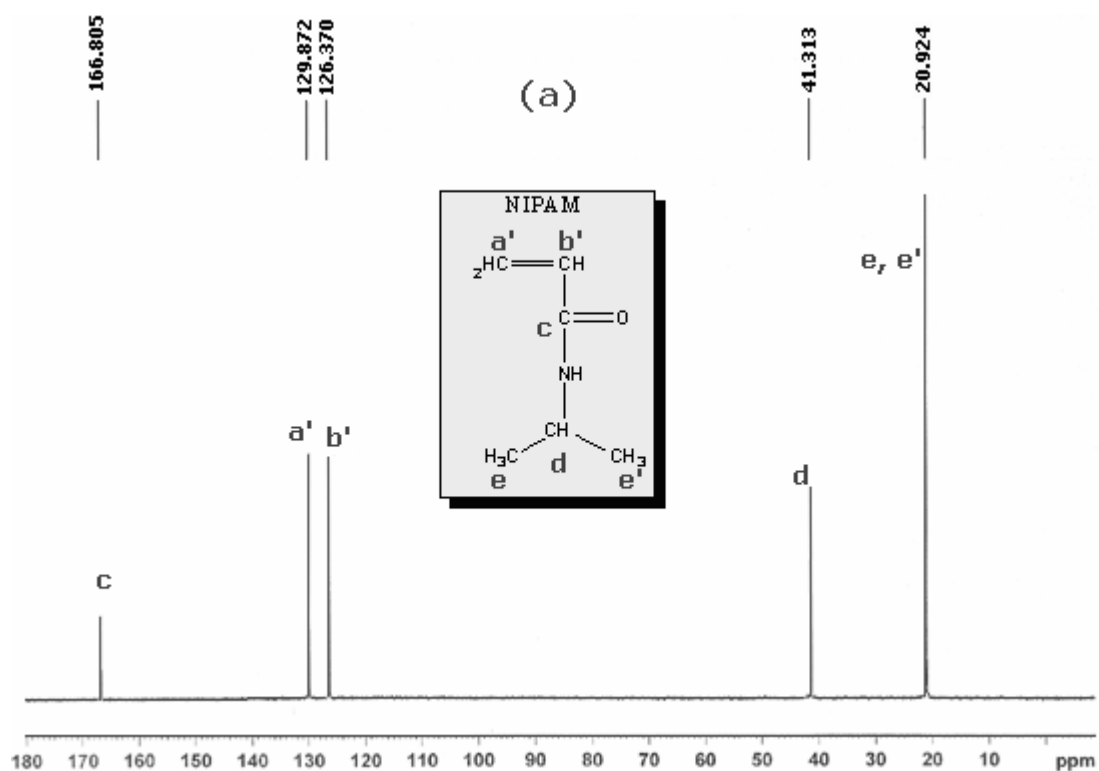


Figure 31 NMR spectra for isolated NIPAM monomer. (a) ^{13}C and (b) ^1H .

Additionally ^1H -NMR spectrum of the sample (still monomer containing) after plasma discharge with no purification is depicted in Figure 32. Protons of vinyl group in monomer and polymer backbone give signals, which are indicated a'-b' and a-b respectively, at the same chemical shifts as in the case of their purified states. As a consequence, data inferred from these clear spectra prove that plasma initiated solid state polymerization of NIPAM under certain parameters gives non-crosslinked PNIPAM polymer in significant amount with no other fragmented or degraded side products.

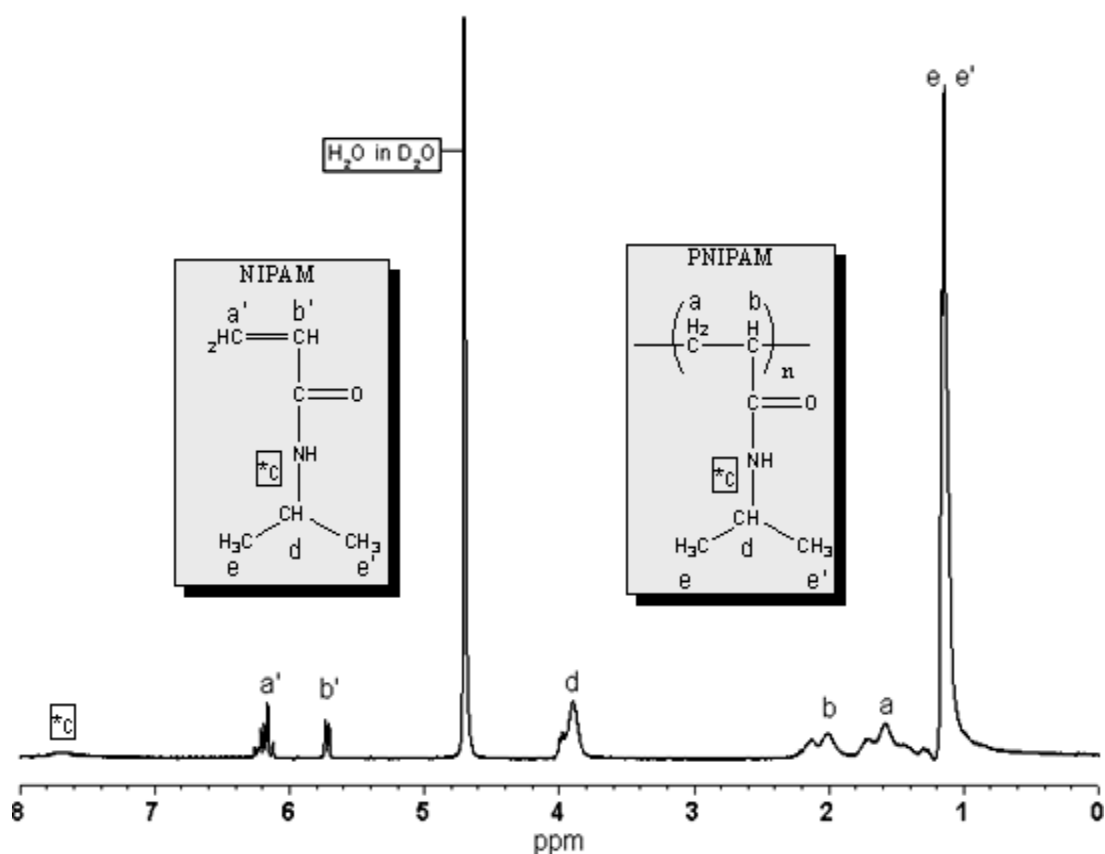


Figure 32 ^1H -NMR spectrum (in D_2O) for raw product mixture.

Table 7 Chemical shifts in ^{13}C and ^1H -NMR spectra of NPAM and PNIPAM.

Sample	Spectrum	CH ₃ (e, e')	CH (b or b')	CH (d)	CH ₂ (a or a')	CO (c)	NH (*c)
NIPAM	^{13}C	20.92	126.37	41.31	129.87	166.81	Sometimes observed at 7.66 ppm in ^1H -NMR
	^1H	1.01	5.58	3.82	6.01	-	
PNIPAM	^{13}C	21.63	41.84	41.84	34.62	175.37	
	^1H	1.13	2.00	3.88	1.56	-	

3.1.4.3 DSC Studies

The DSC thermogram consisting heating and cooling curves of PNIPAM hydrogel is shown in **Figure 33**.

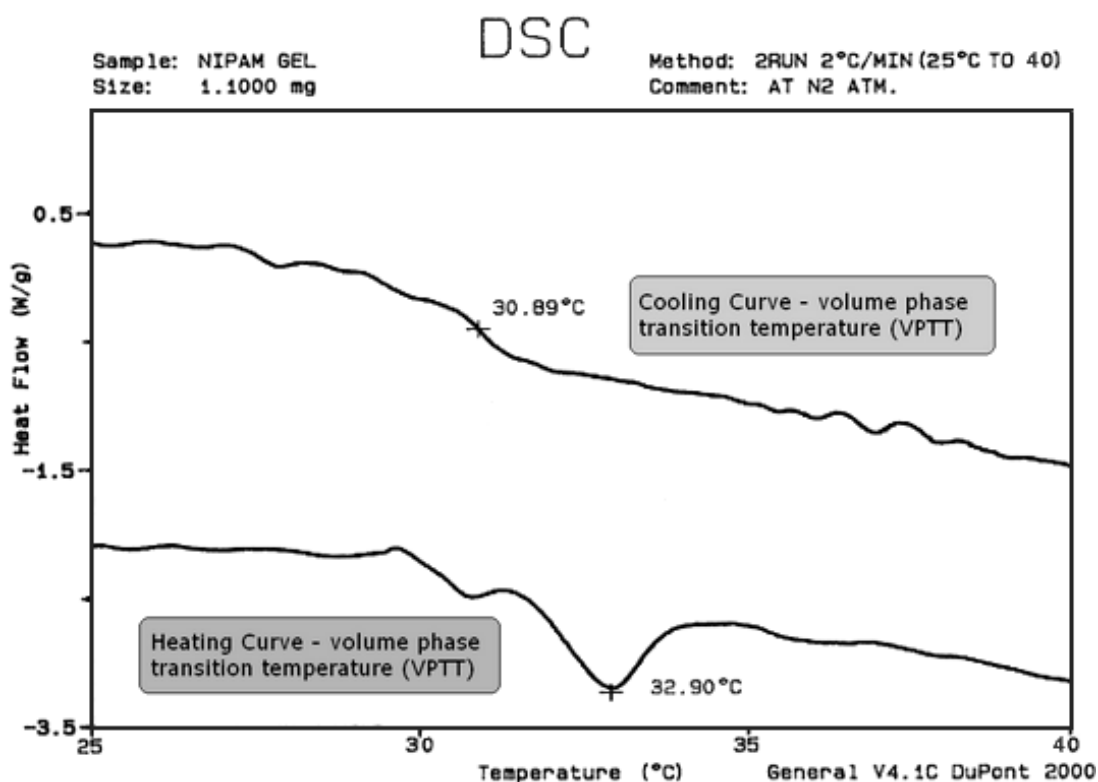


Figure 33 DSC thermogram of the solid state PNIPAM hydrogel at a heating rate of 2°C/min from 25 to 40°C.

The temperature at the peak summits of the DSC endotherm is referred to the volume phase transition temperature (VPTT) of hydrogel. It can be noted from DSC thermogram that PNIPAM hydrogel sample exhibit a similar VPTT around $32 \pm 1^{\circ}\text{C}$ in cooling and heating operations, and there is a good agreement with the value in literature, and variation of $\pm 1^{\circ}\text{C}$ can be attributed to difference in thermal transport rates of deionized water in reference cell and hydrogel filled with deionized water in sample cell. The isolated solution of linear polymer in water, which is totally transparent at room temperature, becomes translucent when heated. This is an indicator of transition at LCST.

3.1.4.4 Scanning Electron Microscopy (SEM)

SEM micrographs of samples are present in Figure 34-36. It is found that the crystalline structure of monomer has a characteristic roughly rugged (crispy) surface morphology. Therefore it is sometimes very difficult to take quality images due to the presence of uncoated moving regions. Chaotic orientation of crystalline structure of monomer is observed in Figure 34. There are plenty of defects, ultramicrocracks due to stress induced deformations and dislocation networks formed during crystal growth especially located at the block boundaries in such a real crystal structure. These defects can either promote or slow down polymerization reaction. On the other hand isolated linear PNIPAM possesses extremely smooth surface morphology as shown in Figure 35. Observed wrinkled surface regime results from removal of solvent (water) during desiccation in preparation of SEM sample. The micrograph given in Figure 36 illustrates the effects on surface properties of monomer crystal flake under certain conditions of 30 W – 1 hr plasma discharge. From these micrographs one can easily deduce, solid state polymerization takes place intensively on the surface of crystalline monomer flakes. Another crucial outcome from existence of partially non polymerized regions under amorphous polymeric surface layer is the protection of inner crystalline bulk of monomer from outer ionizing plasma environment by formation of plasma polymerized thick surface layer.

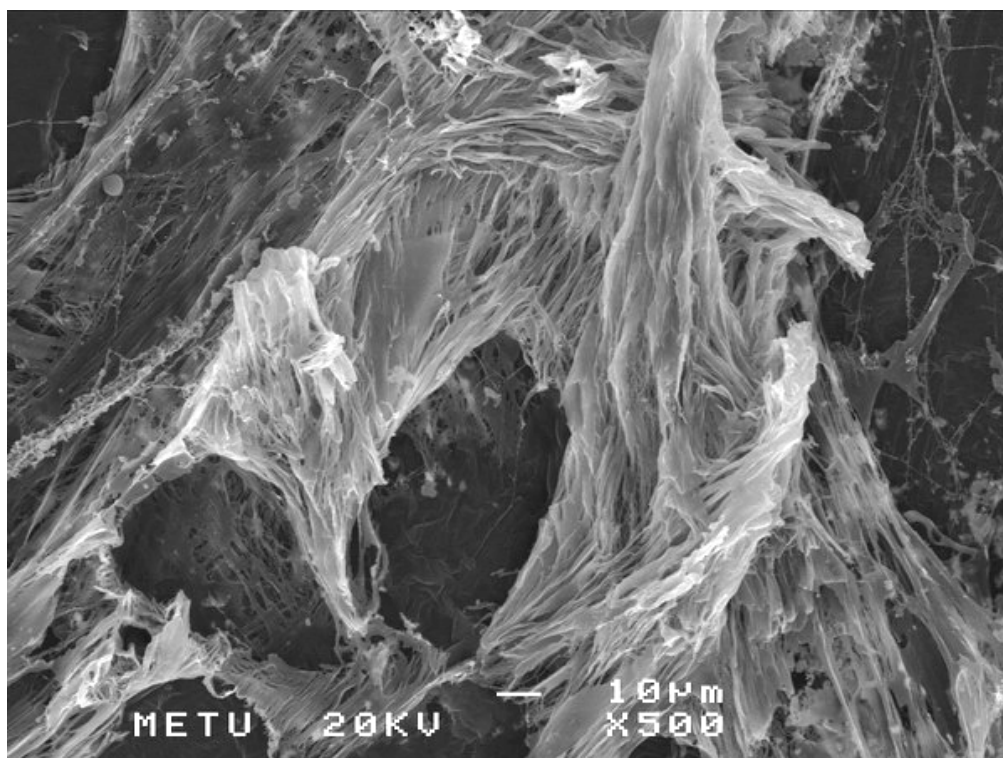


Figure 34 SEM micrographs of crystalline monomer.

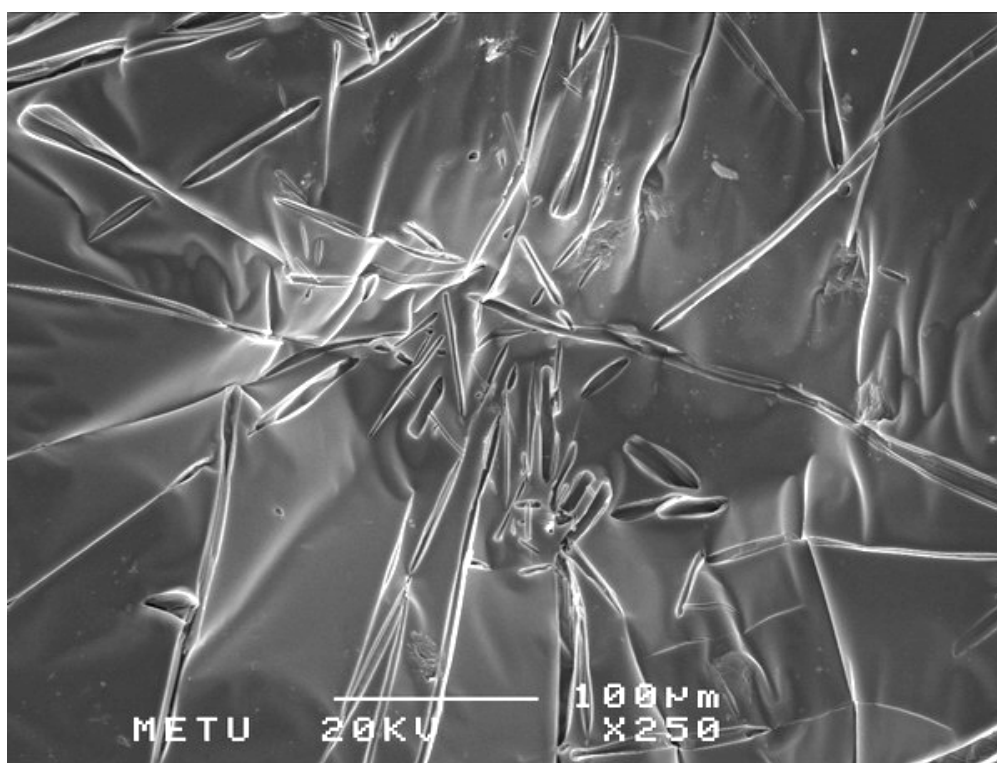


Figure 35 SEM micrographs of amorphous linear polymer isolated by extraction.

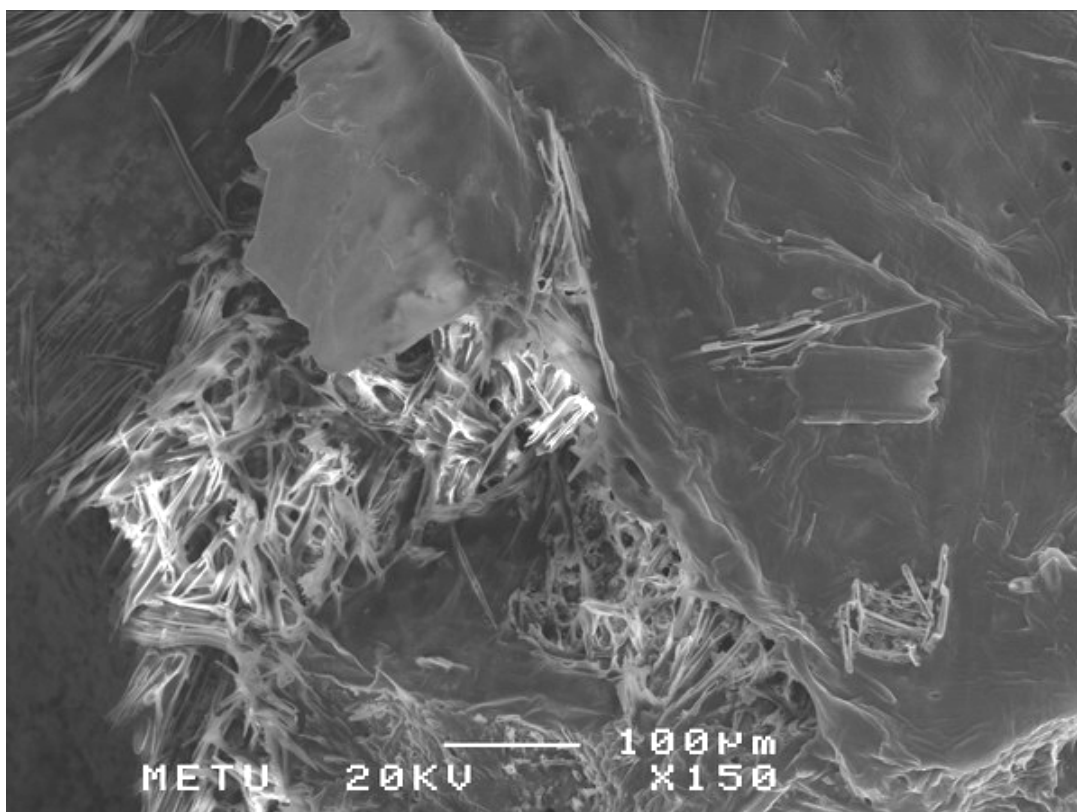


Figure 36 SEM micrographs of sample taken after plasma process having both crystalline inner cores beneath plasma polymerized, amorphous surface layer.

3.1.5 Plasma – surface Interactions

It is well known that introduction of highly energetic radiations such as γ -rays, ultraviolet (UV) or X -rays, into N-substituted acrylamide monomer medium under certain conditions (i.e., favorable temperature and under inert vacuum atmosphere) gives rise to excited sites with varying concentrations from surface to inner layers of monomer depending on penetrating capability of radiation. For example, highly penetrating radiation i.e., γ -rays ensures regular initiation throughout the bulk of the solid monomer, while in the case of UV (40–400 nm) excited site formation is concentrated mostly in the surface layers. Apart from these energetic radiations plasma is a unique phenomenon composed from not only radiation

but also highly energetic electrons at 10^4 K and much cooler molecules and ionized species at about 300 K. Consequently, in a typical plasma discharge medium excitation of monomer molecules of the surface is based on photons of vacuum-UV, V-UV, (40—180 nm), energetic electron bombardment emanated from ionization of working gas (i.e., Ar). After formation of excited sites in the solid monomer matrix surface, dimerization and then polymerization reactions occur successively. Polymerization initiated by plasma induction can be proceed by both a free-radical and an ionic (cationic or anionic) mechanism. It should be emphasized that electrons, ions, radicals and radical ions intermediate and final radiolysis products are all capable of initiating many coincident polymerization reactions especially in the surface volume interacting with the plasma.

Under plasma atmosphere, the formation of polymeric film on the crystalline monomer surface can be explained by two simultaneous mechanisms. First one is the plasma initiated polymerization (P-iP) take place on the surface and in the monomer bulk just below the surface layer. In this mechanism V-UV plays the prominent role for production of excited monomers and radical species in the surface and adjacent inner layers throughout the depth of approximately 100 Å from surface. The surface layer is also bombarded with energetic electrons and ions of working gas (Ar^+) originated from plasma atmosphere. The second mechanism is plasma polymerization (PP) of evaporated monomer where the deposition of ions of excited or fragmented monomer molecules uniformly cover the surface and result in a highly crosslinked polymer network blanket on it. In our case the second mechanism disappeared gradually in the course of time after plasma ignition. This is an outcome of the decrease in monomer evaporation due to formation of polymeric film which covers the surface entirely. This phenomenon is used to explain the sharp decrease of vacuum level in first hour of discharge as shown in Figure 25. In our experiments after 1 hour plasma discharge, plasma will cause some chemical bond breakage and fragmentations from the new crosslinked amorphous surface. This often leads to degradation

and/or further crosslinking of the surface.

Breaking of carbon–carbon bond in the main polymer chain leads to the formation of two free radicals. These free radicals will recombine unless they are able to diffuse away from each other. If they do diffuse away which is more probable in the surface layer than in the bulk the bond remains permanently broken. On the other hand, for crosslink formation, an active radical on each of two molecules must approach each other and react. The difficulty is that the free radicals may be attached to large molecule fragments imbedded in an entangled medium. For that reason crosslinking procedure predominantly occurs on the surface.

Below surface layers, radicals and excited sites are protected from outer atmosphere and depending on the orientation of the monomer molecules polymerization may continue to an extent of residual linear polymer chains. In the light of obtained data the regime change in surface and in the layers underneath, during plasma discharge at predetermined conditions (i.e., discharge power, discharge time, reactor and electrode geometry, working gas flow rate, vacuum level) is proposed in Figure 37.

Especially in the network structure of the surface layer there are chemical crosslinks with tri- and tetra-functional network junctions (b and a respectively). In deeper layers oligomers and linear polymer chains (d) are frequently found between the monomer crystal domains. Some entanglements can act as physical crosslinks in these amorphous polymer domains (c, c', c'').

3.2 Polymerization in Solid State

Although extensive experimental data are available, many theoretical concepts of solid-state polymerization still remain unclear. This polymerization technique lies in the intersection point of the chemistry and

physics of the solid bodies, the chemistry of polymers, and radiation chemistry. In order to understand solid-state polymerization procedure, it is necessary to deal with the crystallographic data of the crystalline monomer in many cases.

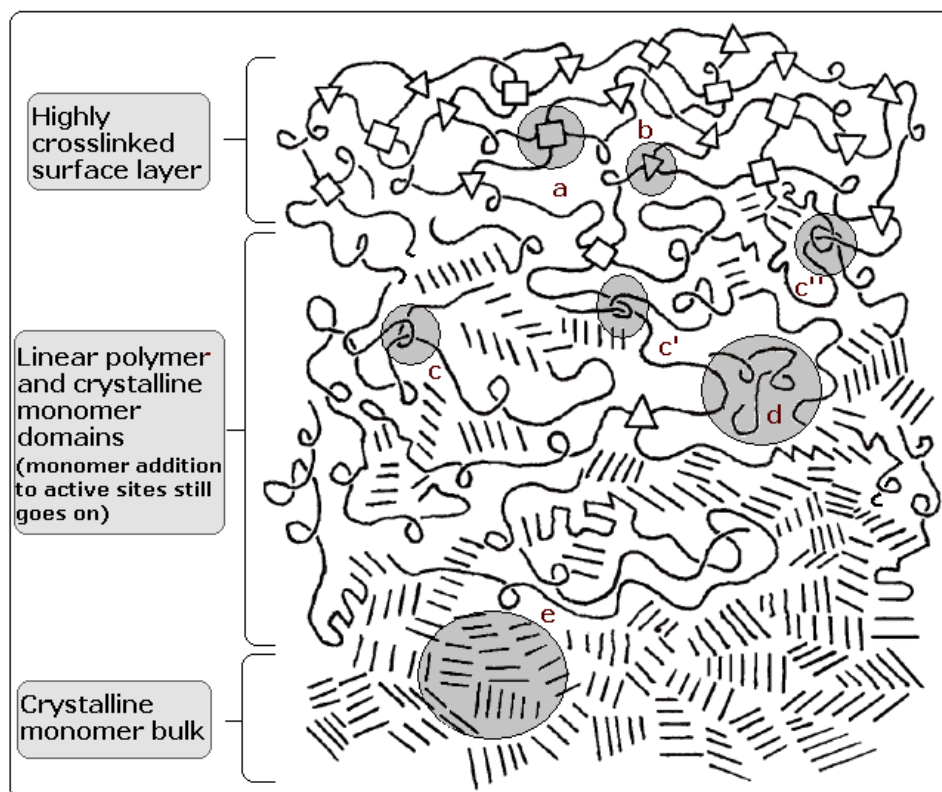


Figure 37 Schematic diagram of surface and underneath layers including linear polymer and crystalline monomer bulk after plasma processing.

3.2.1 Crystallinity Studies

Morphological changes in surface during plasma treatment is studied and discussed in previous section by the help of micrographs obtained from SEM inspections. Effect of crystalline structure or with more detailed statement the effect of the monomer molecular orientations in solid state on polymerization rate will be discussed in this section.

A great deal of information about radiation induced solid-state polymerization of N-substituted acrylamide monomers is accumulated with increase in use of powerful techniques related with crystalline structure characterization especially in the surface region. Among these methods one of the most frequently used is X-ray diffraction (XRD) technique.

In this study diffraction patterns of monomer and synthesized polymer fractions (linear and crosslinked) are discussed. Effects of plasma and post plasma aging period on crystalline structure of NIPAM monomer are also investigated by XRD technique.

3.2.2 X-Ray Investigations of Products

The recorded X-ray diffraction patterns of NIPAM monomer and PNIPAM polymer (linear and crosslinked hydrogel forms) are depicted in Figure 38 and Figure 39 respectively.

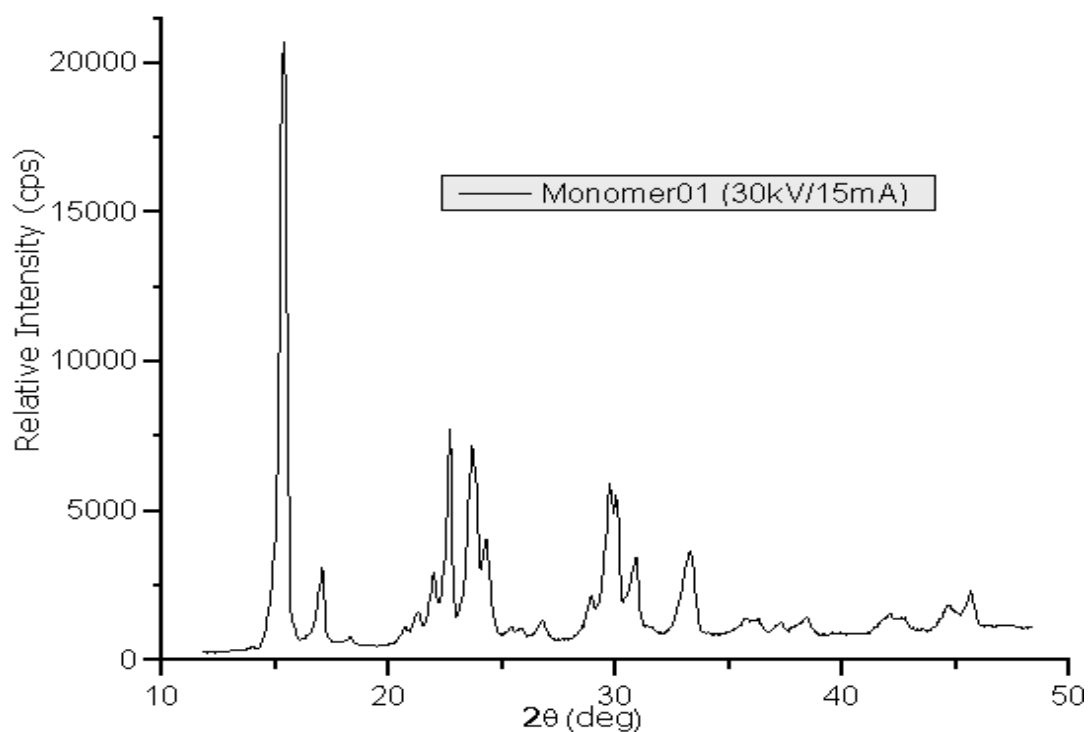


Figure 38 X-ray diffraction pattern of NIPAM monomer.

As evidenced from XRD patterns, illustrated in Figure 38 the spectrum contains a good number of sharp peaks, indicating highly crystalline structure of the NIPAM. As expected, broad peak in the spectra of both crosslinked and linear PNIPAM indicates that these polymers are in the amorphous state. The samples whose X-ray diffraction patterns presented in Figure 39 are extracted from final product mixture where monomer is completely removed and then casted on glass holder before measurement.

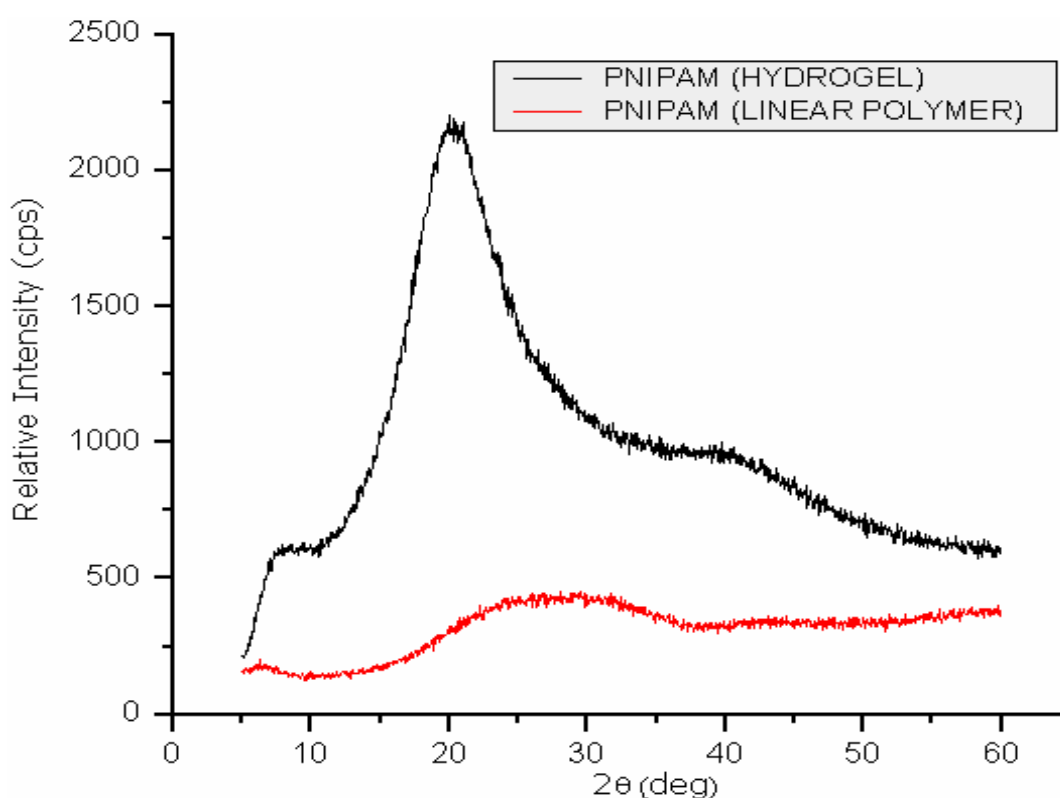


Figure 39 X-ray diffraction patterns of linear and hydrogel PNIPAM.

3.2.3 Aging Studies

Preparation of the referred NIPAM pellets is described in the experimental part. Double sided stripe is used to prevent sample from sliding or displacement on the glass holder and the holder is fixed at the same position of clamps. Hence incident X-ray beam sweeps the same portion of the sample each time. After X-ray investigation of two sets of monomer pellets,

they are treated by plasma at 35 W for 30 minutes. Although, peak intensities vary from sample to sample, the patterns remain unchanged along with x-axis even after plasma treatment of sample surface. After plasma treatment, identical samples were stored under closed and open-air atmospheres. Then X-ray measurements are performed to observe the changes in X-ray patterns at various environments for certain times of aging. Figure 40 and Figure 41 represents these changes.

After plasma application aging conditions are specified differently for both samples. One of these sample pellets was aged in a closed glass vial, while the other one was open to atmosphere at the same temperature for several days. At the end of certain period X-Ray diffractograms were recorded.

For making comparisons between diffractograms, peaks at specific 2θ values are selected. Because they are the strongest ones and the most dramatic changes are observed in them, the selected diffraction peaks for observing plasma and post plasma effects are located at around 15.4° , 22.7° and 29.7° .

At first sight plasma surface treatment of both NIPAM pellets results in a sharp decrease in peak intensities especially at all of the selected 2θ values. This alteration is observed in both sets of sample signals colored black and red. Formation of amorphous crosslinked PNIPAM film in the surface of the sample pellet cause additional scattering of the incident X-ray beams so that decreases the amount of reflected beam reaching to the counter.

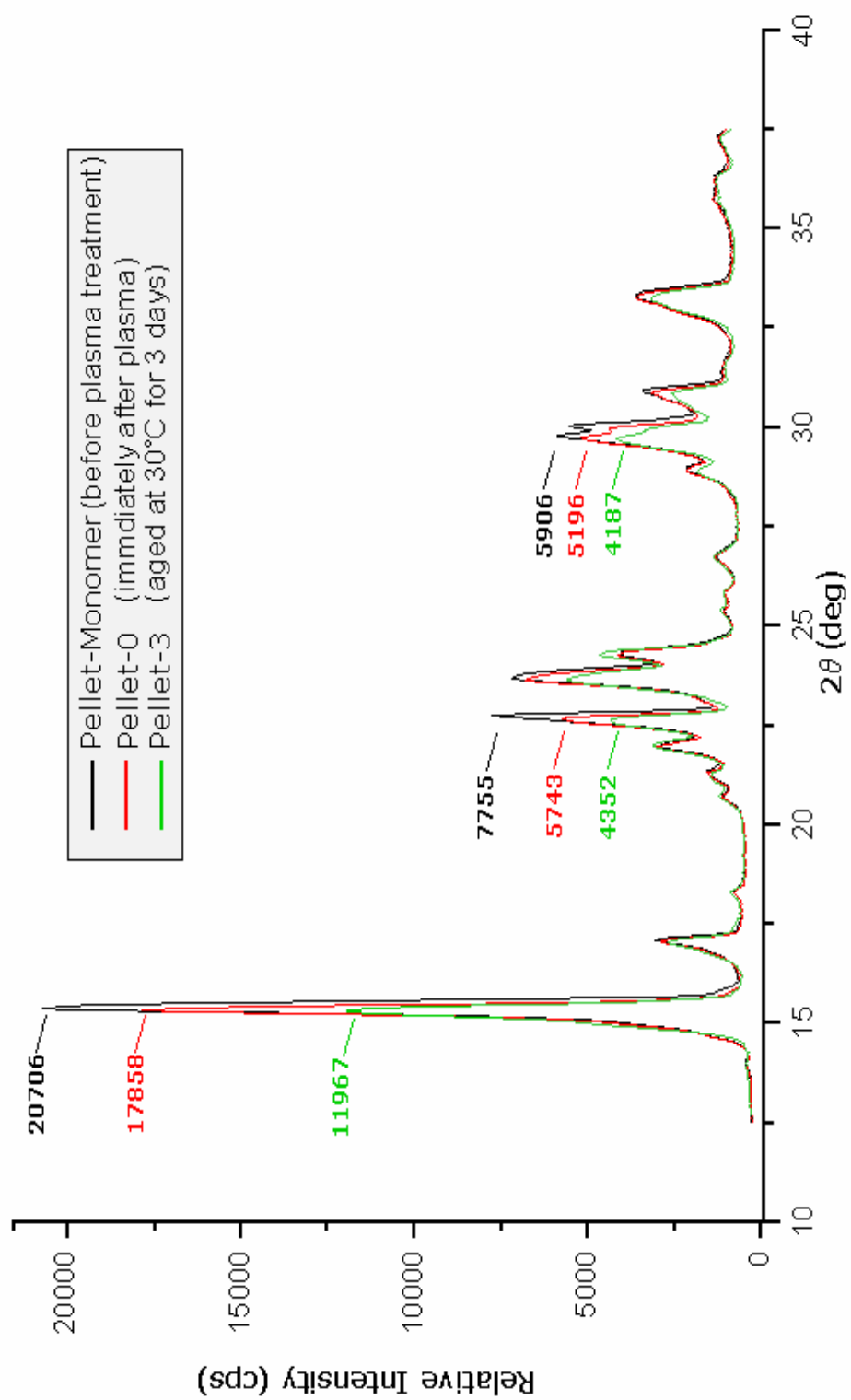


Figure 40 Diffractogram set showing plasma and post-plasma effects on X-ray spectrum of NIPAM pellet stored in open-air.

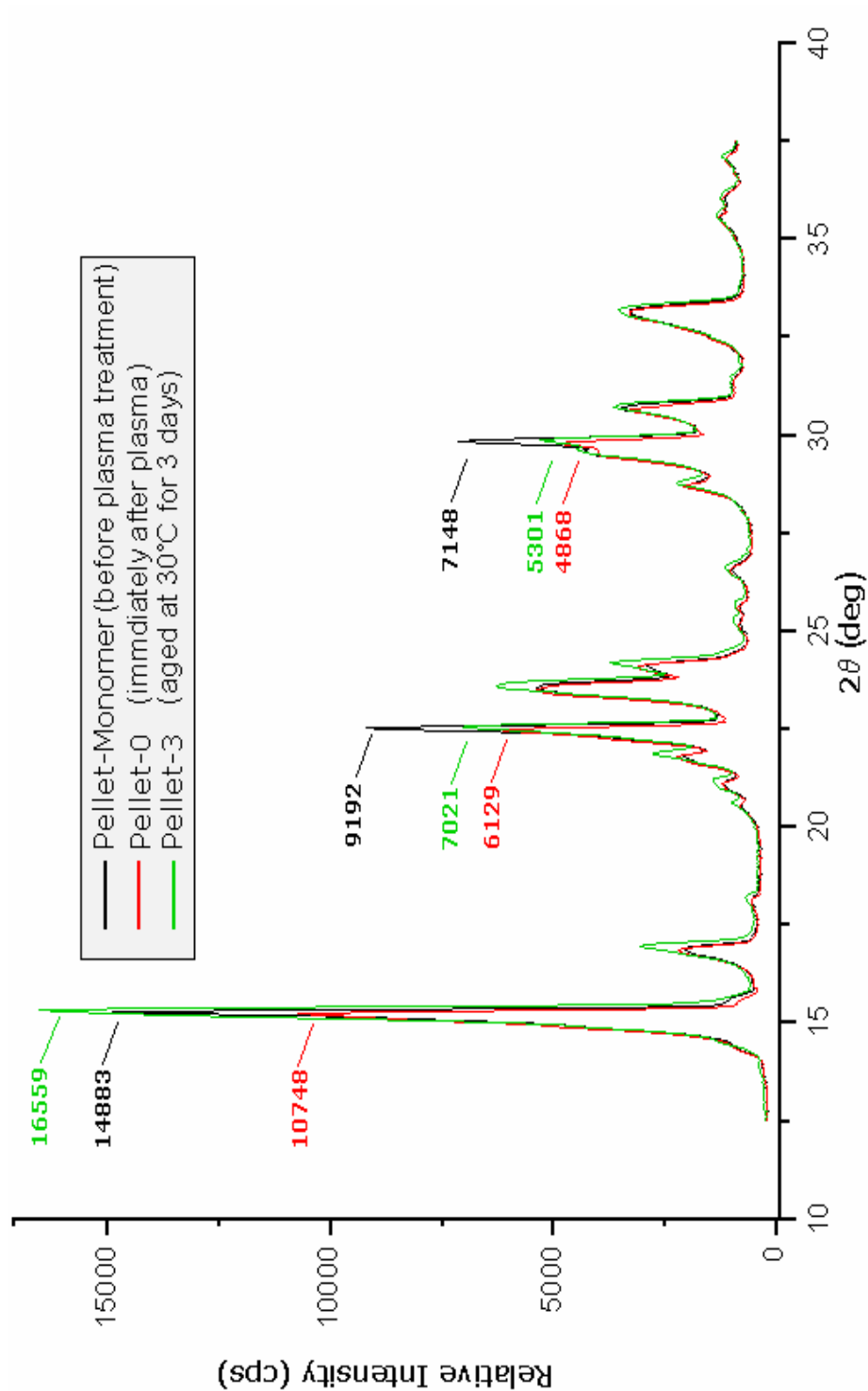


Figure 41 Diffractogram set showing plasma and post-plasma effects on X-ray spectrum of NIPAM pellet stored in a closed vial.

In Figure 40 the signal intensities for the sample opened to atmosphere are diminished significantly (see signals colored red and green). This can be attributed to the sublimation related weight loss of monomer beneath the polymerized surface of the pellet linked. This monomer removal by sublimation is also monitored by change in weight of the pellet in the course of the aging period as given in Figure 42. At the end of 3-day-aging, 92% of monomer is taken away from the pellet by sublimation and after two weeks period, only polymerized amorphous content remains. XRD diffractogram of the two-weeks aged sample turns to the line of crosslinked polymer in Figure 39.

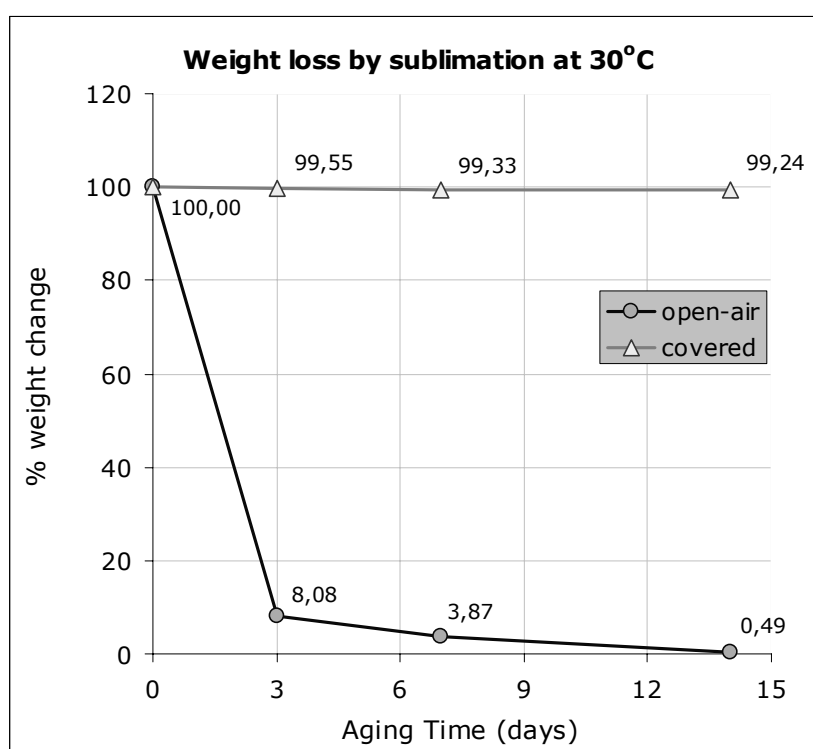


Figure 42 Weight losses of NIPAM pellets stored in closed vial (covered) and open-air after plasma treatment at 30°C.

For the case in which sample aged in closed vial, surprisingly, peak intensities are increased at the end of 3-day aging period with a trend opposite to one in the previous case of open-air. In this case monomer

content in the closed system almost remains constant and sublimation is in equilibrium with deposition for NIPAM monomer. Thanks to this dynamic equilibrium, some of monomer deposited on the polymer film surface. This accounts for increase to some extent in diffraction intensities at all 2θ s, including the selected ones. However, the main reason of increase in amount of reflected beam reaching counter may be explained by the theory of X-ray diffraction in mosaic crystals and by the concept of crystal annealing by some physical effects.

3.2.4 Mosaic Block Model and Kinematical Diffraction Approximation

In general, the interaction of x-rays with a crystal is complicated, and there are two different ways of approach - kinematical and dynamical theories of diffraction.

In the kinematical diffraction, a beam scattered once is not allowed to be scattered for the second, third and so on times. On the contrary, the theory of the dynamical diffraction accounts for scattering of the diffracted beam and other interactions of waves inside the crystal, and thus the mathematical apparatus of the theory is quite complex [191]. Diffraction by an ideal mosaic crystal is best described by a kinematical theory of diffraction, whereas diffraction by an ideal crystal is dynamical and can be described by a much more complex theory of dynamical diffraction where the "ideal mosaic" means that all blocks have the same size and degree of misalignment with respect to other mosaic blocks and the term of "mosaic block" can be defined as a tiny single crystal (microcrystal). Each particle in a polycrystalline material usually consists of multiple mosaic blocks that join together in different orientations.

The kinetic theory of diffraction requires the following postulates:

- A crystal consists of individual mosaic blocks which are slightly misaligned with respect to one another,
- The size of the crystallites is small,
- The misalignment of the crystallites is large enough, so that the interaction of x-rays with matter at the length scale exceeding the size of mosaic blocks is negligible.

Among these approaches, the kinematical approach is the simpler one, and adequately and accurately describes the diffraction of x-rays from mosaic crystals. This is especially true for polycrystalline materials where the size of crystallites is relatively small. Hence, the kinematical theory of diffraction is used in the present study and throughout this thesis.

A simple description of an imperfect (real) crystal, which is NIPAM monomer in our case, is given by a mosaic-block model (Figure 43-a). According to this model crystal structure is imperfect and has many disordered regions [192].

In X-Ray analysis incident beams are reflected from the surfaces of these blocks oriented as mosaic in crystal and are counted by the instrument's detector. Increase in mosaicity of crystal structure by any reason leads to increase in number of scattered beam and thus decrease in number of countable reflected beams. Therefore, intensity of peaks in diffractograms decreases.

Actually, increase in counted reflected X-ray beams for the sample aged in closed vial, is a matter of physical phenomenon. After formation of crosslinked amorphous layer on the surface layer by plasma (Figure 43-b), aging temperature and previously applied radiation effect of plasma cause removal of stress between mosaic blocks of the crystalline monomer which are located just below the amorphous polymer surface in the sample.

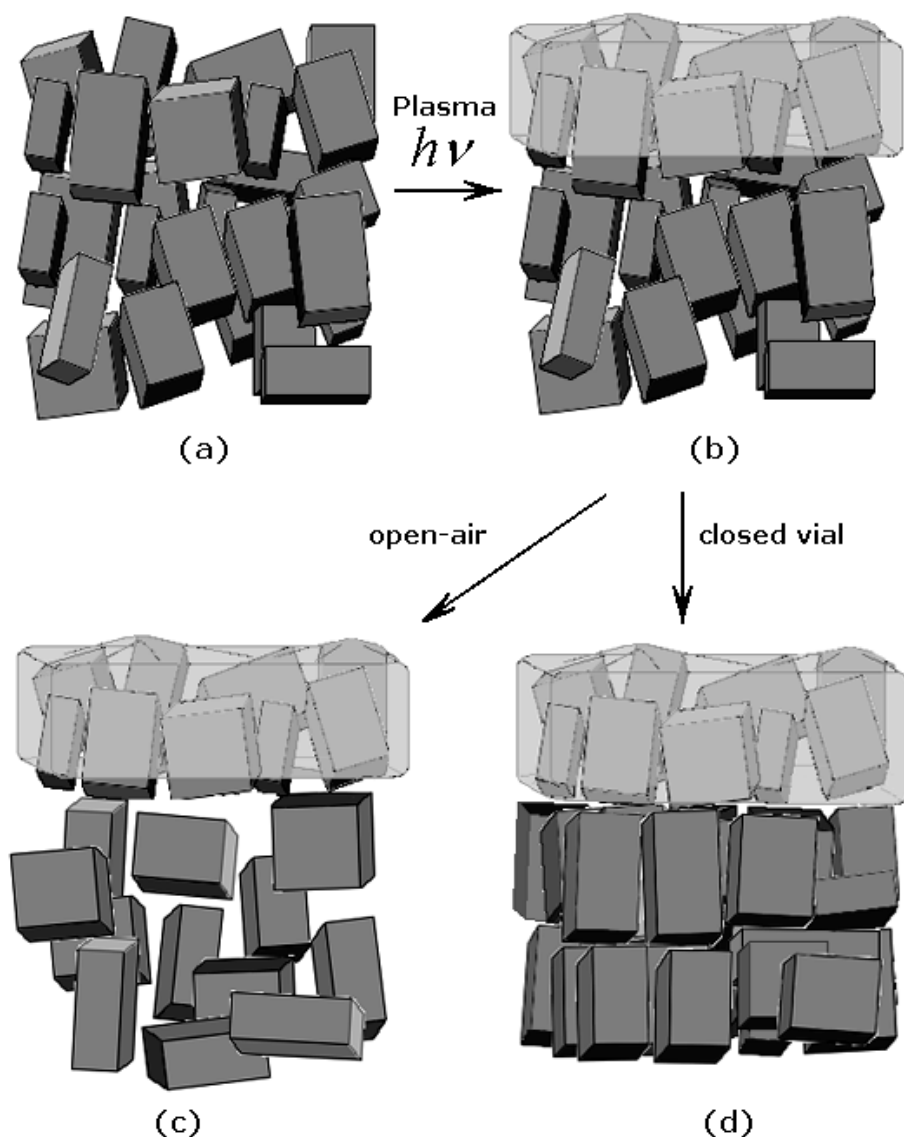


Figure 43 Mosaic model of a NIPAM crystal and effect of aging conditions on orientations of mosaic blocks in the crystal structure.

During aging period dislocation defects within the crystal will be healed. Furthermore, the size of mosaic blocks is possibly increased by recrystallization at the dislocations. Eventually, release of lattice strain, increasing order and size of the mosaic blocks in the crystal results a more ordered orientation of mosaic blocks of crystal surface with improved reflective properties (Figure 43-d). Increase of reflective quality of the inner

monomer layer under amorphous outer surface results more incoming X-ray beams to be reflected so that increases counts per second at all 2θ s. This radiation and temperature induced procedure is reported as “annealing” or “tempering” the crystal. Other methods of macromolecular crystal annealing (MCA) employed quite often in crystallography [193].

On the other hand, under open air conditions O_2 diffuse into the crystalline structure readily and prevent monomer blocks from annealing. Additionally, the easy removal of monomer molecules by sublimation will increase imperfections and number of disordered sites in crystal structure. This phenomenon will left the monomer surface with poorer reflection properties.

Finally, each aging experiment is performed twice under the same conditions. In this way, confirmation of compliance in peak intensity changes is done for parallel cases.

3.2.5 Crystalline Structure and Polymerization in Solid State

Although, complex calculations of the positional parameters used for the evaluation of the packing diagram of the monomer unit cell are beyond the scope of the present study, some calculations and indexing of *d – spacing values* were performed to make some correlations between crystalline structures of acrylamide (AAm) and NIPAM monomers (N-substituted derivative of AAm). The reasons for selecting AAm are based on its structural resemblance to NIPAM and its being most frequently studied in radiation induced solid state polymerization literature. By unveiling and emphasizing the isostructural morphology in crystalline structures of AAm and NIPAM, we intend to obtain a better understanding of the plasma-initiated solid-state polymerization mechanism of NIPAM.

Usanmaz et al. [194] reported the crystal structure of acrylamide for realizing the role of the crystal structure on the reaction mechanism of radiation-

induced polymerization in the solid-state. The crystal lattice is monoclinic, the space group is $P2_1/c$. Other cell parameters are $a = 828.0(2) \text{ pm}$, $b = 578.0(4) \text{ pm}$, $c = 974.9(2) \text{ pm}$, $\beta = 119.62(4)^\circ$, $Z = 4$ molecules/unit cell, $d_x = 1.165 \text{ g/cm}^3$ at -150°C . In the present study using these cell parameters we calculated d – spacing values for AAm by a DOS based computer program, TURBO. Then calculated $1/d^2$ values for AAm are compared with those observed for NIPAM obtained from the d – values at 2θ s corresponding all selected peak summits in the XRD spectrum of NIPAM. From this comparison, it turned out that there is an almost entire matching in d – spacing values which proves that the crystalline structures of AAm and NIPAM are isomorphous at all these 2θ points.

Calculated and observed $1/d^2$ values are tabulated in Table 8 with hkl indices. Small inequalities result from ambiguous procedure of peak maxima selecting which is differing slightly in every one of diffractograms.

3.2.6 Discussions of Polymerization in Crystalline State

In crystalline state polymerization, two fundamentally different cases can be distinguished:

- The polymerization, in which the geometrical arrangement of the molecules in the crystal is of crucial importance in determining their reactivity, named *topochemical polymerization*.
- The polymerization, in which chain propagation is diffusion controlled, i.e., polymerization proceeds with the destruction of the crystalline lattice of the monomer and the formation of an amorphous polymer.

Table 8 X-Ray pattern revealed from comparison AAm with NIPAM.

2θ	$1/d_{AAm}^2$	$1/d_{NIPAM}^2$	h	k	l	I / I_0
15.350	0,030	0,030	0	1	0	100
20.650	0,056	0,054	0	0	-2	2
21.300	0,059	0,058	2	0	-1	3
22.700	0,068	0,065	2	0	-2	33
23.650	0,072	0,071	1	1	-2	27
24.300	0,077	0,075	2	0	0	12
26.750	0,089	0,091	2	1	-1	3
28.900	0,105	0,105	2	0	-3	4
29.700	0,107	0,111	2	1	0	21
30.050	0,119	0,120	0	2	0	11
33.300	0,139	0,138	3	0	-1	13
33.750	0,155	0,159	0	1	-3	2
36.250	0,162	0,163	1	2	-2	2
37.250	0,170	0,172	2	0	-4	2
38.400	0,183	0,182	3	1	-3	3
42.050	0,216	0,217	1	2	-3	2
42.650	0,223	0,223	0	0	-4	2
44.650	0,245	0,243	0	2	-3	3
45.650	0,253	0,254	0	1	-4	6

In crystalline state it is well known that the arrangement and spatial orientation of molecules are strictly determined by crystal packing. Topochemical polymerization phenomenon is more related with monomer's geometrical arrangement in the crystal structure than their chemical properties. In such reactions polymerization of a crystallized monomer occurs without changing the symmetry of the crystal lattice [195]. Therefore, in this type of polymerization the crystalline lattices of the monomer and

those of the polymer completely correspond to each other and the product of this transition is called a *topotactic polymer*. In this case, if the crystal packing of monomers is not suited for the active growing end to propagate, no polymerization occurs [196].

In diffusion controlled polymerization process total deformation of the lattice structure result in the formation of polymers having higher density than their crystalline monomers'. For example solid state polymerization of acrylamide (AAm) is accompanied by reasonable decrease in its volume. In truth obtaining amorphous polymers from the radiation-induced solid state polymerization of vinyl compounds is a frequent occasion. It is also observed in this case.

Although initiation of (nucleation) polymerization of AAm, which consist of dimerization stage, follows the topochemical polymerization procedure, after dimerization step phase separation and diffusion controlled polymerization procedure became dominant. Indeed for AAm monomers to give the dimer radical topochemically, the non-bonding atomic distances (van de Waals contacts) should be in the distance of about 4.3 Å or less [194], but further proceeding of polymerization needs to diffusion (or segmental mobility) of this dimer radical and needs deviation from the lattice monomer orientation further chain propagation steps. On basis of results obtained by product characterization results (SEM) and by crystallographic studies (XRD) proving isomorphological structure of AAm and NIPAM (Table 8), we can suggest that plasma initiated polymerization of NIPAM in solid state follows similar path with AAm. The difference in molecular structure is the isopropyl group on nitrogen atom as shown in Figure 44. The isopropyl group as an N-substituent can cause some increment in distance between monomers which provide additional mobility, on the other hand, causes an increase in the activation energy of solid state polymerization by hampering the chain propagation by the help of probable steric hindrances, which is a dilemma.

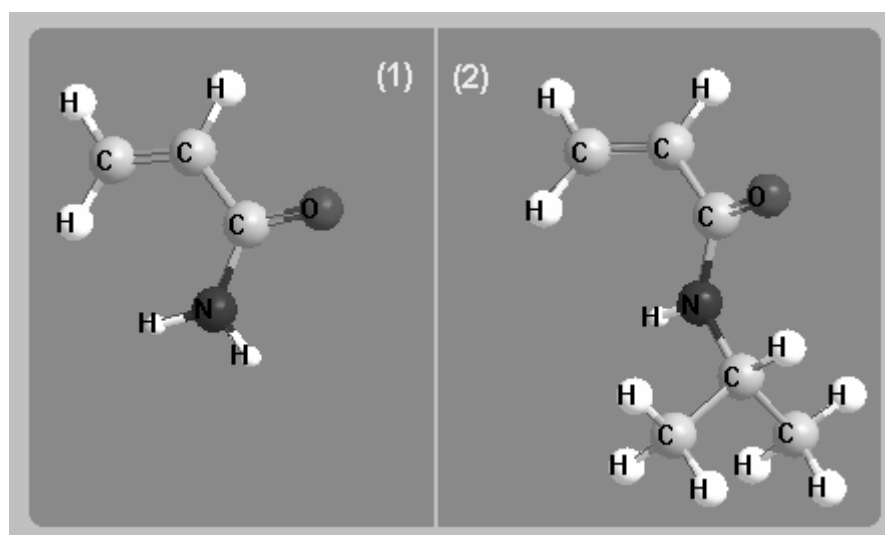


Figure 44 Molecular structures of (1) AAm and (2) NIPAM.

Finally, we are sure that the solid state polymerized NIPAM by plasma treatment possesses amorphous morphology in nature. So we can conclude that after nucleation (or dimerization of adjacent monomer molecules) the polymerization reaction proceeds predominantly according to diffusion controlled mechanism especially at the defects and dislocations in crystalline structure where the restrictions of translational and rotational mobility are minimized. Being sure of the exact mechanism taking place at very beginning of the polymerization is not easy for now. More detailed investigations can be made to provide extra supportive data from more accurate crystallographic calculations (e.g., positional and thermal parameters, bond distances, bond angles of atoms in molecules, etc.), but this is beyond the scope of this study.

3.3 EPR Studies and Post Plasma Radical Decay Kinetics of NIPAM

The act of continuing polymerization, under certain conditions, after removal of the radiation source is an occasionally encountered situation in solid state polymerization, which is called as *post-irradiation polymerization* or *post-polymerization*. It is widely accepted that radiation-induced solid-state polymerization is characterized by the post effect, i.e. by the continuation of

the polymerization of solid monomers outside the irradiation zone. This is seen especially in case of retention of vacuum still on the irradiated species (or keeping medium radical-scavenger free).

In post irradiation studies the interpretation of the obtained data for investigation of radical decay reaction are easier than that in in-source polymerization studies, since effects resulting from chain propagation are not complicated by the superposition of a continuing chain initiation process. In addition, the post-irradiation technique has the advantage that polymer is not exposed to irradiation, which might lead to chain grafting, crosslinking, segmental fragmentations (degradations), etc.

EPR spectroscopy has been mainly used not only for detection of radical species involved in polymerization but also for quantification of radical species by selecting appropriate polymerization conditions and by operating the instrument at optimized conditions. Consequently, the rate constants for radical decay (k) can be easily determined.

3.3.1 Characterization of the Radical

After plasma treatment at about room temperature, NIPAM gives 3-line spectrum obtained with a very good resolution of the resonance signals. From the spectrum given in Figure 45 it can be inferred due to the α proton, at first 2 lines are observed with splitting 27 G, where each line in turn is split into two due to the coupling constant of one of the β proton, and each line further split into 2-line with coupling constant of the second β proton. Consequently a 3-line spectrum covering approximately 110 G of magnetic field with intensity ratio 2:4:2 or 1:2:1 is observed. This outcome is also furnishes us with some general interpretations about initiation step of plasma induced polymerization. The initiation step seems to involve the addition of a hydrogen atom to the vinyl group of NIPAM molecule, detached from another one.

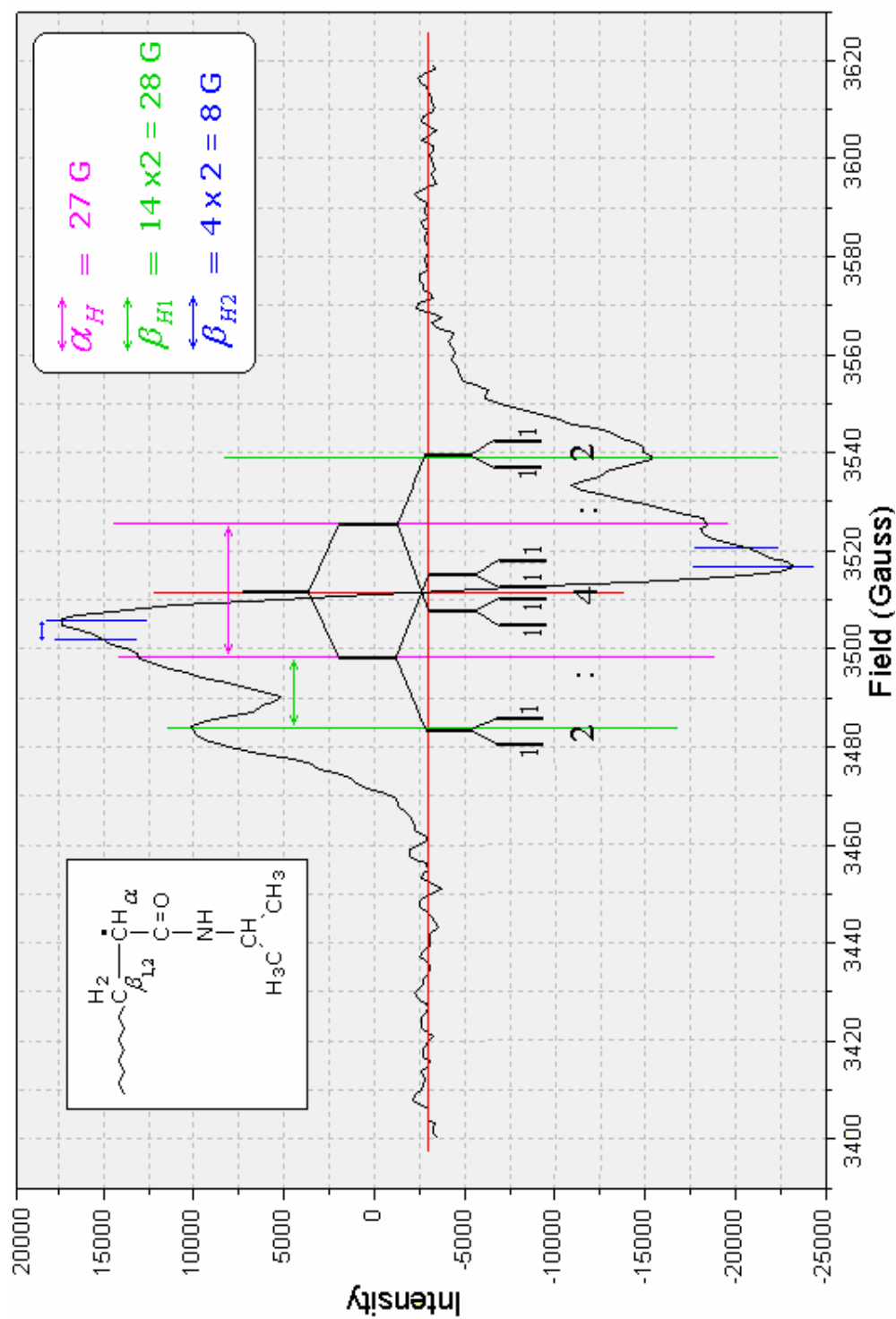


Figure 45 Splittings in stable radical formed under plasma conditions.

From the splitting data we can make some predictions on conformational properties of the propagating radical site on the growing chain. According to McConnell equation given in the introduction part $a_{\alpha}^H = Q_{CH}^H \cdot \rho_C$ the constant of Q_{CH}^C takes the value of 28 gauss which is common for a neutral π radical. By using this equation and $a_{\alpha}^H = 27$ gauss we determined unpaired spin density on the α -carbon atom as, ρ_C , 0.964. This means that 96.4% of the unpaired spin localized in $2p_z$ orbital of the α -carbon in this case. Furthermore by using the semiempirical equation of $a_{\beta}^H \cong B_1 + B_2 \cos^2 \theta$ where $B_1 \cong 4$ gauss, $B_2 \cong 50$ gauss, dihedral angle θ for both of protons in the β position having coupling constants of $\beta_1=28$ gauss and $\beta_2=8$ gauss are found approximately $\theta_1 = 46.1^\circ$ and $\theta_2 = 73.6^\circ$ respectively. The individual conformations can be identified as in Figure 46.

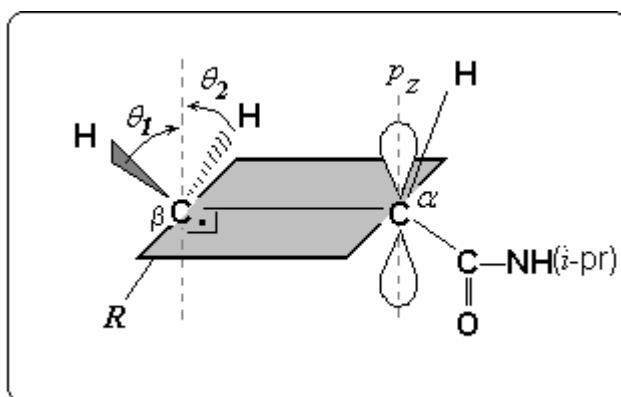


Figure 46 Conformation of protons in the β position in growing chain end.

Here θ is the angle between the p_z orbital axis of the unpaired electron and the projection of the C_{β} —H bond onto a plane perpendicular to the C_{α} — C_{β} bond and R is the reminder of the polymer chain. Due to difference in θ angles, β -protons cause unisotropic splittings.

3.3.2 Thermal Decay of the Radical Signal

In this case EPR data indicate the existence of one initiating radical only [197], suggesting that only the radical produced by the addition of hydrogen atoms survives for an appreciable period of time, which is enough for addition to neighboring monomer unit. In our studies we observed that after 5 weeks at about 20°C there is still EPR signal indicating radicalic activity (Figure 47).

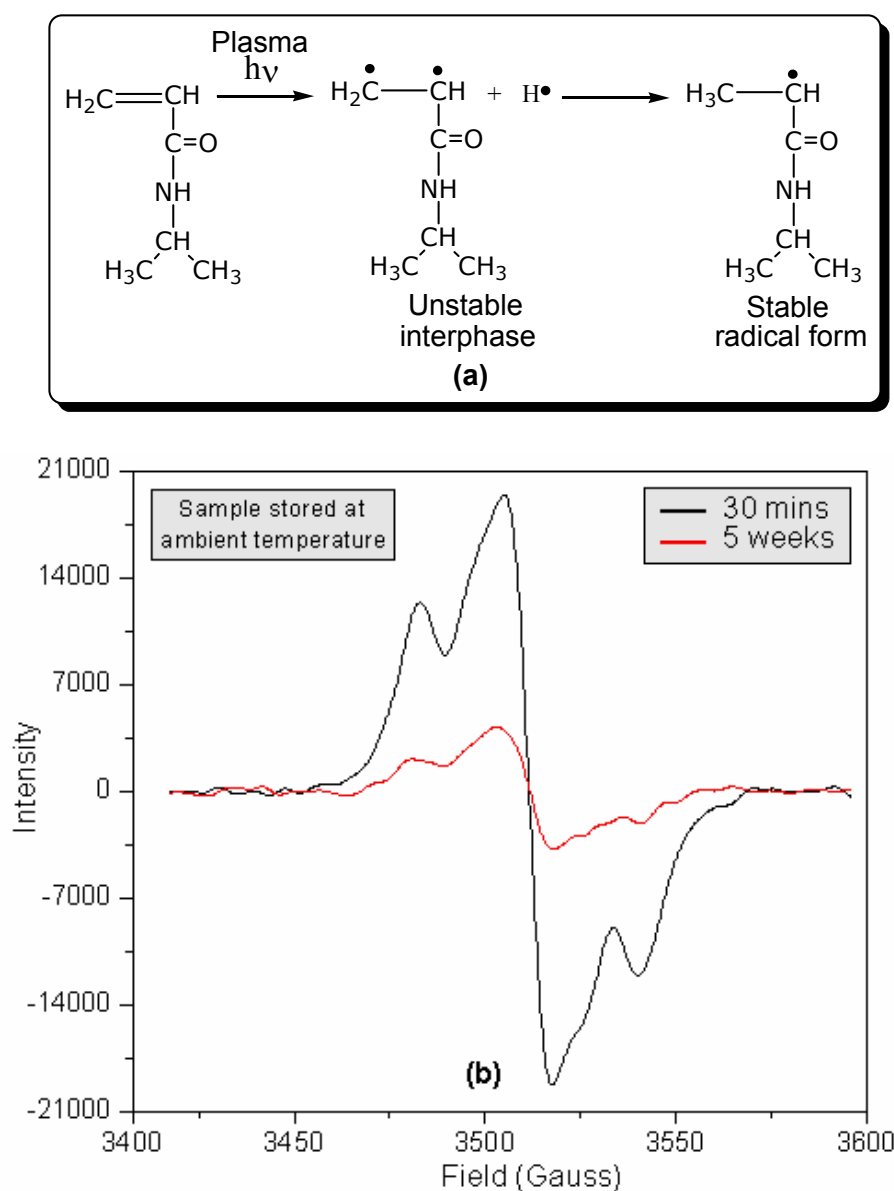


Figure 47 Formation of stable radical under plasma conditions and its signal endurance at ambient temperature in 5 weeks period.

On the other hand at elevated temperatures close to melting point of monomer, radical decays very quickly. For example, at 45°C the radical signal decays completely within 2 hours (Figure 48). This behavior can be explained by recombination of neighboring radicals with increased mobility at temperatures around melting point of the monomer. Therefore at about melting point of NIPAM, 64°C, recombination reaction overwhelms the first order decay reaction. For that reason, we determined the temperature of 30°C as upper limit for radical decay studies.

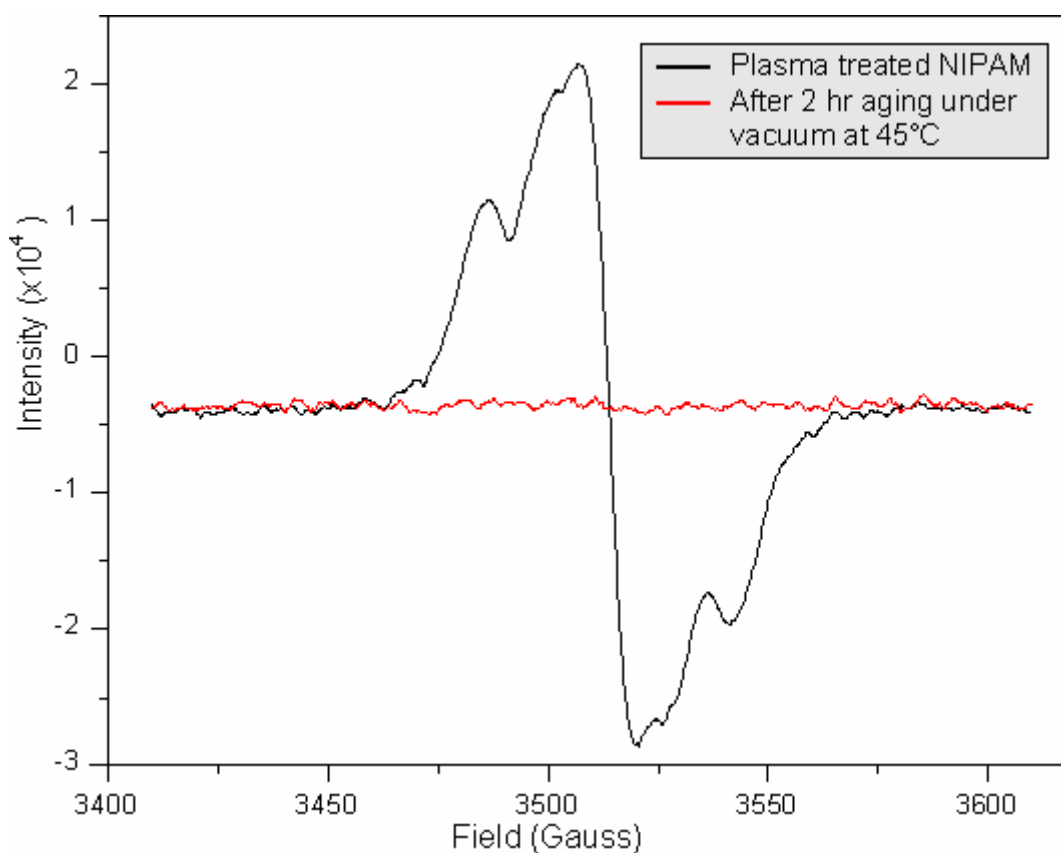


Figure 48 Rapid signal deterioration at 45°C in 2 hours.

From these outcomes we can infer that, at room temperatures plasma treated NIPAM signal is stable and decays very slowly, increasing the temperature promotes recombination type reactions with second order (or bimolecular) kinetics, most probably due to increased mobility of radicals.

3.3.3 Data Collection for Post-plasma Decay Kinetics of Propagating PNIPAM

In the present study, the observed radical signals in the EPR spectra of plasma processed NIPAM crystals are, in fact, due to the species responsible for the growth of the PNIPAM chain. Therefore, evaluation of some kinetic parameters of post-irradiation polymerization by help of quantified data obtained from monitoring the intensity change of radical signal of samples stored at predetermined constant temperatures is quite possible.

The selected temperatures are 7°C, 22°C and 30°C. Since signal shape does not change except decrease in peak-to-peak height one can infer that the existence of one type of radical. In Table 9, 10 and 11 decay data of plasma processed NIPAM at selected temperatures are presented. In these tables $[A]_0$, $[R^\bullet_0]$, $[A]_\infty$, $[R^\bullet]_\infty$, I_∞ and I_0 values are presented in shaded cells. Radical concentrations are calculated by help of standard solution of 4-amino-TEMPO. In investigation of standard solution signal, adjusted parameters of instrument are the same as in case of all other samples. The concentration of the standard is 2.97E-05 mol/L which corresponds to 1.79E+19 number of spin in volume of 1 L. This spin concentration value stands for 3.9E+6 absorption area of EPR signal. By using this number of spin/area ratio we calculate all $[R^\bullet]$ values in **Tables 9, 10 and 11**.

Table 9 Post-plasma decay data of sample stored at 7°C.

Time (hr)	$[A] \times 10^7$ (double int.)	$[R^\bullet] \times 10^{-4}$ mol/L	$[R^\bullet]/[R^\bullet_0]$	$\ln \frac{[R^\bullet_0] - [R^\bullet]_\infty}{[R^\bullet] - [R^\bullet]_\infty}$	I peak to peak height.	I/I_0	$\ln \frac{I_0 - I_\infty}{I - I_\infty}$
0	2.02	1.53	1.000	0.000	40724.7	1.00	0
24	1.85	1.41	0.920	0.264	40032.1	0.98	0,07
72	1.74	1.32	0.864	0.503	37586.4	0.92	0,39
96	1.68	1.28	0.833	0.663	37090.8	0.91	0,46
336	1.32	1.01	0.656	-	30926.7	0.76	-

Table 10 Post-plasma decay data of sample stored at 22°C.

Time (hr)	[A]x10 ⁷ (double int.)	[R•]x10 ⁻⁴ mol/L	[R•]/[R•] ₀	$\ln \frac{[R•]_0 - [R•]_\infty}{[R•] - [R•]_\infty}$	<i>I</i> peak to peak height.	<i>I</i> / <i>I</i> ₀	$\ln \frac{I_0 - I_\infty}{I - I_\infty}$
0	1.42	1.08	1.000	0.000	34282.6	1.00	0.00
24	1.37	1.04	0.965	0.068	30318.2	0.88	0.28
48	1.22	0.93	0.859	0.312	27110.5	0.79	0.59
72	1.10	0.84	0.777	0.550	25907.3	0.76	0.73
144	0.96	0.73	0.676	0.955	23561.6	0.69	1.09
240	0.90	0.68	0.631	1.205	22469.0	0.66	1.31
336	0.79	0.60	0.558	1.838	21339.6	0.62	1.62
408	0.70	0.53	0.492	3.354	19941.4	0.58	2.19
480	0.67	0.51	0.474	-	18127.0	0.53	-

Table 11 Post-plasma decay data of sample stored at 30°C.

Time (hr)	[A]x10 ⁷ (double int.)	[R•]x10 ⁻⁴ mol/L	[R•]/[R•] ₀	$\ln \frac{[R•]_0 - [R•]_\infty}{[R•] - [R•]_\infty}$	<i>I</i> peak to peak height.	<i>I</i> / <i>I</i> ₀	$\ln \frac{I_0 - I_\infty}{I - I_\infty}$
0	5.92	4.50	1.000	0.000	13180.0	1.00	0.00
24	3.66	2.78	0.618	0.577	8389.9	0.64	0.64
48	2.94	2.24	0.497	0.861	7001.6	0.53	0.94
72	2.45	1.86	0.414	1.115	5851.2	0.44	1.29
144	2.25	1.71	0.381	1.238	5329.2	0.40	1.49
240	1.42	1.08	0.241	2.045	3858.9	0.29	2.54
336	7.61	0.58	0.128	-	3057.7	0.23	-

The first derivative and its absorption signal of standard 4-amino-TEMPO are shown in Figure 49-a and Figure 49-b respectively. Double integral of the first derivative gives the quantity of the area under the absorption curve which is 3.9E+6 in our case.

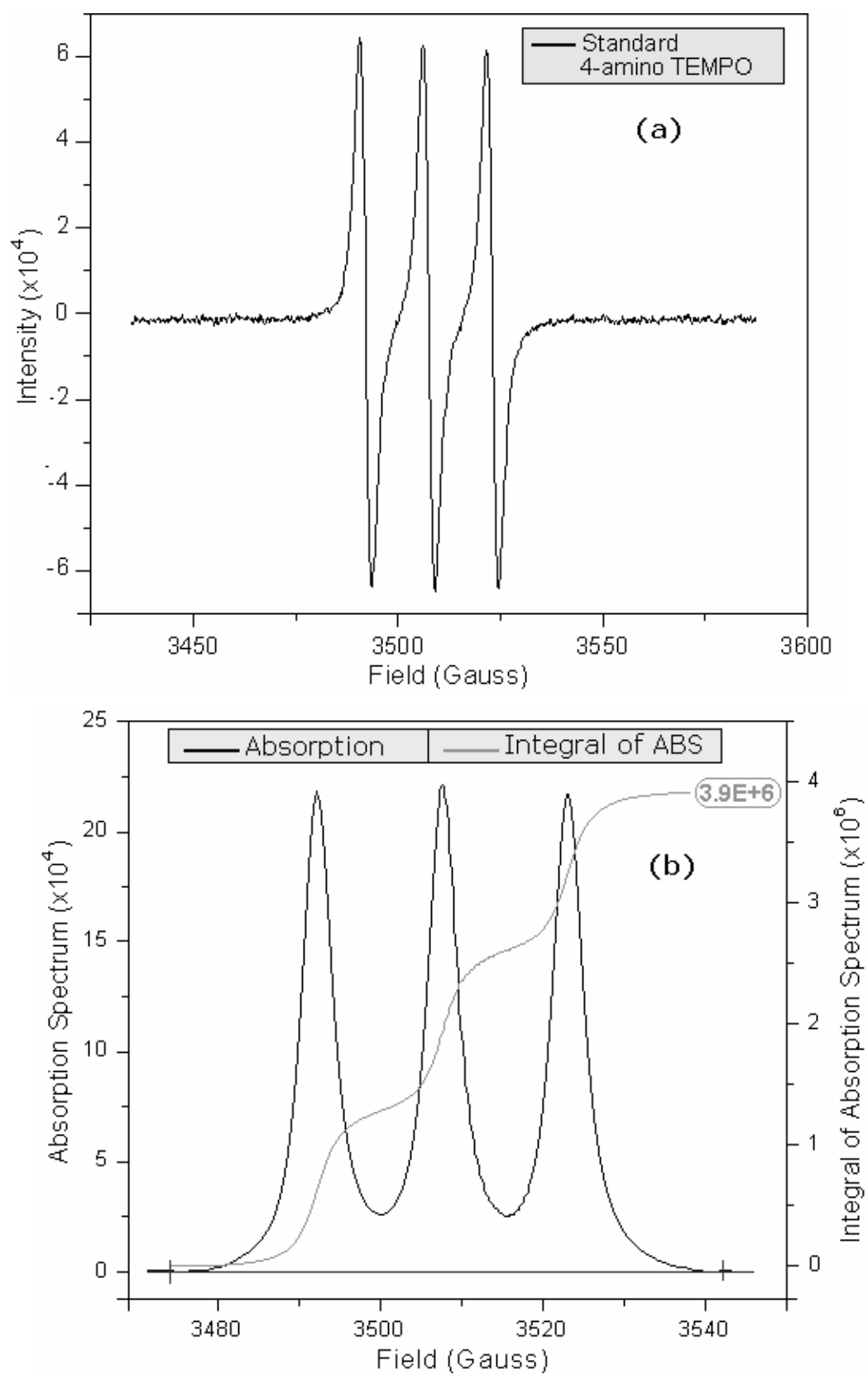


Figure 49 First derivative (a) and absorption (b) curves of 4-amino-TEMPO used as a standard for quantitation of spin concentration.

3.3.4 Decay Kinetics of PNIPAM Radicals

After plasma treatment of NIPAM monomer formation of monomeric radicals (nucleation mechanism) and propagation of polymerization reaction primarily in the surface layers of the NIPAM crystals are reported and discussed in the previous parts of the present thesis.

At suitable temperature range radical formed after plasma-processing in solid state decays by first-order kinetics. Decay kinetics of the radicals was studied by using two methods based on radical concentration and on peak-to-peak height. Considering $[R^\bullet_0]$ and I as the values at initial time and $[R^\bullet]_\infty$ and I_∞ as the values at time after which no significant change occurs in radical signal anymore, calculations were made.

The changes in the concentration of the initiating radical with time: at a series of constant temperatures are shown in Figure 51. At each temperature the rate of disappearance of radical was initially very high, but then decreased to a relatively low value. This will elucidate the kinetic picture of the post-irradiation radical decay reaction and the integrated rate equation for the first order radical decay can be written as

$$-\frac{d[R^\bullet_0]}{dt} = k_p[R^\bullet_0][M] \quad (3.1)$$

where; $[R^\bullet_0]$ is the initial concentration of the radical can be regarded as $[A_0]$, area under EPR curve and $[M]$ is the concentration of monomer [198]. Assuming the monomer concentration to remain unchanged by the first addition

$$-\frac{d[R^\bullet_0]}{dt} = k[R^\bullet_0] \quad (3.2)$$

where $k = k_p[M]$ so that the post irradiation polymerization reaction has the first-order kinetics with respect to initiating radical concentration, $[R^\bullet_0]$. This equation is derived by assuming 100 % conversion. Since the percent conversion during post polymerization of NIPAM did not reach 100 % conversion [199].

$$\ln \frac{([A] - [A]_\infty)}{([A]_0 - [A]_\infty)} = -k t \quad (3.3)$$

where; $[A]_\infty$ is the limiting radical concentration at the end of decay. The equation above is used to find the rate constants of the radical decay reaction at selected temperatures. After calculating $[R^\bullet]$ values by using radical concentration of the standard solution, $\ln([R^\bullet]_0 - [R^\bullet]_\infty / [R^\bullet] - [R^\bullet]_\infty)$ is plotted against time for each data set collected at three different temperatures in Figure 50. These plots are also obtained by use of peak-to-peak heights of the EPR signals and similarly used for the investigation of the radical decay mechanisms. Thus these peak-to-peak height data ($\ln([I]_0 - [I]_\infty / [I] - [I]_\infty)$) is also plotted against the same time values in similar graphs. To eliminate any confusion, y-axis named as $\ln([X]_0 - [X]_\infty / [X] - [X]_\infty)$ and $X = [R^\bullet]$ when using radical concentration values from double integrated signal areas; $X = [I]$ when using data set from peak-to-peak height measurements.

For determination of the limiting value, which is very important for the calculations of the radical decay process, the spectrums of the samples storing at constant temperature are taken at definite times, and by calculation of area under absorption curves, radical decay profiles are acquired. The radical decay profiles are belongs to the samples kept at three different temperatures as represented in Figure 51. In limiting condition, the active end of the propagating chain reaches a monomer free medium; anyway, it is possibly surrounded by other entangled polymer chains [200]. The same practical approach is employed for these plot sets where $X = [R^\bullet]$ and $X = [I]$.

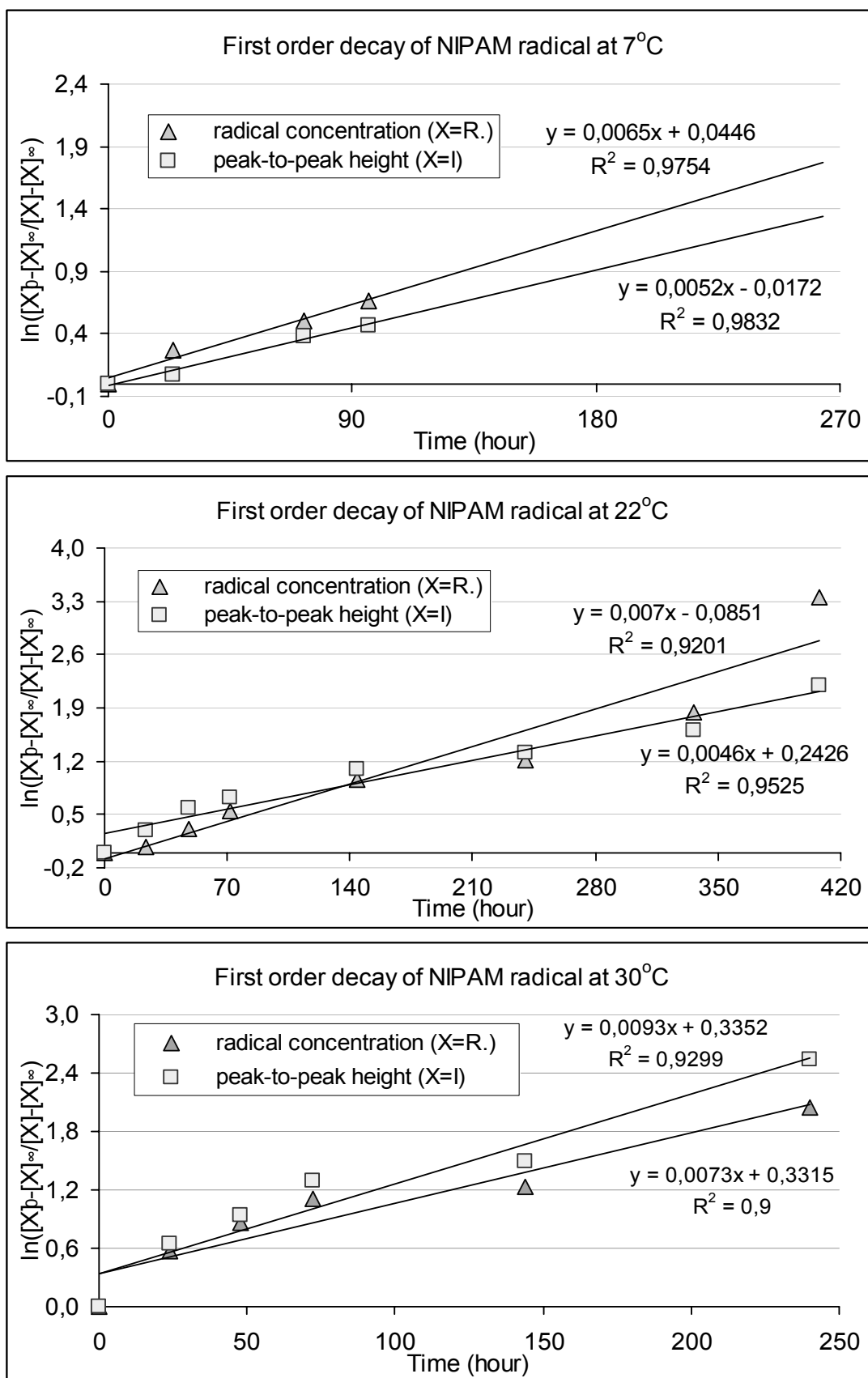


Figure 50 First-order decay lines of PNIPAM radicals at 7°C, 22°C and 30°C.

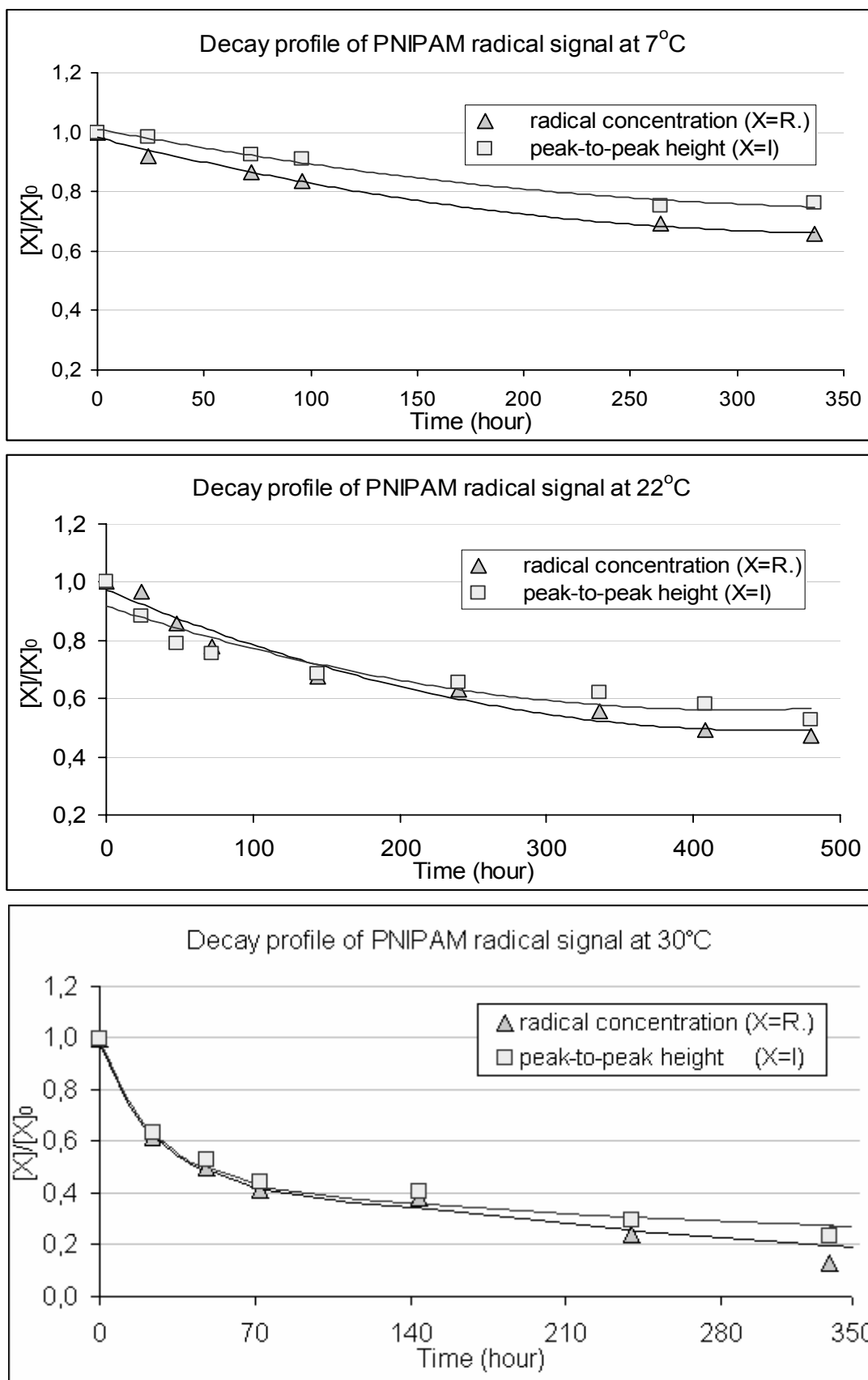


Figure 51 Decay radical profiles of PNIPAM radical at 7°C, 22°C and 30°C.

From the decay curves at different temperatures, it is obvious that PNIPAM radical decays according to the first-order mechanism between 7°C and 30°C. It can also be noticed that the polymerization of NIPAM in solid state proceeded for long periods of time after plasma processing. From the decay profiles of the radicals we can suggest that by elevation of the temperature decay kinetics of the radical deviates from the first-order mechanism and becomes look like a second-order one. This is an expected alteration because we proposed a bimolecular decay mechanism for the radical stored at 45°C previously. Continuous decrease in signal intensities are also depicted in PNIPAM radical's spectrum sets of first derivative curves and integrated absorption curves in Figures 53-58.

Two calculation methods are employed during radical decay studies. Calculated first-order rate constants from the slope of the radical decay lines for both methods are tabulated in Table 12. By using these data $\ln k$ is plotted against $1/T$ in Figure 52. In this time line obtained from radical concentration method data set possesses higher R-squared value.

Table 12 Data used in calculation of activation energy of post-plasma radical decay.

$T (^{\circ}\text{C})$	$T (\text{K})$	$1/T \times 10^{-3} (\text{K}^{-1})$	$k (\text{hr}^{-1})$ from radical concentration	$k (\text{hr}^{-1})$ from peak-to-peak height.	$\ln k$ from radical concentration	$\ln k$ from peak-to-peak height.
7	280.15	3.57	6.50 E-03	5.20 E-03	- 5.04	- 5.26
22	295.15	3.39	7.00 E-03	4.60 E-03	- 4.96	- 5.38
30	303.15	3.30	7.30 E-03	9.30 E-03	- 4.92	- 4.68

By using the Arrhenius equation,

$$k = Ae^{-E_a / RT} \quad (3.4)$$

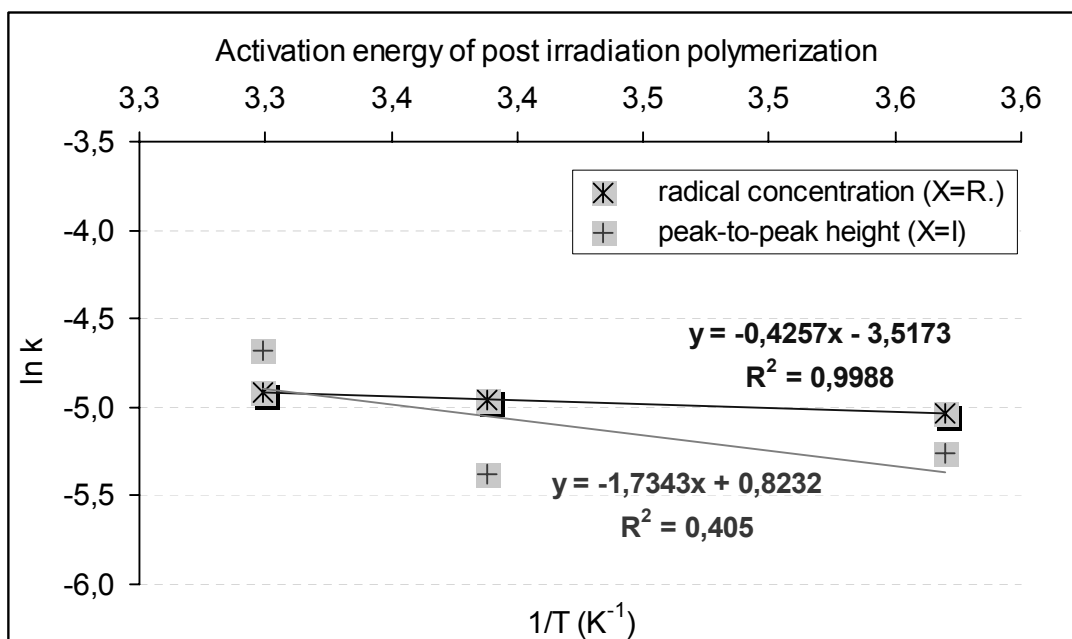


Figure 52 Arrhenius plots of first order PNIPAM radical decay.

The overall activation energy for post plasma radical decay was calculated as 3.53 joule/mol from radical concentration data and 14.42 joule/mol from peak-to-peak height data. From comparison of these two methods, it seems that, radical concentration method is more powerful in terms of statistical relative predictiveness than peak-to-peak height method. There is much less deviation from the linearity. Since the activation energy is positive, temperature rise would increase the post-plasma reaction rate. Relatively low value of the activation energy means that reaction can take place readily at suitable temperature range (Table 12).

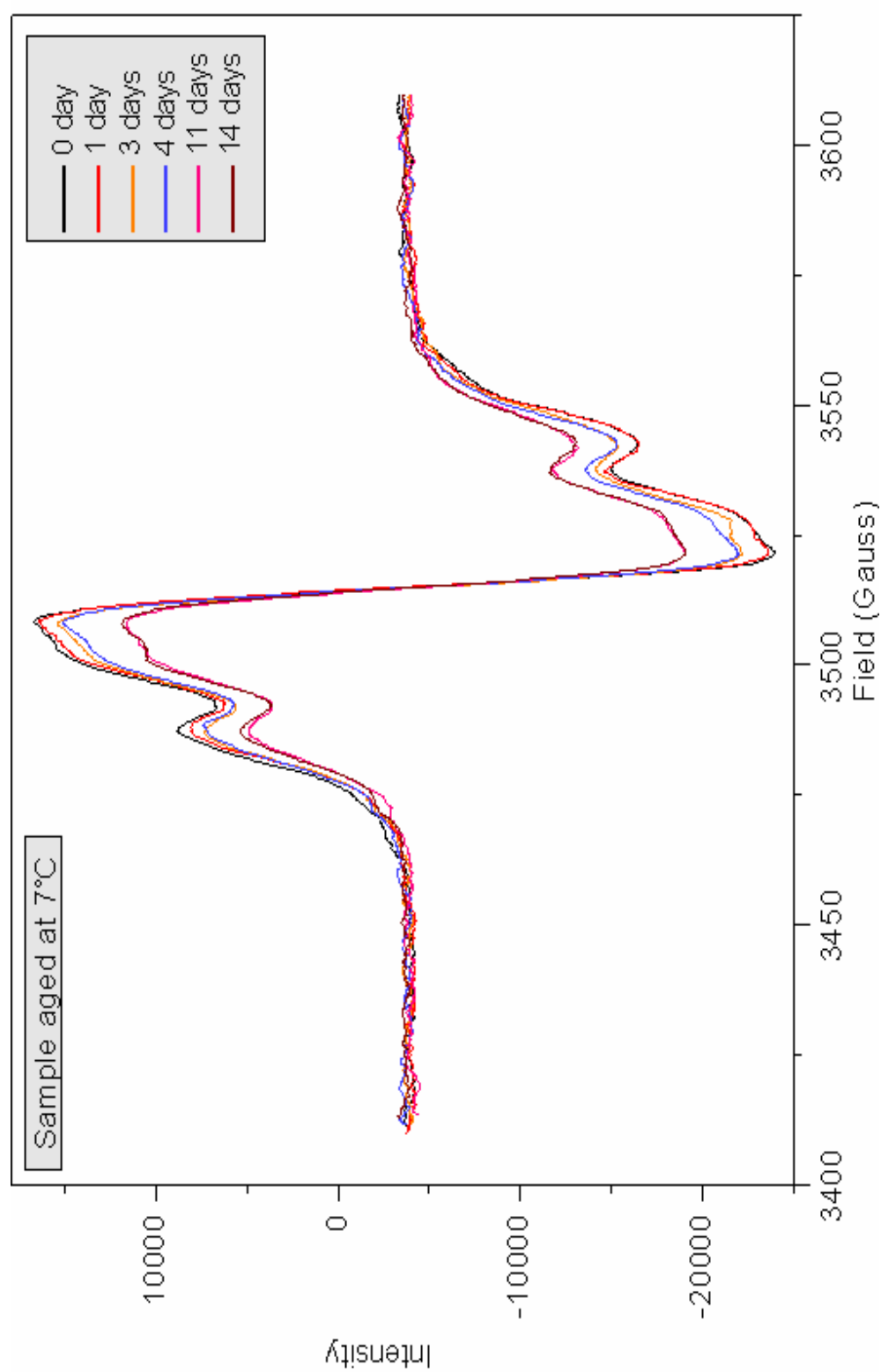


Figure 53 EPR spectrum set for PNIPAM radical decay at 7°C.

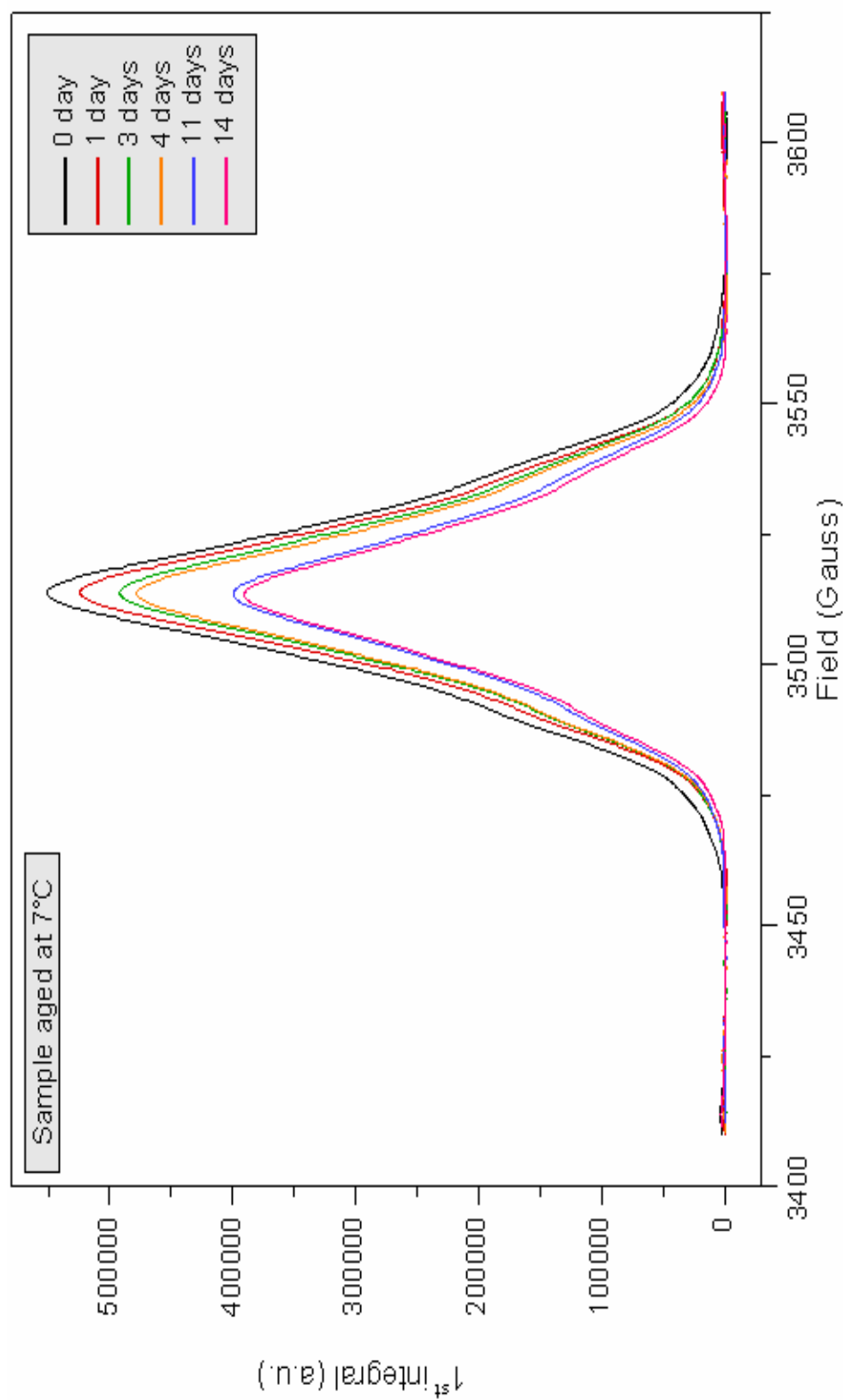


Figure 54 Integrated absorption curve set for PNIPAM radical decay at 7°C.

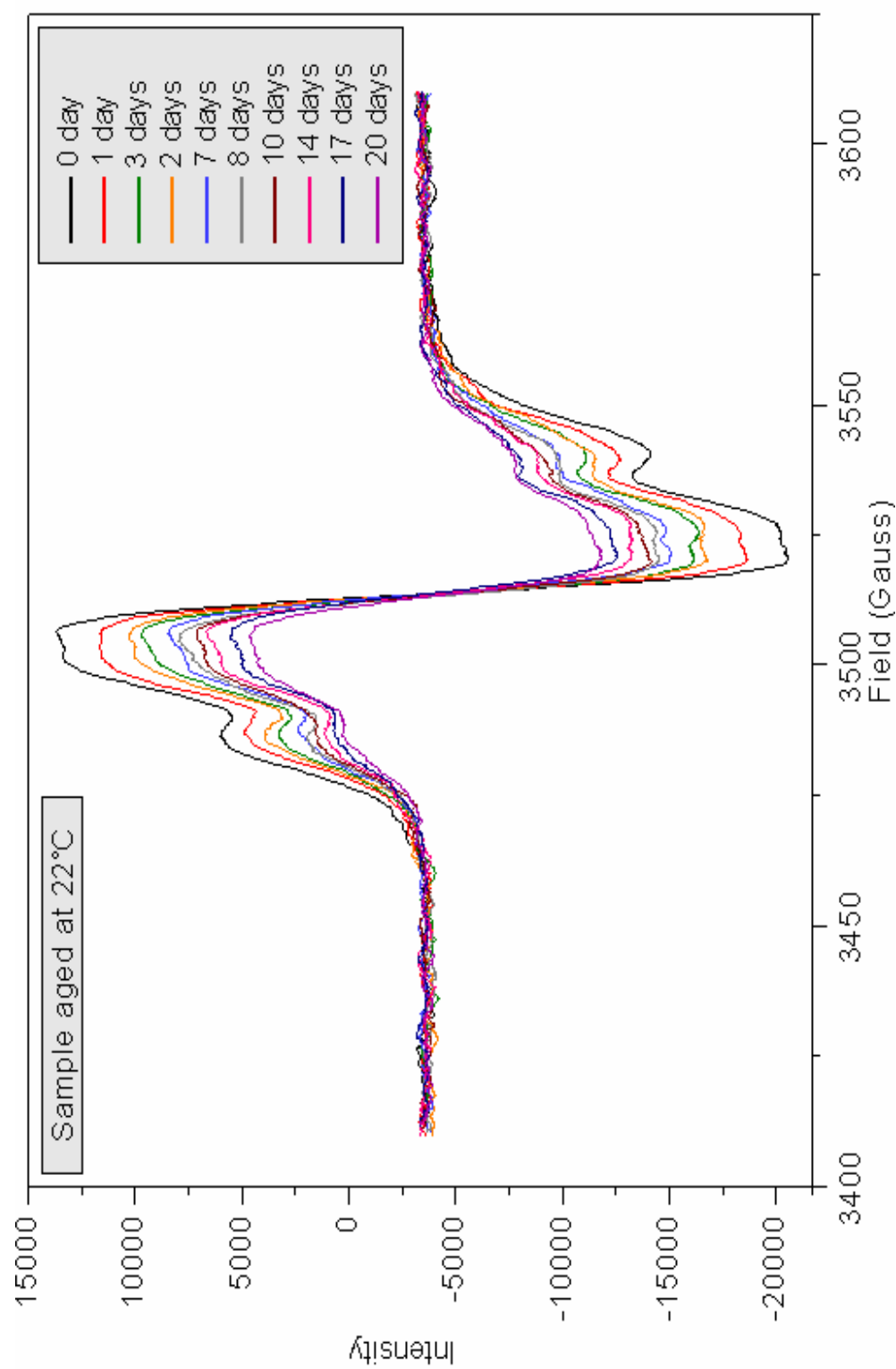


Figure 55 EPR spectrum set for PNIPAM radical decay at 22°C.

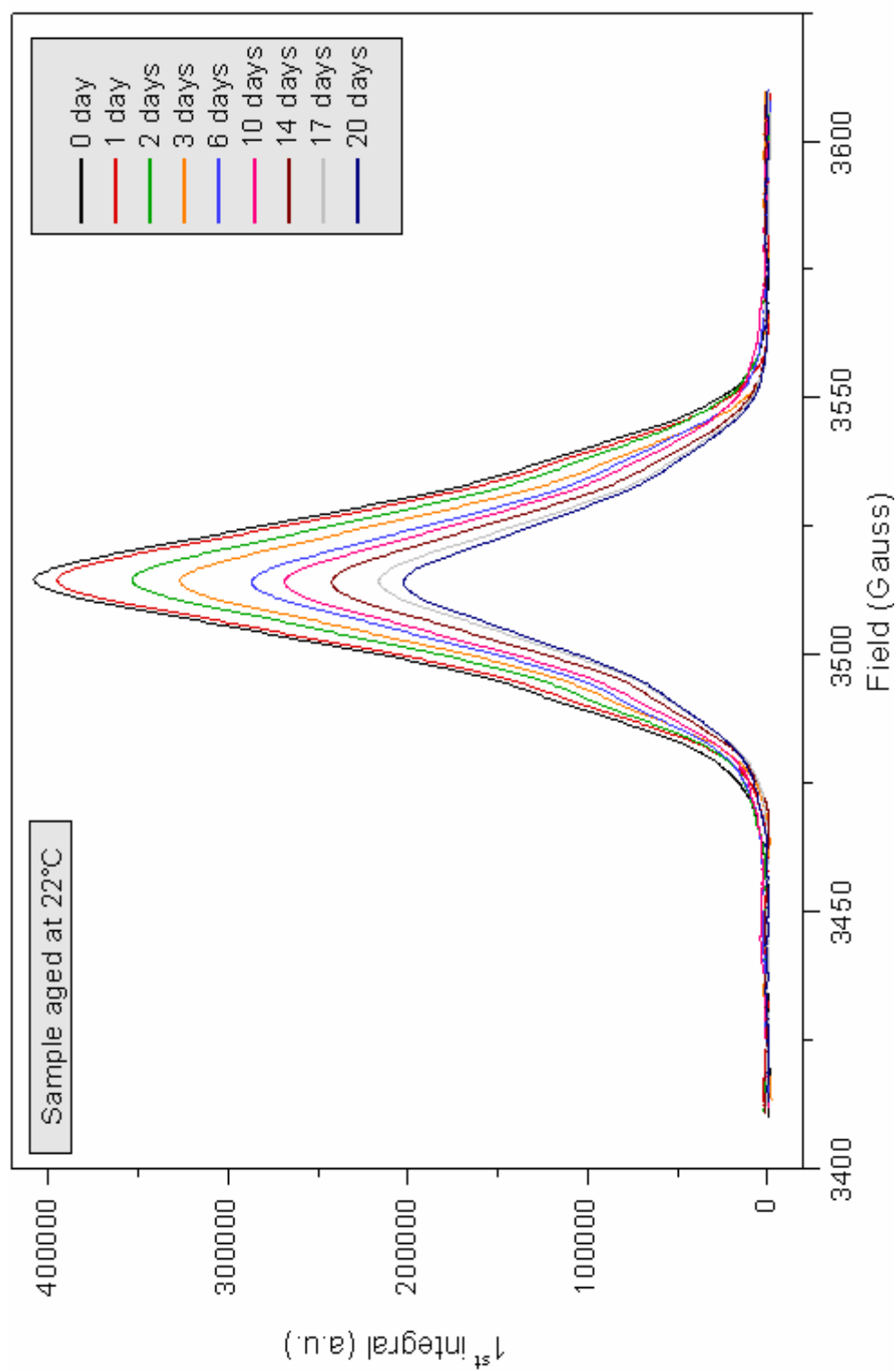


Figure 56 Integrated absorption curve set for PNIPAM radical decay at 22°C.

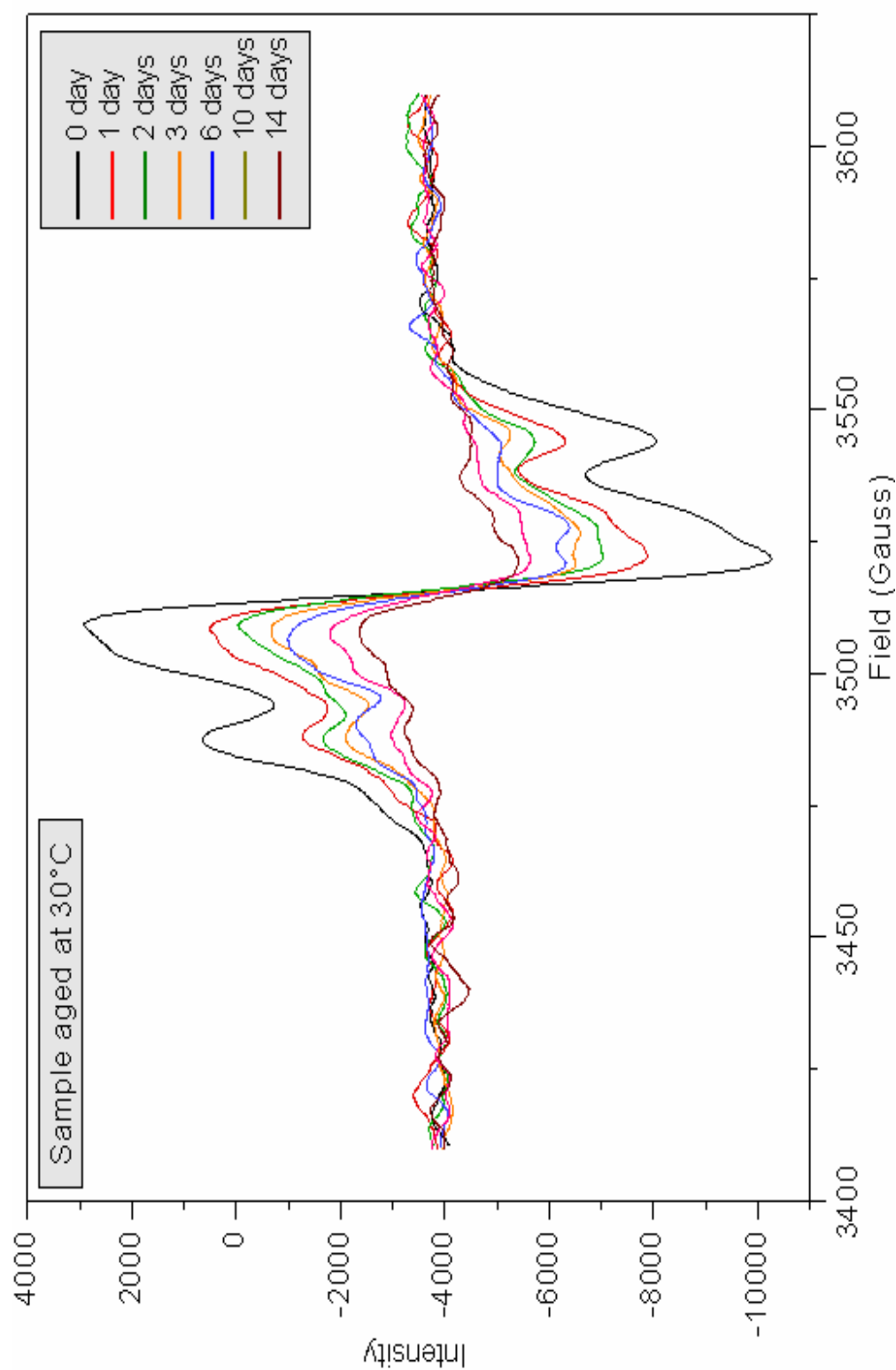


Figure 57 EPR spectrum set for PNIPAM radical decay at 30°C.

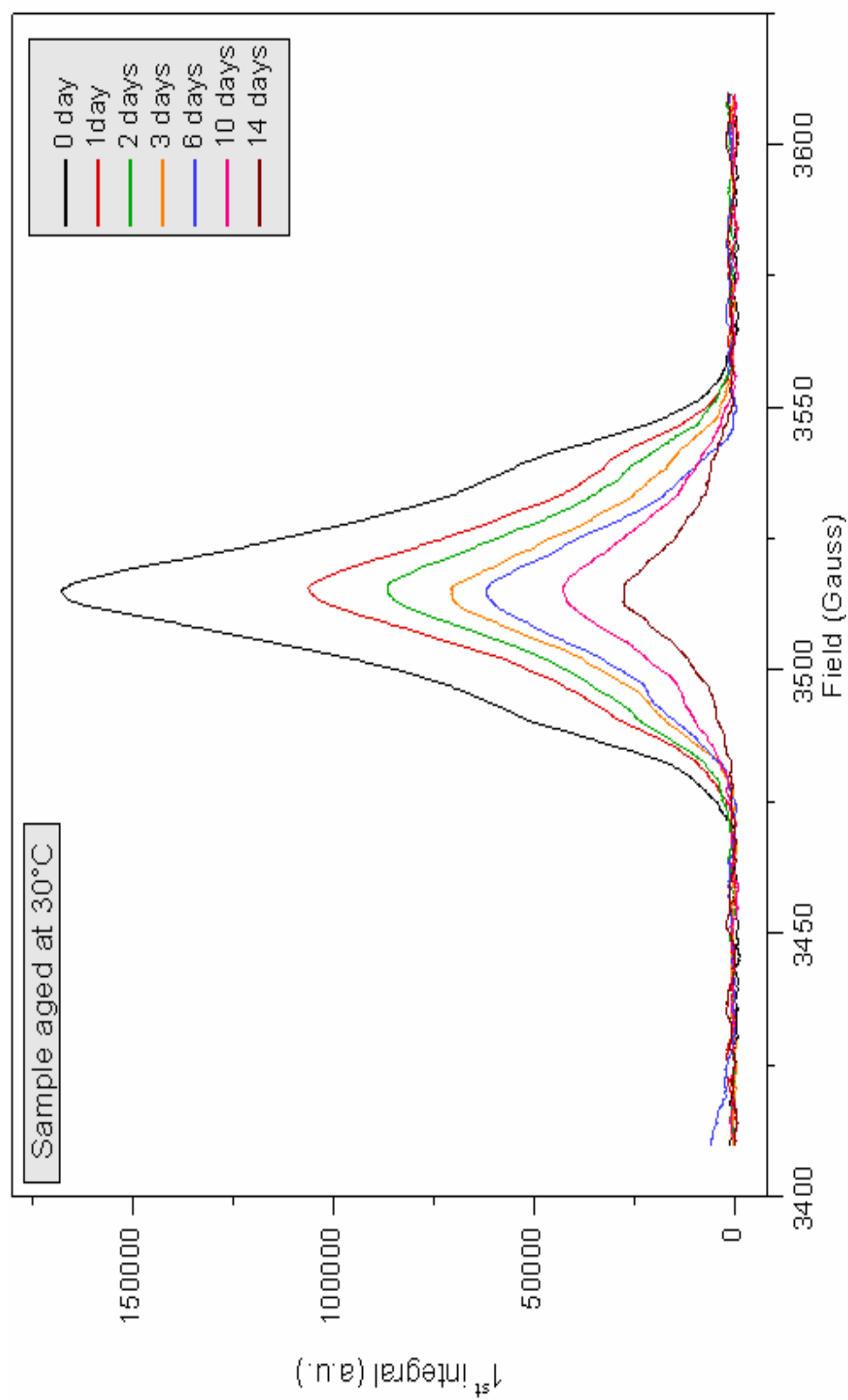


Figure 58 Integrated absorption curve set for PNIPAM radical decay at 30°C.

3.3.5 Peroxide Radical Formation and its Decay

Since the plasma treatment of crystalline state monomer creates radicals it is highly sensitive to oxygen (O_2) inhibition effect when air is introduced into the medium. Oxygen is known to inhibit radical reactions as far as it penetrates inside the solid crystal lattice of the monomer. In our case radicals formed intensively on the surface of the monomer crystals due to low penetration (approximately 100 Å) nature of the plasma as discussed before. For that reason when air is introduced into the medium by breaking vacuum radical signal of the plasma processed sample, exhibits a drastic fall in intensity and striking change in shape as shown in Figure 59.

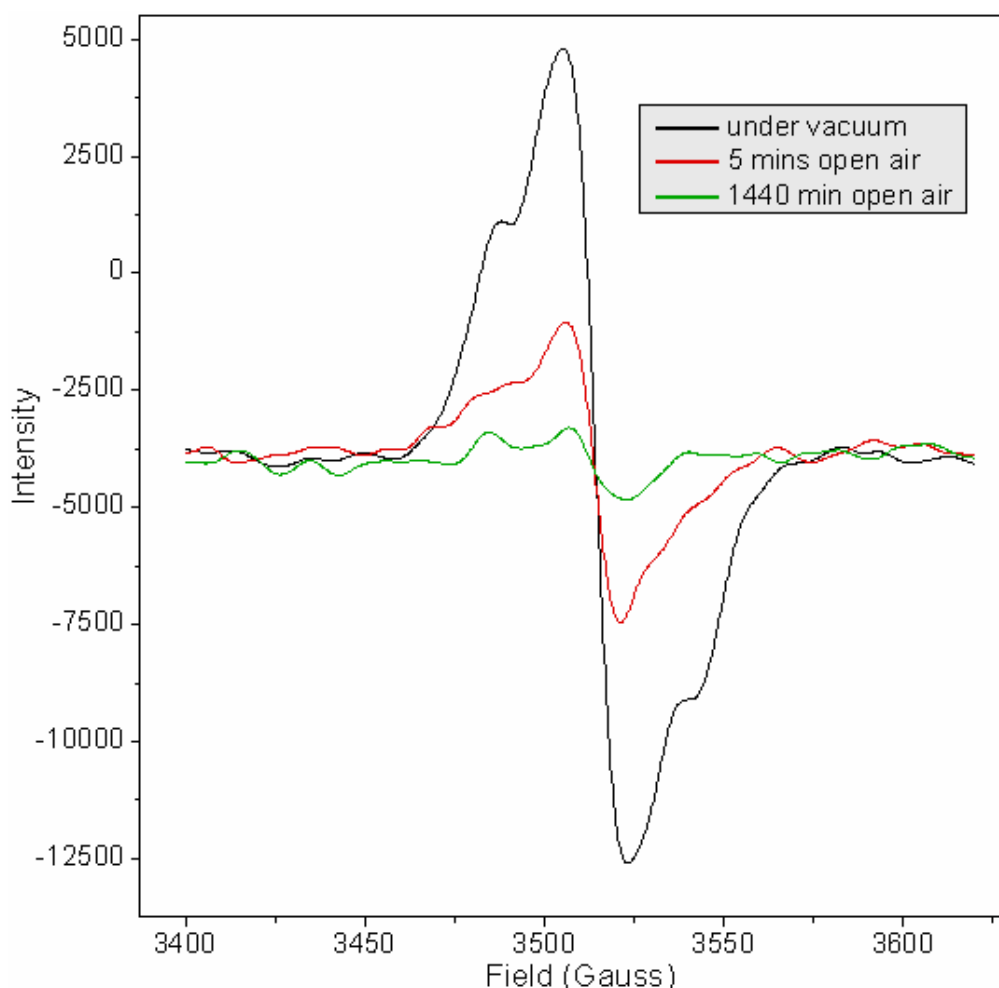


Figure 59 Peroxide formation by vacuum break and its decay at 22°C.

Additionally molecular oxygen can diffuse in the amorphous perimeters of the polymer formed by plasma treatment more rapidly than a highly crystalline medium. Formed peroxide radical is identified by its signal's well known shape which is asymmetric due to g-anisotropy (three principal components of the anisotropic g-tensor) and absence of hyperfine interactions (where the unpaired spin is mostly localized on outer oxygen atom) (Figure 60). This peroxide radical is not stable at room conditions and decays according to second-order kinetics. Its decay profile and second-order decay kinetic line at 22°C are given in Figure 61 and Figure 62 with respectively by using data set in Table 13.

Table 13 Second-order decay data of peroxide stored at 22°C.

Time (min)	$[A] \times 10^{-6}$ (double int.)	$[R^\bullet] \times 10^{-5}$ mol/L	$[R^\bullet]/[R^\bullet_0]$	$\frac{1}{[R^\bullet]} \times 10^5$
0	8.50	6.47	1.00	0.16
5	2.43	1.85	0.29	0.54
17	2.07	1.57	0.24	0.64
30	1.90	1.44	0.22	0.70
45	1.59	1.21	0.19	0.83
60	1.25	0.95	0.15	1.05
120	0.68	0.52	0.08	1.93
1440	0.44	0.33	0.05	3.01

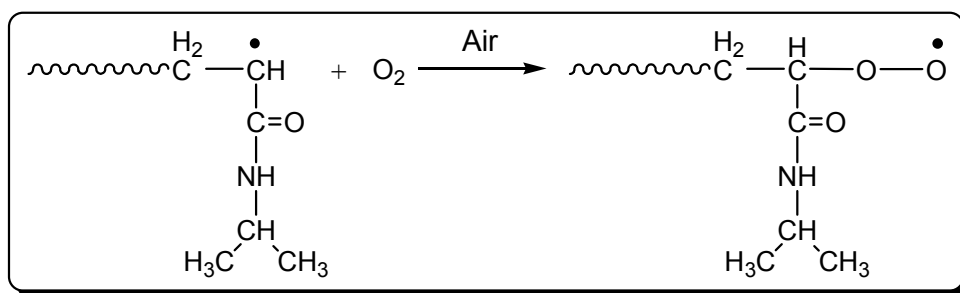


Figure 60 Formation of peroxide radical on growing chain end of PNIPAM.

After opening sample to air and quick formation of the peroxide radicals at the perimeters of its surface, shape of the 3-line spectrum undergoes a metamorphosis. Detailed change can be seen in Figure 63 especially after 5 minutes.

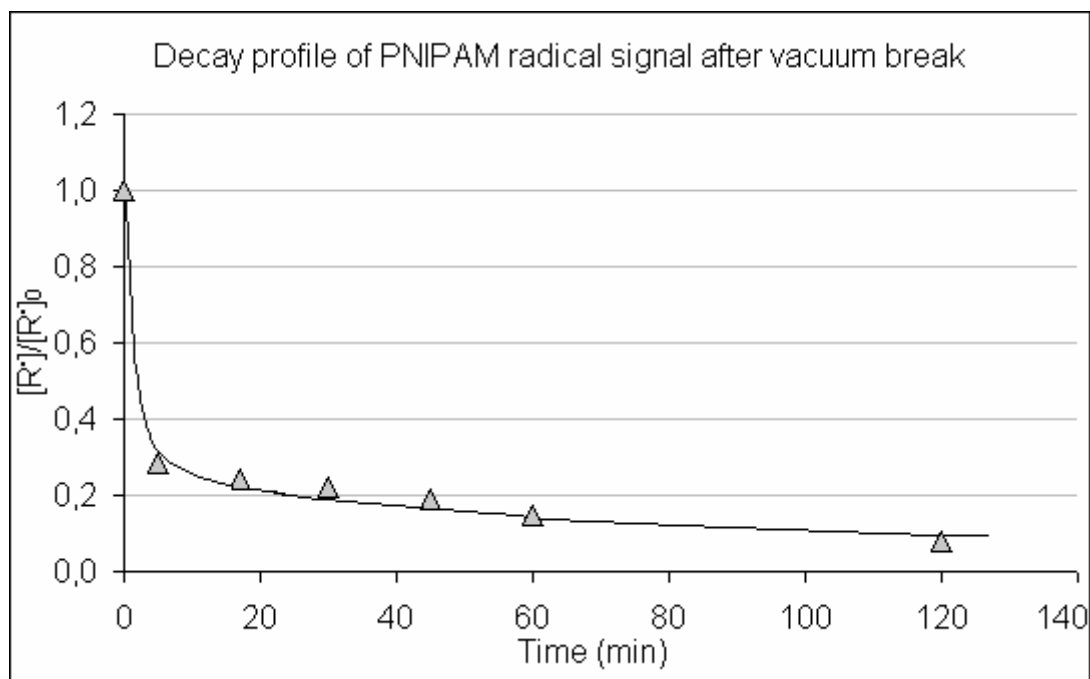


Figure 61 Decay radical profiles of peroxide radical at 22°C.

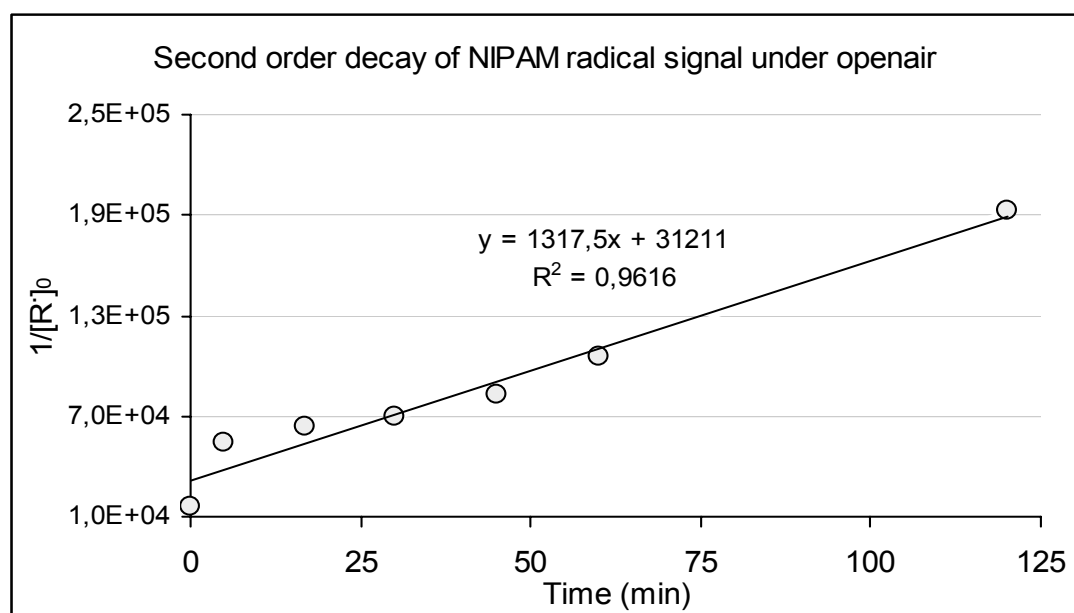


Figure 62 Second-order decay line of PNIPAM radicals at 22°C.

At the end of 1 day, the EPR signal which is taken at 1440 mins completely turns to typical peroxide radical in shape.

Second-order decay mechanism stipulates the following equation as rate expression

$$\frac{d[R^\bullet]}{dt} = -k_t [R^\bullet]^2 \quad (3.5)$$

and its integrated form

$$\frac{1}{[R^\bullet]} - \frac{1}{[R_0^\bullet]} = k_t t \quad (3.6)$$

where, k_t is the second-order decay constant at time of t . Due to reaction reaches completion, the use of limiting value in calculations is unnecessary (at the end of 24 hours peak intensity decreases to 5% of its initial value-see Table 9). From the beginning of this procedure both signals of propagating PNIPAM and its peroxide spectrums are superposed. For that reason we did not prefer to make alternative kinetic calculations by using peak-to-peak height data. Due to both coincided spectrum possess different shapes in nature making calculations with data based on method of peak-to-peak height will bring error markedly in the course of the shape transformation. Thus the second-order rate constant obtained from radical concentration method for the thermal decay reaction of peroxide radical is found $1.32\text{E}+03 \text{ L hour}^{-1} \text{ mol}^{-1}$. Integrated absorption spectrum set for decay process of peroxide radical at 22°C is given in Figure 64. Because integration of these absorption lines will give the absolute radicalic amount in the sample tube, use of radical concentration method gives the best results in kinetic calculations.

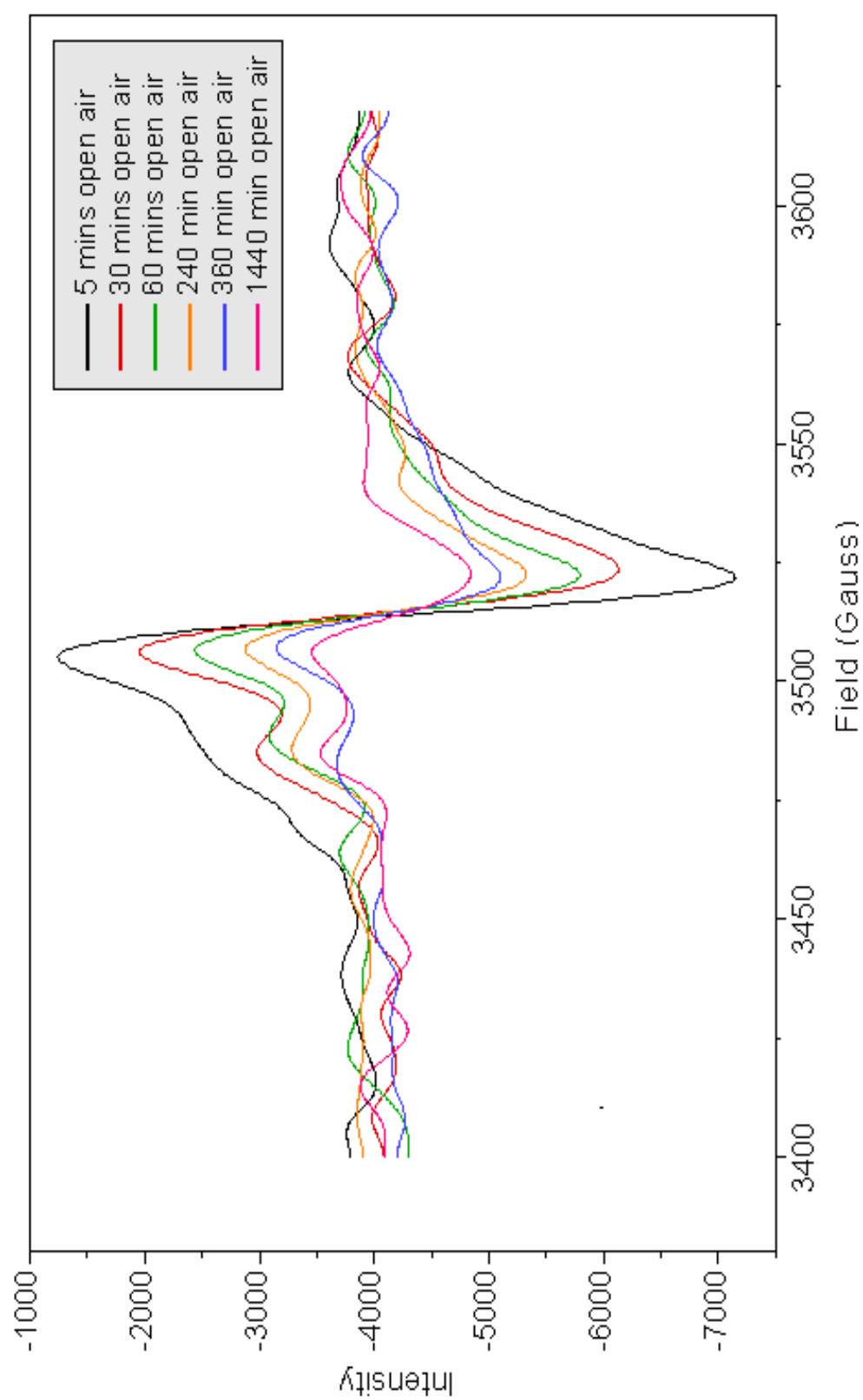


Figure 63 EPR spectrum set for decaying peroxide radical at 22°C.

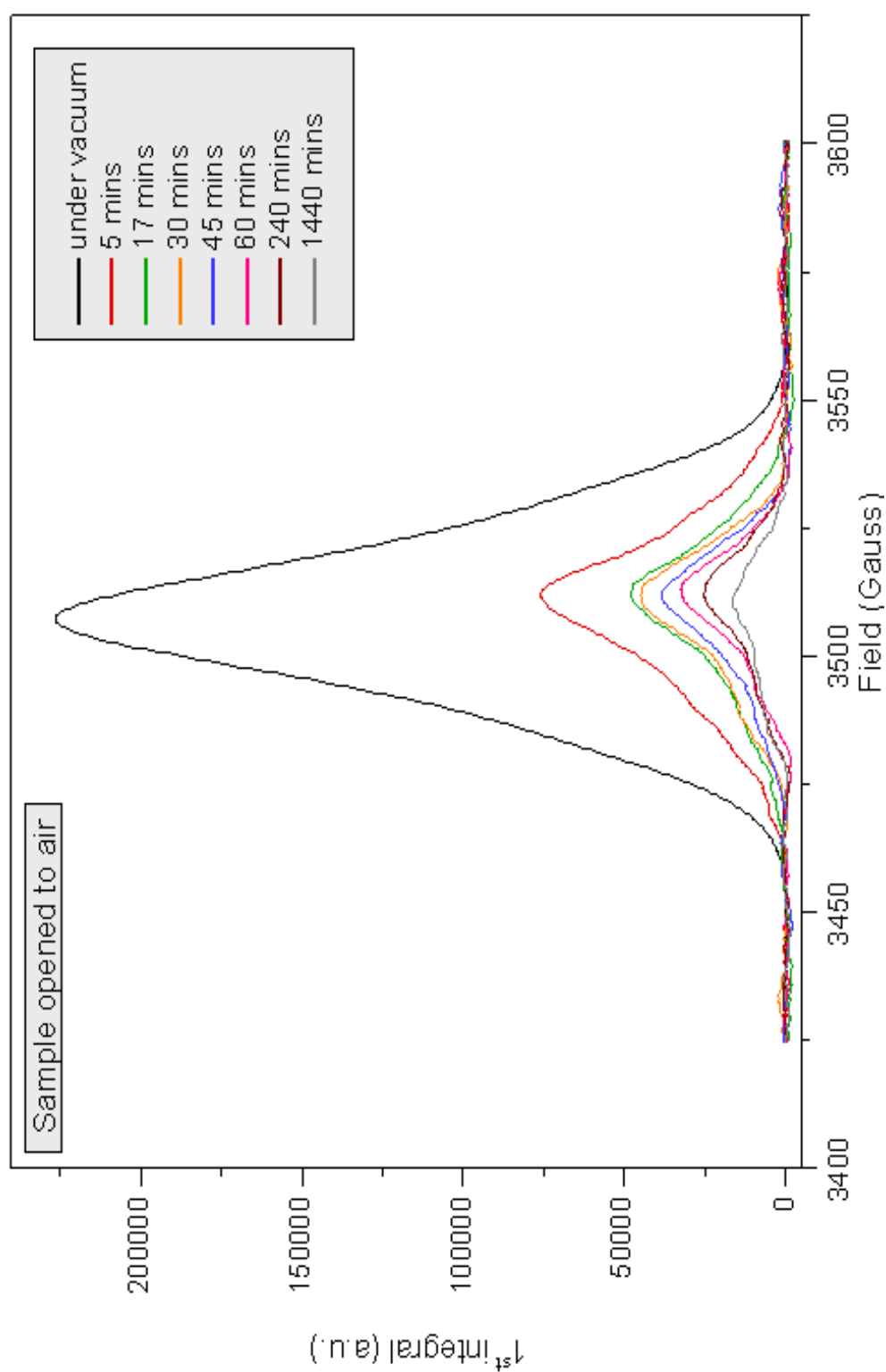


Figure 64 Integrated absorption curve set for decaying peroxide radical at 22°C.

CHAPTER 4

Conclusions

- Plasma can be proposed as a novel and clean radiation induced solid state polymerization method for N-isopropylacrylamide (NIPAM) leading to its crosslinked (gel) and linear polymers, both with similar thermal transition response characteristics.
- According to the X-ray data NIPAM and AAm are isomorphous, so that polymerization mechanisms of both monomers in solid state are most probably alike, with polymerization mechanisms being mostly diffusion controlled.
- Post plasma polymerizations of NIPAM in solid state proceed by radicalic mechanism as investigated by EPR method, as is also observed that post plasma polymerization reaction is highly sensitive to O₂ as a radical inhibitor.
- At temperatures between 5 to 30°C the radical is found to decay with first order kinetics whereas at temperatures close to 45°C (melting point of NIPAM), propagating radicals most probably recombine with a biradicalic kinetic.

REFERENCES

1. R. d'Agostino, P. Favia, C. Oehr, M. R. Wertheimer, *Plasma Processes and Polymers*, 2 (2005) pp. 7–15.
2. Mark D. Smith, *Plasma Technology*, Kirk-Othmer Encyclopedia of Chemical Technology, DOI: 10.1002/0471238961.1612011919130920.a01.
3. Hynek Biederman, *Plasma Polymer Films*, Imperial Collage Press, 2004.
4. W. Crookes, *Proceedings of the Royal Society of London*, Vol. 25. (1876 - 1877), pp. 303-314.
5. R. K. DeKosky, *Isis*, Vol. 67, No. 1. (Mar., 1976), pp. 36-60.
6. N. Tesla, U.S. Patent No: 454,622 *System of Electric Lighting*, Patented: June 1891.
7. N. Tesla, U.S. Patent No: 645,576 *System of Transmission of Electrical Energy*, Patented: March 1900.
8. N. Tesla, U.S. Patent No: 649,621 *Apparatus For Transmission of Electrical Energy*, Patented: May 1900.
9. Donald M. Mattox, *The Foundations of Vacuum Coating Technology*, Noyes Publications, 2003.
10. L. Tonks and I. Langmuir, *Physical Review*, Vol. 33, (1929) pp. 195-211.

11. L. Tonks, The American Journal of Physics, Vol. 35, (1967) pp. 857-858.
12. K.T. Compton, I. Langmuir, Reviews of Modern Physics, Vol. 2, No.2, pp. (1930) 123-242.
13. I. Langmuir, K.T. Compton, Reviews of Modern Physics, Vol. 3, No.2, pp. (1931) 191-258.
14. I. Langmuir and H.A. Jones, Physical Review, Vol. 31, (1928) pp. 357-404.
15. A. Bogaerts, E. Neyts, R. Gijbels, J. van der Mullen, Spectrochimica Acta Part B 57 (2002) pp. 609–658.
16. C.-M. Chan, T.-M. Ko, H. Hiraoka, Surface Science Reports, 24 (1996), pp. 1-54.
17. F.S. Denes, S. Manolache, Progress in Polymer Science, 29 (2004) pp. 815–885.
18. Y. Uyama, K. Kato, and Y. Ikada, Advances in Polymer Science, Vol. 137, (1998), pp. 1-39.
19. E.F. Castro Vidaurre, C.A. Achete, F. Gallo, D. Garcia, R. Simão, A.C. Habert, Materials Research, Vol. 5, No. 1, (2002) pp. 37-41.
20. P.K. Chu, J.Y. Chen, L.P. Wang, N. Huang, Materials Science and Engineering R 36 (2002) pp. 143–206.
21. D. Klee, H. Höcker, Advances in Polymer Science, Vol. 149, (2000) pp. 1-57.

22. B. Gupta, N. Anjum, *Advances in Polymer Science*, Vol.162, (2003) pp. 35-61.
23. E. Sardella, P. Favia, R. Gristina, M. Nardulli, R. d'Agostino, *Plasma Processes and Polymers*, 3, (2006) pp. 456–469.
24. K.S. Siow, L. Britcher, S. Kumar, H.J. Griesser, *Plasma Processes and Polymers* 3, (2006) pp. 392–418.
25. A. Ohl, K. Schröder, *Surface and Coatings Technology* 116–119 (1999) pp. 820–830.
26. M. Dhayal, H.G. Jeong, J.S. Choi, *Applied Surface Science* 252 (2005) pp. 1710–1715.
27. F. Brétagnot, A. Valsesia, G. Ceccone, P. Colpo, D. Gilliland, L. Ceriotti, M. Hasiwa, F. Rossi, *Plasma Processes and Polymers*, 3, (2006) pp. 443–455.
28. Y.I Kima, T.S Park, J.H Kanga, M.C Lee, J.T Kimb, J.H Park, H.K Baik, *Sensors and Actuators B* 119 (2006) 592–599.
29. M. Laroussi, *Plasma Processes and Polymers* 2, (2005) 391–400.
30. A.G. Whittaker, E.M. Graham, R.L. Baxter, A.C. Jones, P.R. Richardson, G. Meek, G.A. Campbell, A. Aitken, H.C. Baxter, *Journal of Hospital Infection*, 56 (2004) pp. 37–41.
31. D.B. Haddow, S. MacNeil, R.D. Short, *Plasma Processes and Polymers*, 3, (2006) pp. 419–430.

32. A.R.-Addamo, C. Riccardi, E. Selli, R. Barni, M. Piselli, G. Poletti, F. Orsini, B. Marcandalli, M.R. Massafra, L. Meda, *Surface and Coatings Technology* 174 –175 (2003) pp. 886–890.
33. Shijian Luo, Chapter 1 - *Surface Modification Of Textile Fibers And Cords By Plasma Polymerization For Improvement Of Adhesion To Polymeric Matrices*, Doctoral thesis, Division of Research and Advanced Studies of the University of Cincinnati (2002).
34. E. Selli, C. Riccardi, M.R. Massafra, B. Marcandalli, *Macromolecular Chemistry and Physics*, 202, (2001) pp. 1672-1678.
35. Y. Taga, *Surface and Coatings Technology* 112 (1999) pp. 339–346.
36. L. Bromberg, D.R. Cohn, A. Rabinovich, J. Heywood, *International Journal of Hydrogen Energy* 26 (2001) pp. 1115–1121.
37. J.D. Dale, M.D. Checkel and P.R. Smy, *Prog. Energy Combust. Sci.* Vol. 23., (1997) pp. 379-398.
38. M.S. Chung, S.H. Kim, M.J. Jeon, B.K. Kang, *Displays* 28 (2007) pp. 74–80.
39. H. Sato, T. Sakai, M. Matsubayashi, K. Hata, H. Miyake, K. Hiramatsu, A. Oshita, Y. Saito, *Vacuum* 80 (2006) pp. 798–801.
40. M. Taniguchi, H. Nagao, M. Hiramatsu, Y. Ando, M. Hori, *Diamond & Related Materials* 14 (2005) pp. 855–858.
41. D. Hegemann, H. Brunner, C. Oehr, *Surface and Coatings Technology* 142-144 (2001) pp. 849-855.

42. S. Yu. Suzdal'tsev and R. K. Yafarov, Technical Physics Letters, Vol. 27, No. 8, 2001, pp. 656–658.
43. H. Kinoshita, I. Ippei, H. Sakai, N. Ohmae, Diamond & Related Materials, (Unedited Accepted Manuscript) doi: 10.1016/j.diamond.2007.08.0
44. H. Brachhold, R. Müller, G. Pross, *Plasma Reactions*, Ullmann's Encyclopedia of Industrial Chemistry, DOI: 10.1002/14356007.a20_427, Wiley-VCH Verlag.
45. E. Pfender, Plasma Chemistry and Plasma Processing, Vol. 19, No. 1, (1999) pp. 1-31.
46. E. Gariboldi, B. Previtali, Journal of Materials Processing Technology 160 (2005) pp. 77–89.
47. W.J. Xu, J.C. Fang, Y.S. Lu, Journal of Materials Processing Technology, 129 (2002) pp. 152-156.
48. J. Hu, H.L. Tsai, International Journal of Heat and Mass Transfer 50 (2007) pp. 833–846.
49. A. Ureña, E. Otero, M.V. Utrilla, C.J. Múñez, Journal of Materials Processing Technology 182 (2007) pp. 624–631.
50. D. Elanski, J.-W. Lim, K. Mimura, M. Isshiki, Journal of Alloys and Compounds 421 (2006) pp. 209–216.
51. D. Elanski, J.-W. Lim, K. Mimura, M. Isshiki, Journal of Alloys and Compounds 413 (2006) pp. 251–258.
52. T. Hammer, Contrib. Plasma Phys. 39 (1999) 5, pp. 441-462.

53. Hyun-Ha Kim, *Plasma Processes and Polymers* 1, (2004) pp. 91–110.
54. Amutha Rani, D. et al., *Plasma treatment of air pollution control residues*, *Waste Management* (2007), doi:10.1016/j.wasman.2007.06.008.
55. H. Huang, L. Tang, *Energy Conversion and Management* 48 (2007) pp. 1331–1337.
56. G. Herdrich, M. Auweter-Kurtz, *Vacuum* 80 (2006) pp. 1138–1143.
57. M. Betti, L. Aldave de las Heras / *Spectrochimica Acta Part B* 59 (2004) pp. 1359–1376.
58. W. Yang, H. Zhang, A. Yu, Q. Jin, *Microchemical Journal*, 66 (2000) pp. 147-170.
59. U Fantz, *Plasma Sources Science and Technology*, 15 (2006) S137–S147.
60. M. Tajmar, J. González, G. Saccoccia, G. Noci, H. Laakso, *Planetary and Space Science* 50 (2002) pp. 1355 – 1360.
61. H. Sou, Y. Takao, T. Noutsuka, Y. Mori, K. Uemura, H. Nakashima, *Vacuum* 59 (2000) pp. 73-79.
62. K-Y. Lee, S-i. Honda, M. Katayama, T. Kuzuoka, Y-G. Baek, S. Ohkura, K. Aoki, T. Hirao, K. Oura, *Thin Solid Films* 464–465 (2004) pp. 194– 198.
63. H.J. Lee, H.J. Yoon, J.K Lee, *Computer Physics Communications* 177 (2007) pp. 106–107.

64. C. Seoul, W-J. Song, Journal Of Materials Science: Materials In Electronics 12 (2001) pp. 51-55.
65. P.A. Hobson, S. Wedge, Jon A.E. Wasey, I. Sage, W.L. Barnes, Advanced Materials, Communications, 14, No. 19 (2002) pp. 1393-1396.
66. B.R. Rogersa, T.S. Cale, Vacuum 65 (2002) pp. 267–279.
67. S. J. Pearton, D.P. Norton, Plasma Processes and Polymers 2, (2005) pp. 16–37.
68. Banqiu Wu, Journal of Vacuum Science and Technology B 24(1) Jan/Feb 2006, pp. 1-15.
69. André Anders, Surface and Coatings Technology 156 (2002) pp. 3–12.
70. W. Chen, L. Dai, H. Jiang, T.J. Bunning, Plasma Processes and Polymers, 2, (2005) pp. 279–292.
71. M.C. Jobanputra, M.F. Durstock, S.J. Clarson, Journal of Applied Polymer Science, Vol. 87, (2003) pp. 523–528.
72. A. Hiratsuka, I. Karube, Electroanalysis, 12, No. 9, (2000) pp. 695-702.
73. A. Partridge, P. Harris, T. Hirotsu, S. Kurosawa, Plasmas and Polymers, Vol. 5, No. 3/4, (2000) pp. 191-200.
74. D.C. Schram, J.A.M. van der Mullen and M.C.M. van de Sanden Plasma Physics and Controlled Fusion 36, (1994) B65-B78.

75. U. Vohrer, D. Hegemann C. Oehr, *Analytical & Bioanalytical Chemistry*, 375 (2003) pp. 929–934.
76. *Cold Plasma Materials Fabrication: From Fundamentals to Applications*, Alfred Grill, Wiley-IEEE Press, 1994.
77. J.R. Hollahan, R.S. Rosler, In *Thin Film Processes*, Editors: Vossen J.L. and Kern W., pp. 335, New York: Academic Press, 1978.
78. Chuan Li, J.H. Hsieh, W.M. Huang, *Surface & Coatings Technology* 198 (2005) pp. 372– 378.
79. C. Busch, I. Möller and H. Soltwisch, *Plasma Sources Sci. Technol.* 10 (2001) pp. 250–259.
80. J.T. Gudmundsson, *Journal of Physics D: Applied Physics* 35 (2002) pp. 328–341.
81. H. Yasuda, In *New Methods of Polymer Synthesis*, Vol. 2, Editors: Ebdon J.R. and Eastmond G.C., pp. 161, Blackie Academic & Professional, 1995.
82. H. Yasuda, In *Thin Film Processes*, Editors: Vossen J.L. and Kern W., pp. 361, New York: Academic Press, 1978.
83. H. Yasuda Q. Yu, *Plasma Chemistry and Plasma Processing*, Vol. 24, No. 2 (2004) pp.325-351.
84. J.G.A. Terlingen, Chapter 2 - Introduction of functional groups at polymer surfaces by Glow discharge techniques, Doctoral thesis, Universiteit Twente (1993).

85. P. Krüger, R. Knes, J. Friedrich, *Surface and Coatings Technology* 112 (1999) pp. 240–244.
86. D.F. O’Kane, K.L. Mittal, *Journal of Vacuum Science and Technology* Vol.11, Issue 3 (1974) pp. 567-569.
87. J. P. Chang, J. W. Coburn, *Journal of Vacuum Science Technology A* Vol.21, Issue5 (2003) pp. 145-151.
88. F.L. Hopwood, T.J. Phillips, *Proc. Phys. Soc. (London)*, 50, (1938) pp. 438.
89. Adolphe Chapiro, *Radiation Chemistry of Polymeric Systems*, Wiley (Interscience), New York, 1962.
90. E. Collinson, F.S. Dainton, G.S. McNaughton, *Transactions of the Faraday Society*, 53, (1957) pp. 476-498 (2 parts).
91. E. Collinson, F.S. Dainton, G.S. McNaughton, *Transactions of the Faraday Society*, 53, (1957) pp. 357-362.
92. Arthur Charlesby, *Atomic Radiation and Polymers*, Pergamon, New York 1960.
93. Y. Tabata, In *Vinyl Polymerization Part II*, Editor: George E. Ham, 305, Marcel Dekker 1969.
94. J.V. Schmitz, E.J. Lawton, *Science*, 113, (1951) pp. 718.
95. R. Worrall, S. H. Pinner, *Journal of Polymer Science*, 34, (1959) pp. 229.

96. E. Collinson, F.S. Dainton, and H.A. Gillis, *Journal of Physical Chemistry*, 63, (1959) pp. 909.
97. A. Chapiro, V. Stannett, *J. chim. phys.*, 56, (1959) pp. 830.
98. T.H. Fadner, H. Morawetz, *Journal of Polymer Science*, 45 (1960) pp. 475.
99. J. Benard, *Reactivity of Solids*, J.H. de Boer *et. al.*, Elsevier, Amsterdam, 1960, pp. 362.
100. W.E. Garner, T.J. Jennings, *Proceedings of the Royal Society of London Ser. A* 224, (1954) pp. 460-471.
101. G. Adler, W. Reams, *The Journal of Chemical Physics*, Vol.32, No:6, (1960) pp. 1698-1700.
102. H. Morawetz, *Science*, Vol. 152, No. 3723 (6 May 1966) pp. 705-711.
103. J. Žurakovska-Országh, A. Gumulka, *Radiat. 4th Symp. Radiat. Chem. Hungary, Prep., B/34. Proc. 4th Tihany Symp. Radt. Chem. Akad. Kiado, Budapest*, (1976) pp. 401-409.
104. J. Žurakovska-Országh, A. Gumulka, *Radiation Physics and Chemistry*, Vol. 15, (1980) pp. 571-575.
105. J. Žurakovska-Országh, A. Gumulka, J. Bartnik, *Radiation Physics and Chemistry*, Vol. 23, No. 4, (1984) pp. 385-392.
106. A.J. Restaino, R. B. Mesrobian, H. Morawetz, D. S. Ballantine, G. J. Dienes, and D. J. Metz, *Journal of American Chemical Society*, 78, (1956) pp. 2939-2943.

107. G. Adler, *The Journal of Chemical Physics*, Vol. 31, (1959) 848.
108. B. Baysal, G. Adler, D. Ballantine, P. Colombo, *Journal of Polymer Science*, Vol. 44, (1960) pp. 117-127.
109. I.N. Levine, *Physical Chemistry*, 4th Edition, McGraw-Hill, Inc., 1995.
110. P.B. Ayscough, *Electron Spin Resonance in Chemistry*, London, Methuen; New York, Barnes & Noble, 1967.
111. Atkins, P. W., *Atkins' Physical Chemistry*, 1940-Oxford; New York: Oxford University Press, (2002).
112. Silbey, Robert J., *Physical Chemistry*, New York: Wiley, (2001)
113. S.Ya. Pshezhetskii, A.G. Kotov, V.K. Milinchuk, V.A. Roginskii, and V.I. Tupikkov, *EPR of free radicals in radiation chemistry*, translated from Russian by P. Shelnitz, translation edited by T. Pick., New York, Wiley, 1974.
114. C.C. Rowlands, D.M. Murphy In *Encyclopedia of Spectroscopy and Spectrometry*, Vol. 1 (A-L), Editors: J.C. Lindon, G.E. Tranter, J.L. Holmes, Chapter: EPR Spectroscopy, Theory, (2000) pp. 445-456.
115. H.M. McConnell, *J. Chem. Phys.*, 24 (1956) pp. 632.
116. R. Bersohn, *J. Chem. Phys.*, 24 (1956) pp. 1054.
117. S.I. Weissman, *J. Chem. Phys.*, 25 (1956) pp. 890.
118. H.S. Jarrett, *J. Chem. Phys.*, 26 (1956) pp. 1289.

119. J.R. Bolton, A. Carrington, A.D. McLachlan, *Molec. Phys.* 5 (1962) pp. 31.
120. D.B. Chesnut, *J. Chem. Phys.*, 29 (1958) pp. 43.
121. D. Lazdins, M. Karplus, *J. Chem. Phys.*, 44 (1966) pp. 1680.
122. W. Derbyshire, *Molec. Phys.* 5 (1962) pp. 225.
123. C. Heller, H.M. McConnell, *J. Chem. Phys.*, 32 (1960) pp. 1535.
124. D.K. Roylance, *An EPR Investigation of Polymer Fracture*, University of Utah, Ph.D. Dissertation (1968) pp. 146.
125. A.J. Nanassy, *Journal of Applied Polymer Science*, Vol. 16 (1972) pp. 2577-2582.
126. I.Y. Galaev and B. Mattiasson, *TIBTECH* Vol. 17 (August 1999) pp. 335-340.
127. A.S. Hoffman, P.S. Stayton, *Macromolecular Symposia*, 207 (2004) pp. 139-151.
128. E.S. Gil, S.M. Hudson, *Progress in Polymer Science*, 29 (2004) pp. 1173–1222.
129. Allan S. Hoffman, *Clinical Chemistry* 46:9 (2000) pp. 1478-1486.
130. T. Shimoboji, E. Larenas, T. Fowler, A.S. Hoffman, P.S. Stayton, *Bioconjugate Chemistry*, 14 (2003) pp. 517-525.
131. P. Gupta, K. Vermani and S. Garg, *Drug Discovery Today (DDT)*, Vol. 7, No. 10 (May 2002) pp. 569-579.

132. B. Jeong and A. Gutowska, *TRENDS in Biotechnology* Vol.20 No.7 July (2002) pp. 305-311.
133. A. Kikuchi, T. Okano, *Progress in Polymer Science*, 27 (2002) pp. 1165–1193.
134. H.-Hui Lin, Y.-Ling Cheng, *Macromolecules*, 34 (2001) pp. 3710-3711.
135. T. Magoshi, H. Ziani-Cherif, S. Ohya, Y. Nakayama, T. Matsuda, *Langmuir*, 18 (2002) pp. 4862-4872.
136. M. Kurisawa, M. Yokoyama, T. Okano, *Journal of Controlled Release*, 69 (2000) pp. 127–137.
137. J.-Christophe Leroux, E. Roux, D. Le Garrec, K.Hong , D.C. Drummon, *Journal of Controlled Release* 72 (2001) pp. 71–84.
138. Jean-François Lutz, Ö. Akdemir, A. Hoth, *Journal of American Chemical Society*, 128 (2006) pp. 13046-13047.
139. E.H. Sprech, A. Neuman, H.T. Neher, U.S. Pat. 2,773,063; Rohm & Haas, (1956).
140. CIBA, Ltd., Br. Pat. 746,747; (1956).
141. E.H. Sprech, A. Neuman, H.T. Neher, H. T. Br. Pat. 772,196; Rohm & Haas, (1956).
142. X. Wang, X. Qiu, C. Wu, *Macromolecules*, 31 (1998) pp. 2972.
143. X. Wang, C. Wu, *Macromolecules*, 32 (1999) pp. 4299.
144. G. Zhang, C. Wu, *J. Am. Chem. Soc.*, 123 (2001) pp. 1376.

145. W. Zhang, S. Zou, C. Wang, X. Zhang, J. Phys. Chem. B, 104 (2000) pp. 10258.
146. T. L. Lowe, J. Virtanen, H. Tenhu, Langmuir, 15 (1999) pp. 4259-4265.
147. N. Hatto, T. Cosgrove, M.J. Snowden, Polymer 41 (2000) pp. 7133–7137
148. T.L. Lowe, J. Virtanen, H. Tenhu, Polymer, 40 (1999) pp. 2595–2603.
149. E. C. Muniz, G. Geuskens, Macromolecules, 34 (2001) pp. 4480-4484.
150. T. L. Lowe, H. Tenhu, Macromolecules, 31 (1998) pp. 1590-1594.
151. R. Xie, Y. Li, L-Yin Chu, Journal of Membrane Science 289 (2007) pp. 76–85.
152. R. Xie, L-Yin Chu, W-Mei Chen, W. Xiao, H-Dong Wang, J-Bo Qu, Journal of Membrane Science 258 (2005) pp. 157–166.
153. Y.V. Pan, R.A. Wesley, R. Luginbuhl, D.D. Denton, B.D. Ratner, Biomacromolecules, 2 (2001) pp. 32-36.
154. S. Ohya, Y. Nakayama, T. Matsuda, Biomacromolecules, 2 (2001) pp. 856-863.
155. J. R. Caldwell, R. Gilkey, U.S. Pat. 2,882,255; Eastman Kodak Co., (1959).
156. H.G. Schild, Progress in Polymer Science, Vol. 17 (1992) pp.163-249.
157. K. Otake, H. Inomata, M. Konno, S. Saito, Macromolecules 23 (1990) pp. 283-289.

158. S. Hirotsu, Journal of the Physical Society of Japan, 56 (1987) pp. 233-242.
159. K. Otake, Inomata, H.; Konno, M.; Saito, S. Journal of Chemical Physics, 91 (1989) pp. 1345-1350.
160. A. Ben-Naim, *Hydrophobic Interactions*, Plenum Press, New York (1980).
161. H. Dautzenberg, Y. Gao, M. Hahn, Langmuir, 16 (2000) pp. 9070-9081.
162. M. Shibayama, T. Tanaka, *Volume phase transition and related phenomena of polymer gels*, Advances in Polymer Science, 109 (1993) pp. 1–62.
163. G. Chen, A.S. Hoffman, Nature, Vol. 373 (1995) pp. 49-52.
164. A.S. Hoffman, et al., Journal of Biomedical Materials Research, 52 (2000) pp. 577–86.
165. S. Fujishige, K. Kubota, I. Ando, Journal of Physical Chemistry, 93 (1989) pp. 3311-3313.
166. C. Boutris, E. G. Chatzi, C. Kiparissides, Polymer Vol. 38 No. 10, (1997) pp. 2567 -2570.
167. H.Y. Liu, X.X. Zhu, Polymer 40 (1999) pp. 6985–6990.
168. H. Feil, Y.H. Bae, J. Feijen, S.W. Kim, Macromolecules, 26 (1993) pp. 2496-2500.

169. H.G. Schild, D.A. Tirrell, *Journal of Physical Chemistry*, 94 (1990) pp. 4352-4356.
170. E.I. Tiktopulo, V.E. Bychkova, J. Rička, O.B. Ptitsyn, *Macromolecules*, 27 (1994) pp. 2879-2882.
171. T. Tokuhiro T. Amiya, A. Mamada, T. Tanaka, *Macromolecules*, 24 (1991) pp. 2936-2943.
172. Y. Maeda, T. Higuchi, I. Ikeda, *Langmuir*, 16 (2000) pp. 7503-7509.
173. A. Kirpach, D. Adolf, *Macromolecular Symposia*, 237 (2006) pp. 7–17.
174. R. Walter, J. Rička, Ch. Quellet, R. Nyffenegger, Th. Binker, *Macromolecules*, 29 (1996) pp. 4019-4028.
175. C.K. Chee, S. Rimmer, I. Soutar, L. Swanson, *Polymer* 42 (2001) pp. 5079-5087.
176. X. Wang, X. Qiu, C. Wu, *Macromolecules*, 31 (1998) pp. 2972-2976.
177. M. Meewes, J. Rička, M. de Silva, R. Nyffenegger, Th. Binkert, *Macromolecules*, 24 (1991) pp. 5811-5816.
178. K. Kubota, S. Fujishig, I. Ando, *Journal of Physical Chemistry*, 94 (1990) pp. 5154-5158.
179. Lay-Theng Lee, B. Cabane, *Macromolecules*, 30 (1997) pp. 6559-6566.
180. T. Terada, T. Inaba, H. Kitano, Y. Maeda, N. Tsukida, *Macromolecular Chemistry and Physics*, 195 (1994) pp. 3261-3270.

181. E. Vesterinen, A. Dobrodumov, H. Tenhu, *Macromolecules*, 30 (1997) pp. 1311-1316.
182. F.M. Winnik, M.F. Ottaviani, Stefan H. Boßmann, Wenseng Pan, M. Garcia-Garibay, N.J. Turro, *Macromolecules*, 26 (1993) pp. 4577-4585.
183. S. Siggia, "Quantitative Organic Analysis via Functional Groups" 3rd Edition, Wiley, New York, 1966.
184. H.J. Lucas, D. Pressman, *Industrial and Engineering Chemistry, Analytical Edition*, 10, 140, (1938)
185. J. H. O'Donnell, P. J. Pomery, R. D. Sothman, *Macromol. Chem.* Vol.181 (1980) pp 409-419.
186. R.M. Silverstein, F.X. Webster, *Spectrometric Identification of Organic Compounds*, 6th Edition, Wiley, 1997.
187. B.Mattiasson, A.Kumar I.Yu. Galaev, *Journal of Molecular Recognition*, Vol. 11 (1998) pp. 211–216.
188. S.J. Han, M.K. Yoo, Y.K. Sung, Y.M. Lee, C.S. Cho, *Macromol. Rapid Commun.* 19 (1998) pp. 403–407.
189. E. Díez-Peña, I. Quijada-Garrido, J.M. Barrales-Rienda, M. Wilhelm, H.W. Spiess, *Macromolecular Chemistry and Physics*, 203, (2002) pp. 491-502.
190. F. Zeng, Z. Tong, H. Feng, *Polymer*, Vol. 38 No. 22, (1997) pp. 5539-5544.

191. V.K. Pecharsky, P.Y. Zanalij, *Fundamentals of Powder Diffraction and Structural Characterization of Materials*, Springer, 2005.
192. C. Nave, *Acta Cryst.* (1998). D54, pp. 848-853.
193. B. Leif Hanson, Constance A. Schall, Gerard J. Bunick, *Journal of Structural Biology*, 142 (2003) pp. 77–87.
194. A. Usanmaz, *Turkish Journal of Chemistry*, 21 (1997) pp. 304-312.
195. K. Tajima, T. Aida, *Chemical Communications*, (2000) pp. 2399 – 2412.
196. V.S. Ivanov, *New Concepts in Polymer Science: Radiation Chemistry of Polymers*, VSP (1992).
197. H. Morawetz, *Journal of Polymer Science: Part A-1* vol. 4 (1966) pp. 2487-2492.
198. M.J. Bowden J.H. O'Donnell, *Macromolecules*, Vol. 1, No. 6 (1968) pp. 499-505.
199. U. Ramelow, B.M. Baysal, *Journal of Applied Polymer Science*, Vol. 35 (1988) pp. 937-952.
200. C. Chachaty, M. Latimar, and A. Forchioni, *Journal of Polymer Science*, 13 (1975) pp. 189.

CURRICULUM VITAE

PERSONAL INFORMATION

Surname, Name: Ünver, Alper
Nationality: Turkish (T.C.)
Date and Place of Birth: 02 July 1977, Ankara
Marital Status: Single
Phone: +90 312 241 32 24
Fax: +90 312 210 12 80
E-mail: alperu77@gmail.com

EDUCATION

Degree	Institution	Year of Graduation
MS	METU Chemistry Department	2002
BS	HACETTEPE UNIVERSITY Chemistry Department	1999
High School	Anittepe High School, Ankara	1994

WORK EXPERIENCE

Year	Place	Enrollment
2002-2007	METU Department of Chemistry	Research Assistant
1998 August	ASKI	Intern Research Student

FOREIGN LANGUAGES

Advanced English

PUBLICATIONS

1. Alper Ünver, Nursel Dilsiz, Mürvet Volkan, Güneri Akovalı, Journal of Applied Polymer Science, Volume 96, Issue 5 (2005) Pages 1654 – 1661.
2. Nursel Dilsiz, Alper Ünver, Journal of Applied Polymer Science, Volume 101, Issue 4 (2006) Pages 2538 – 2545.

HOBBIES

Anatolian archaeology, sailing, photography